Influence of Stress on Bone Vasculature and Breast Cancer Bone Metastasis

By

Patrick Louis Mulcrone

Dissertation

Submitted to the Faculty of the

Graduate School of Vanderbilt University

in partial fulfillment of the requirements

for the degree of

DOCTOR OF PHILOSOPHY

in

Cancer Biology

August 11th, 2017

Nashville, Tennessee

Approved:

Jin Chen, M.D., Ph.D.

Ginger E. Holt, M.D.

John S. Penn, Ph.D.

Florent Elefteriou, Ph.D.

Julie A. Sterling, Ph.D.

To my grandparents:
James Ball for his stoicism, hard work, and devotion to his family,
Carol Ball for her quiet strength, kind heart, and love,
Helen Mulcrone for her loving spirit, common sense, and sense of humor,
& James L. Mulcrone, who's legacy I am proud to carry on.

ACKNOWLEDGEMENTS

Firstly, I would like to acknowledge the two scientists that gave me the research opportunities that led to the science documented in this dissertation. Dr. Florent Elefteriou is a brilliant scientist filled with ideas, new methodologies, and a strong work ethic, and I became a more independent scientist and thinker because of his training. Dr. Julie Sterling, in addition to being incredibly supportive and truthful, is a researcher that understands the "big picture" of her studies and knows how to develop projects into sound, high quality science. Her training and guidance impacted my thought processes as a scientist, and I am grateful that she allowed me to join her lab in 2015 so I could stay at Vanderbilt University to complete my dissertation work.

Secondly, the other members of my dissertation committee each influenced my training in unique ways. Dr. Ginger Holt brought a clinical expertise that constantly reminded me of why research is essential for humanity and critically significant. Dr. John Penn is a fantastic researcher, but more importantly, he is a student advocate to the utmost degree. He was always honest with me regarding my research and my path during graduate school, and I would not have been able to complete this program without his guidance. Lastly, my Committee Chair, Dr. Jin Chen, has been an invaluable resource, not only for scientific ideas and protocols, but also for life and career advice. She, like Dr. Penn, was always respectfully honest with my throughout my time here at Vanderbilt. I hope to emulate her training and mentorship style in my future career.

During my six years at Vanderbilt, I worked with many wonderful people. Any member of the Elefteriou and Sterling Labs that I had the privilege to work with on any project, thank you so much. Specifically, I would like to recognize Dr. Preston Campbell, a former member of the Elefteriou Lab. Dr. Campbell was a great mentor who trained me in the ways of bone biology and tumor metastasis

research, along with being incredibly supportive of the many ideas I had, one of which became the basis for this dissertation. However, I am most grateful for the strong friendship his family and mine have developed of the past six years.

My research would not have been possible without the many grants and funding sources provided by the Vanderbilt Interdisciplinary Graduate Program, The National Cancer Institute, and the Department of Veterans' Affairs. Also, I'd like to thank my fellow Vanderbilt Graduate students; we kept each other sane through it all.

The completion of this dissertation would not have been possible without my supportive, large family. My kind and intelligent parents, Dr. Jim Mulcrone and Dr. Susan Ball-Kell, stressed the importance of education early on in my life, and were always encouraging in my pursuit of a career in science. My stepparents, Dr. John Kell and Dr. Renee Mulcrone, are amazing people, and I am eternally grateful to have them in my life. I would also like to thank my in-laws, Col. Uday Dadwal and Sarita Singh Dadwal, who are very loving and wise people that gave unconditional support from across the world. My brother Ryan always makes me laugh, my sister Lauren is always up for a good conversation, and the younger ones, Shannyn, Erynn, and Aedan, are wonderful young adults who will have great impact on the world. I love all five of you so much.

Finally, but definitely not least of all, I would like to thank my lovely wife, Dr. Ushashi Dadwal. Your love, kindness, intelligence, warmth, free spirit, and devotion are traits I aspire to emulate. I love you with all of my heart and soul, and could not have finished this degree without you. My one and only, my back-up brain, we have such a long, exciting road ahead of us.

TABLE OF CONTENTS

Page

Appendix

LIST OF FIGURES

Figure **Page**

LIST OF ABBREVIATIONS

ACA	Affordable Care Act
ANG-2	Angiopoietin 2
AREG	Amphiregulin
β2AR	Beta 2 Adrenergic Receptor
BMEC	Bone Marrow Endothelial Cell
BMP	Bone Morphogenic Protein
BMSC	Bone Marrow Stromal Cell
BV	Bone Volume
cAMP	Cyclic Adenosine Monophosphate
CAR	CXCL12 Abundant Reticular Cell
CARV	Carvedilol
CCL5	C-C Motif Chemokine 5
cDNA	Complementary DNA
CIS	Chronic Immobilization Stress
CM	Conditioned Media
CRC	Colorectal Cancer
Dll4	Delta Like Ligand 4
DMFS	Distant Metastasis Free Survival
ECM	Extracellular Matrix
EGF	Epidermal Growth Factor
ELISA	Enzyme Linked Immunosorbent Assay
EMT	Epithelial to Mesenchymal Transition

EPI	Epinephrine
ER	Estrogen Receptor
ESL-1	E-Selectin Ligand 1
FAK	Focal Adhesion Kinase
FGF-2	Fibroblast Growth Factor 2
GAP	GTPase Activating Protein
GEF	Guanidine Nucleotide Exchange Factor
GFP	Green Fluorescent Protein
GIST	Gastro-intestinal Stromal Tumor
GP130	Glycoprotein 130
GPCR	G Protein Coupled Receptor
GRK	G Protein Couple Receptor Kinase
HER2	Human Epidermal Growth Factor 2
HIF	Hypoxia Inducible Factor
HPA	Hypothalamic Pituitary Axis
ICAM	Intercellular Adhesion Molecule
IFN	Interferon
IL-11	Interleukin 11
IL-17	Interleukin 17
IL-1β	Interleukin 1 Beta
IL-3	Interleukin 3
IL-6	Interleukin 6
IL-8	Interleukin 8

IL6-R	Interleukin 6 Receptor
ISO	Isoproterenol
ITG	Integrin
KM	Kaplan Meier
LEPR+	Leptin Receptor Positive
LIF	Leukemia Inhibitory Factor
LIFR	Leukemia Inhibitory Factor Receptor
Luc	Luciferase
M-CSF	Macrophage Colony Stimulating Factor
MET	Mesenchymal to Epithelial Transition
MMP	Matrix Metalloproteinase
NE	Norepinephrine
NGF	Nerve Growth Factor
NSCLC	Non-small Cell Lung Cancer
OPG	Osteoprotegerin
OSX	Osterix
PBS	Phosphate Buffered Saline
PDAC	Pancreatic Ductal Adenocarcinoma
PDGFR	Platelet Derived Growth Factor Receptor
PGE	Prostaglandin E
PKA	Protein Kinase A
pNET	Pancreatic Neuroendocrine Tumor
PR	Progesterone Receptor

PSGL-1	P-Selectin Ligand 1
PSNS	Parasympathetic Nervous System
PTH	Parathyroid Hormone
PTHrP	Parathyroid Hormone Related Protein
PUR	Polyurethane
qPCR	Quantitative Polymerase Chain Reaction
RA	Rheumatoid Arthritis
RANK	Receptor Activator of Nf-kB
RANKL	Receptor Activator of Nf-kB Ligand
RCC	Renal Cell Carcinoma
RTK	Receptor Tyrosine Kinase
SCF	Stem Cell Factor
SDF-1	Stromal Derived Factor 1
SELE	E-Selectin
SELP	P-Selectin
SMI	Small Molecule Inhibitor
SNS	Sympathetic Nervous System
TB	Trabecular Bone
TGF	Transforming Growth Factor
TIBD	Tumor Induced Bone Disease
TNBC	Triple Negative Breast Cancer
TNF	Tumor Necrosis Factor
TRAP	Tartrate Resistant Acid Phosphatase

TSP	Thrombospondin
TV	Total Volume
VCAM	Vascular Cell Adhesion Molecule
VEGF	Vascular Endothelial Growth Factor
VEGFR	Vascular Endothelial Growth Factor Receptor
WT	Wild Type
ZA	Zoledronic Acid
μCT	Microcomputed Tomography

ORIGNIAL PUBLICATIONS

1. **P.L. Mulcrone**, J.P. Campbell, L. Clément-Demange, A.L. Anbinder, A.R. Merkel, R.A. Brekken, J.A. Sterling, and F. Elefteriou; Skeletal Colonization by Breast Cancer Is Stimulated by an Osteoblast and β2AR-dependent Neo-angiogenic Switch. *Journal of Bone & Mineral Research.* 2017 Mar 16. doi: 10.1002/jbmr.3133

2. D. Buenrostro, **P.L. Mulcrone**, P. Owens, and J.A. Sterling; The Bone Microenvironment: A Fertile Soil for Tumor Growth. *Current Osteoporosis Reports.* 2016 Jun 2.

3. J.P. Campbell, **P. L. Mulcrone**, S.K. Masood, M. Karolak, A. Merkel, K. Hebron, A. Zijlstra, J. Sterling, and F. Elefteriou: TRIzol and Alu qPCR-based quantification of metastatic seeding within the skeleton. *Nature Scientific Reports.* 2015 Aug 14;5:12635. doi: 10.1038/srep12635

CHAPTER I

Background Information and Dissertation Focus

Cancer Introduction

As stated by to the World Health Organization, cancer is the second leading cause of death in the USA behind heart disease. Worldwide, cancer accounts for approximately 13% of all deaths, warranting more funds, time, and investment to understand the pathology of this disease (1). At its most basic, cancer is a group of diseases that originates because of uncontrolled cell proliferation due to mutations in the genome. These so-called "driver mutations" can be caused by exposure to environmental toxins, like chemicals found in cigarettes, or due to genetics, as people with Li-Fraumeni Disease who have a mutation in the tumor suppressor gene TP53 and are at a much higher risk of developing multiple types of cancer (2). Additionally, driver mutations can lead to other genetic changes, giving rise to other driver mutations as well as myriad of "passenger mutations." Because of this characteristic, tumors can be incredibly heterogeneous not only intertumorally, between different patients that have the same classification of cancer, but even intratumorally, between different sections of one tumor in a single patient (3). This biological diversity has made it difficult to completely eradicate many tumor types and can also lead to drug-resistant tumors that either grow during initial treatment or recur months to years later.

Advances in cancer research over many decades have illuminated specific traits of tumors, designated the "Hallmarks of Cancer" by Drs. Douglas Hannahan and Robert Weinberg. These characteristics are believed to be essential to cancer development and progression, covering a wide range of biological processes (4, 5). Although one could argue that each of these characteristics is influenced by the host cells of a microenvironment where a tumor grows, some of these hallmarks are

more tumor centric: genetic instability, deregulated cellular metabolism, resisting cell death, avoiding destruction by the immune system, capability to invade and metastasize, evading growth suppressors, and immortal cellular replication. There are some hallmarks, however, that heavily involve host cell types, or the stroma; tumor-promoting inflammation, sustaining proliferative signaling, and angiogenesis, which is the formation of new blood vessels, involve the immune system, cancer-associated fibroblasts and pericytes, and endothelial cells, respectively. These interactions between tumors and the stroma allow the tumors to become malignant neoplasms, grow exponentially, and evolve into diffuse, metastatic disease. Once cancer advances to this stage, it is more difficult to treat and, in many cases, incurable.

Cancer Metastasis

Metastasis is defined as the event when tumor cells travel from the initial site of disease to a separate site in the body, and this event accounts for a vast majority of cancer-related deaths (6). Tumors metastasize to specific secondary organs due to intrinsic properties of both the primary tumor and those secondary sites; these secondary sites being fertile “soil” for the “seeds” of the primary tumor (7). A strong example of this behavior is observed in colorectal cancer (CRC). This tumor type commonly metastasizes to the liver via the hepatic portal vein, a structure that carries blood from the gastrointestinal tract to the liver. It is this structure that forms a direct connection between these two organs, exposing metastatic CRC cells to the liver microenvironment. Furthermore, advanced prostate cancer almost exclusively spreads to bone because this tumor type responds favorably to proteins and the physical make-up of the bone. In turn, prostate cancer cells secrete factors such as androgens that activate osteoblasts, causing the release of bone morphogenic proteins (BMPs) and TGF-β, which are known to drive prostate tumor progression.

One of the most common sites of metastasis is the bone. Regarding specific cancer subtypes, breast, prostate, lung, melanoma, multiple myeloma, many of which are among the most commonly diagnosed cancers, all metastasize to bone. Anthracyclines, such as doxorubicin, as well as radiation are standard lines of therapy for patients that present with bone lesions (8). While these treatments are non-specific, more translational studies now focus on ways to explicitly target the tumor cells that establish in the bone as well as prevent actions of the multitude of cells in the bone microenvironment with which the tumors interact.

Breast Cancer Subtypes

Specifically looking at breast cancer, a subtype that commonly metastasizes to bone, this disease is the most commonly diagnosed cancer in women and the second-leading cause of cancer-related deaths in women in the USA. Screenings for breast cancer have increased over the last three decades, and the survival rate has reflected that advancement. However, most breast cancer deaths are due to diffuse metastatic disease; it is estimated that around 90% of breast cancer deaths are due to metastases, and there are currently no cures once the tumor has spread (1, 9). Breast cancer commonly metastasizes to lungs, liver, brain, and bone, and has a recurrence rate of 20-30% (10). Moreover, the median survival time of patients with metastatic breast cancer is roughly 3 years, yet this depends on the subtype, stage at diagnosis, and treatment regimen (11).

There are multiple subtypes of breast cancer that are distinguished by receptor status as well as cell of origin of the tumor in the breast tissue. The presence of any of the following proteins: Estrogen Receptor (ER), Progesterone Receptor (PR), and Human Epidermal Growth Factor Receptor 2 (HER2), classify breast tumors and identify prognosis and potential therapy options.

Triple negative breast cancers (TNBC) lack expression of all three of the aforementioned receptor proteins and account for approximately 20% of breast tumors. They have poor prognosis, are poorly differentiated, and are treated with chemotherapies. HER2+ cancers, representing about 20% of breast cancer diagnoses, have strong expression of the HER2 receptor, and are treated with trastuzumab, a monoclonal antibody that binds HER2 and blocks downstream signaling of that receptor. Luminal breast cancers make up the other 60% of breast cancer diagnoses. They range in receptor status and in prognosis. This type of breast tumor can be ER and/or PR positive and can be treated with anti-hormonal therapies like anti-estrogens. Relating these subtypes to bone metastasis, all have been reported to metastasize to the bone. TNBC are viewed as the most aggressive category, and certain groups report that ER+ breast cancers are the most common subtype that produces bone lesions (12). Up to 75% of patients with diffuse metastatic breast cancer will develop a bone lesion, and this can manifest as one of many skeletal related events. These include hypercalcemia, spinal cord compression, severe bone pain, and pathological fractures (13).

Breast Cancer Metastasis to Bone

The metastatic process is one that occurs rarely and is biologically inefficient. In reference to breast cancer, a tumor grows at a primary site somewhere in breast tissue, increasing in size and acquiring multiple mutations that promote this growth (**Figure 1**). In order for this tumor to survive due to its incredible growth potential, it must create and co-op blood vessel networks through the process of angiogenesis. Tumors commandeer blood vessel networks through hypoxic signaling cues, like secretion of growth factors such as vascular endothelial growth factor (VEGF), that guide blood vessel growth toward the tumor mass. The initial tumor, now malignant, can then locally invade as well as intravasate into the circulatory and lymphatic systems after undergoing epithelial to mesenchymal (EMT) transition.

While many cells from a primary tumor may intravasate, only a very small percentage are able to survive in circulation, leading to systemic dissemination of a tumor in a host. Eventually, tumor cells that successfully colonize bone must exit circulation and extravasate into a secondary tissue; this requires interactions with circulating immune cells, endothelial cells, and mesenchymal to epithelial (MET) transition. Tumor cells that arrive in bone can remain dormant for as long as a decade before commandeering the homeostatic processes of the bone microenvironment and becoming a secondary lesion (9, 14, 15). Much research is needed to understand the process of bone metastases, treatment options for these types of lesions, and factors that promote or hinder this process. It is clear, however, that the cells of the host microenvironment have a role in tumor progression and need to be further investigated in the context of basic, translational, and clinical research.

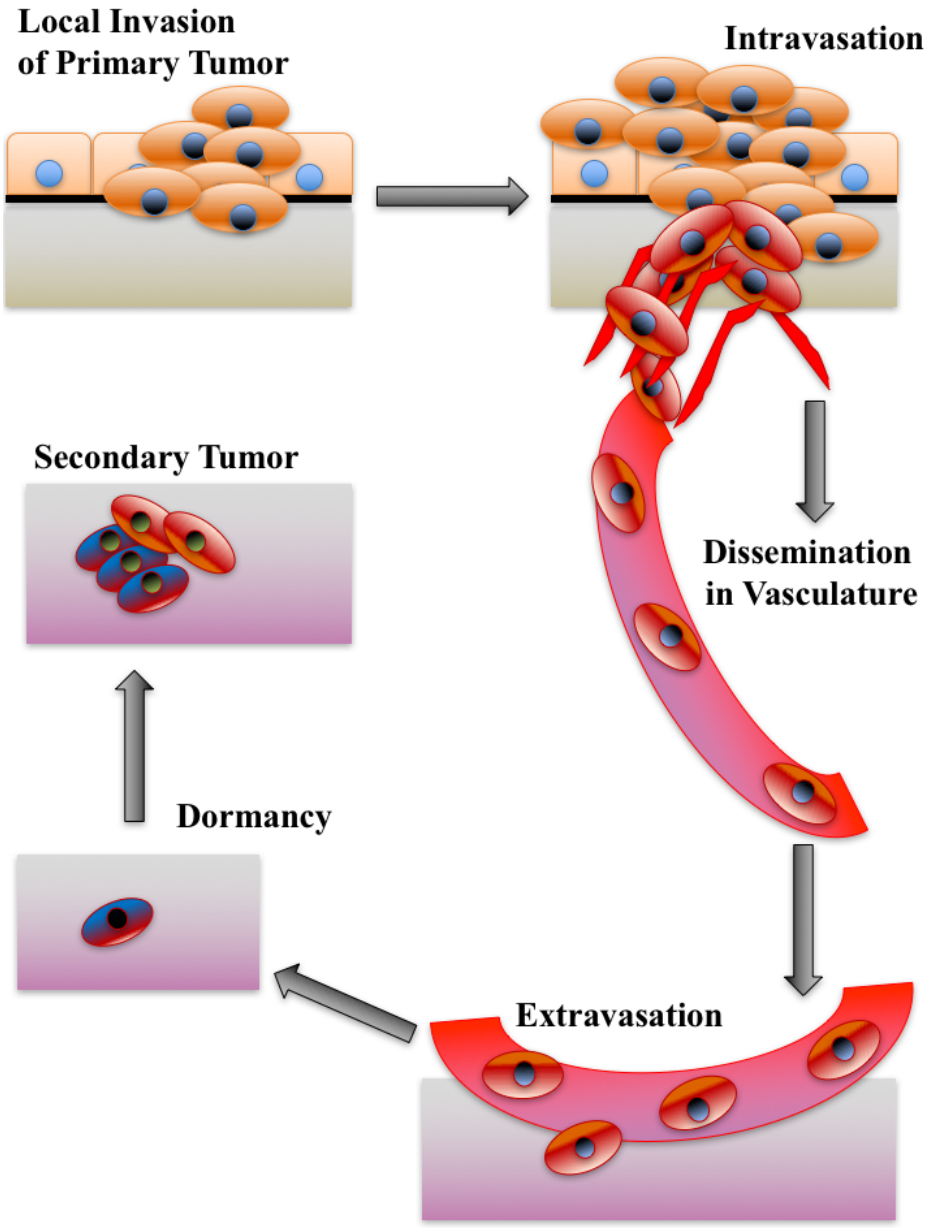

Figure 1: The Metastatic Cascade. Tumor initiation begins with a mutation of normal cells at a primary location. The tumor grows and can invade locally. If the tumor is able to commandeer vasculature, this will allow it to grow exponentially, as the vessels provide nutrients for survival. Also, this compromised network provides a conduit to the circulatory and lymphatic systems. A fraction of the tumor cells will survive in circulation, becoming systemically disseminated. An even smaller percentage extravasates from the blood stream into a secondary organ. These successfully metastasized cells can either remain dormant for as long as a decade, or begin proliferating, creating a secondary lesion.

The Vicious Cycle of Bone Metastasis

A pioneer in the field of bone biology and metastasis, Dr. Gregory Mundy, described the process of bone metastasis as "The Vicious Cycle" (14). Essentially, tumor cells that are present in the bone secrete factors such as Parathyroid Hormone Related Protein (PTHrP) and Interleukins 6, 8, and 11 (IL-6, IL-8, IL-11) that activate osteoblasts. These activated osteoblasts produce RANKL, a cytokine that binds its receptor RANK that is present on pre-osteoclasts, causing them to mature into fully functional osteoclasts. These cells of the myeloid lineage are then able to resorb bone, releasing a myriad of factors like Transforming Growth Factor Beta (TGF-β), Bone Morphogenic Proteins (BMPs), and calcium into the bone microenvironment that promote tumor growth and feed forward this destructive cycle. Breast cancer and multiple myeloma bone lesions tend to present in clinic as osteolytic, while prostate cancer bone lesions are most commonly osteosclerotic, validating both osteoclast and osteoblast-targeted therapies (16).

Elucidation of The Vicious Cycle has revealed how important the multitudes of stromal cells of the bone microenvironment are for cancer progression. Because of this, current standard of care therapies for patients with bone lesions target proteins produced by stromal cells as well as their activity. Denosumab is an antibody that targets receptor activator of Nf-kB ligand (RANKL) that is produced by osteoblasts and prevents it from binding its receptor, RANK, thus reducing osteoclastogenesis (17). Bisphosphonates are a class of drugs that prevent osteoclast resorption by binding hydroxyapatite present in bone tissue, thus stopping bone destruction and reducing bone pain for patients. The most commonly used bisphosphonate currently is Zoledronic Acid (ZA), and there is a debate in the bone field as to whether bisphosphonates also inhibit tumor growth (18). The field of bone-targeted therapies is not without its pitfalls. A drug called Odanacatib that targets Cathepsin K, a protease made by osteoclasts, showed promise in the laboratory, but was not successful in human trials due to

cardiovascular side effects (19). It is extremely important to note that these treatments for bone metastases are only palliative, reinforcing the need for more research to elucidate the biology of bone metastatic lesions and how to effectively treat them.

Cells of the Bone Microenvironment: Osteoblasts, Osteoclasts, and Osteocytes

Osteoblasts are known as the "bone-forming" cells. These cells are derivatives of mesenchymal cells and drive bone formation through the production of cytokines and deposition of matrix proteins. Osteo-chondroprogenitor cells differentiate down the osteoblast lineage through transcriptional activity of Runx2, leading to the induction of osteoblastic genes related to collagen deposition and matrix mineralization (20).. These cells are producers of macrophage colony stimulating factor (M-CSF) and RANKL, both of which are needed for formation of the bone resorbing osteoclasts (21-23). Osteoblasts are also able to produce osteoprotegerin (OPG), a decoy receptor for RANKL as a mechanism of negative regulation of bone turnover (22). Certain tumors, such as prostate cancer, produce osteosclerotic lesions. This type of bone lesion is characterized by increased deposition of compromised bone tissue, which is linked to overstimulated osteoblast activity.

Osteoclasts, known as the bone-resorbing cells, are a multinucleated cell population of the myeloid lineage that is responsible for bone destruction in the context of both bone homeostasis and cancer (23). As previously mentioned, M-CSF and RANKL, produced by osteoblasts as well as osteocytes, bind receptors present on pre-osteoclasts, causing them to differentiate and become active bone resorbing cells. Mature, activated osteoclasts create resorption pits on the bone surface via the release many proteases like matrix metalloproteinase 9 (MMP9), Cathepsin K, and H+ ions to create an acidic environment apt for bone destruction (14). This process is tightly regulated by cellular communication from osteoblasts and other cell types found in bone. Parathyroid hormone (PTH) as well

as prostaglandin E (PGE) have been reported to positively regulate secretion of H+ in osteoclasts, thus promoting resorption (23).

Osteocytes are the mature forms of osteoblasts, the most abundant cell in bone, and are embedded in the calcified tissue of the bone. These cells have protrusions and are believed to be highly communicative within the bone microenvironment. They have functions related to mechanosensing, bone remodeling, and mineral metabolism (24). Although more research is needed even to fully understand their biology, it has been reported that osteocytes can secrete adenosine nucleotides that facilitate breast cancer cell migration and can respond to physical changes in bone due to tumor growth, which caused them to secrete cytokines and matrix metalloproteinases (MMPs) that promote tumor growth (25). Interestingly, Sottnik *et al*. revealed that increased pressure on MLO-Y4 osteocytes promoted production of C-C motif chemokine 5 (CCL5), which enhanced migration and invasion of multiple prostate cancer lines (26). This study suggests that certain physical parameters of the bone microenvironment can enhance tumor progression, and that osteocytes may contribute to tumor progression through these types of mechanisms. Osteocytes can also influence other bone stromal cells in manners that promote tumor progression. Delgado-Calle *et al*. revealed that bidirectional Notch signaling between multiple myeloma cells and osteocytes can lead to increased pre-osteoclast recruitment, tumor cell proliferation, and decreased osteoblast activity and differentiation (27).

RANKL and OPG Are Key for Bone Homeostasis and Cancer Metastasis

As previously stated, osteoblasts are the bone-forming cells of the bone microenvironment. Furthermore, these cells generate growth factors and cytokines that regulate bone homeostasis and also affect cancer progression. Two of these principal proteins are RANKL and OPG.

RANKL, receptor activator of NF-κB ligand, is a member of the tumor necrosis factor (TNF) family of ligands that has a membrane-bound form and a soluble form caused by proteolytic cleavage or alternative mRNA splicing. Once a hexameric complex is formed between 3 ligands and 3 RANK receptors, a signaling cascade through the NF-κB pathway is initiated. Target genes of this pathway that are transcribed promote inflammation, osteoclastogenesis, and epithelial proliferation (28, 29). It is through osteoclast differentiation that RANKL regulates bone homeostasis. Additional pathways activated by RANKL signaling include PI3K-AKT, MEK-ERK, and JNK c-FOS/c-JUN. Regarding cancer pathology, many types of cancer, including sarcomas and breast cancers, have been reported to express RANK and respond to RANKL in a manner that promotes disease progression (30).

Osteoprotegerin (OPG) is a member of the TNF superfamily of receptors. This secreted decoy receptor is responsible for negatively regulating bone resorption through binding RANKL and preventing its downstream activity (22, 31). Bone homeostasis is highly dependent on the ratio of RANKL to OPG; more RANKL leads to bone resorption, while more OPG leads to reduced resorption. Multiple myeloma cells degrade OPG, which ultimately shifts the RANKL/OPG ratio to a tumor-promoting value (32). The mechanism of the drug Denosumab mimics that of OPG and is used as a treatment for osteoporosis and tumor-induced bone disease (TIBD).

Interleukin 6 (IL-6) in Bone Biology and Cancer

Another protein that plays a role in both bone biology and cancer progression, and is produced by osteoblasts, is IL-6. This protein is a pro-inflammatory cytokine that is involved in many biological processes and present in many tissues. It signals by binding a heterotrimeric receptor complex containing one IL6-R protein, either soluble or membrane-bound, and two membrane-bound GP130 proteins, and activates the JAK/STAT and NF-κB pathways (33). These two isoforms of the IL6

receptor are synthesized through alternative splicing of the IL6-R gene, or through proteolytic processing of membrane-bound IL6R upstream of its transmembrane domain via ADAM17 activity (34, 35). Signaling through the membrane-bound IL6-R is considered the canonical pathway, and the receptor complex containing the soluble form of IL6-R is designated as trans-signaling. In the context of bone biology, IL-6 promotes osteoclast formation and activity through increased RANKL expression; Il6KO mice are reported to have reduced bone degradation and low levels of Rankl and Il-17 (33). Johnson *et al.* revealed that specific loss of gp130 in osteoblasts and osteocytes led to reduced trabecular bone formation in mice, highlighting the role of this cytokine in bone formation and homeostasis (36). Furthermore, injury to bone is known to increase expression of IL-6 in multiple bone stromal cells, including osteoblasts, and infiltrating monocytes to initiate bone healing (37).

IL-6 is a tumor promoting protein and contributes to cancer cachexia (33, 38, 39). STAT3 activation downstream of IL-6 is linked to muscle atrophy and exacerbates this wasting phenotype in tumor models (39). Many of the osteotropic tumor types, such as breast, prostate, and multiple myeloma, secrete elevated amounts of this cytokine. Hartman and colleagues showed that the TNBC subtype relies heavily on IL-6 for its tumorigenicity (40). To further complicate cancer pathology, tumors can also stimulate the stroma to produce IL-6, indicating that multiple pools of this cytokine can promote tumor progression. This phenomenon was reinforced by Zheng *et al*.; they demonstrated that specific blockade of either tumor-derived human IL-6 or stromal derived mouse Il-6 reduced bone lesion area, increased apoptotic tumor cell percentage, and minimized serum RANKL levels (41). As far as clinical treatments targeting IL-6 are concerned, tocilizumab, a monoclonal antibody that targets IL6R, is currently FDA approved to treat rheumatoid arthritis. As this drug has shown efficacy in studies targeting HER2+ tumors that are also hormone receptor negative, it could be a viable option for the treatment of metastatic breast cancer tumors (42).

The Sympathetic Nervous System Signals via Adrenergic Receptors and Regulates Bone Remodeling

More research is needed to investigate processes that regulate the many distinct cells involved in the "vicious cycle" of cancer-induced bone destruction, which could reveal new targets for the treatment and prevention of bone metastases. In addition to cells listed in the previous section, the bone microenvironment contains both Parasympathetic Nervous System (PSNS) and Sympathetic Nervous System (SNS) nerves (21). The SNS regulates the "Fight or Flight" response and signals via activation of the Hypothalamic-Pituitary Axis (HPA) and release of catecholamines in the adrenal gland and innervated tissues. Peripheral sympathetic nerves that innervate the bone release norepinephrine (NE), a neurotransmitter that binds adrenergic receptors present on target cells (43). NE is known to bind beta2-adrenergic receptors (β2ARs) present on osteoblasts. Upon SNS activation, NE is released by sympathetic nerve fibers. Activation of β2AR leads to increased RANKL production by osteoblasts, osteoclastogenesis, and bone turnover (44). In addition to changes in bone turnover, β2AR activation leads to alterations in inflammation and cell trafficking in bone tissue.. It is well reported that SNS innervation of the bone marrow is a regulatory mechanism for hematopoiesis and immune cell response to injury (45). Previous work has shown that Isoproterenol (ISO), a synthetic βAR agonist, increased RANKL production by osteoblasts and bone remodeling (44, 46). Also, both osteoblast-specific and global β2AR knockout mice exhibit a high bone mass, indicating the β2AR in osteoblasts triggers this bone phenotype (46, 47). A direct role of the nerves on tumor progression in bone metastases is an expanding area of research. Even though stress has not been shown to directly cause cancer, it is linked to reduced patient survival and exacerbation of the disease (48-50).

Previous work from our lab has reinforced the role that SNS has on the progression of breast cancer bone metastases. Campbell and colleagues report that increased levels of osteoblastic RANKL

caused by ISO treatment induced the migration of MDA-MB-231 breast cancer cells *in vitro* in a transwell assay. Addition of OPG to the activated osteoblasts prevented that migration, strongly implicated a RANKL-dependent migration. Furthermore treatment in an experimental bone metastasis mouse model, ISO promoted the colonization of bone in MDA-MB-231s, but not in MDA-MB-231s with low levels of the RANK receptor (51). RANKL has been linked to worse clinical outcomes in breast cancer patients, as well as melanoma bone metastases (53-53)

Adrenergic Signaling in Cancer Progression

Adrenergic receptors belong to the family of G-protein coupled receptors (GPCRs), the largest family of eukaryotic receptor proteins. The structure of GPCRs is well studied, as these receptors are known to be heptahelical with seven transmembrane α-helices spanning the cell membrane, have an extracellular N-terminus, and an intracellular C-terminus (54). GPCR signaling relies on many effector proteins and signal transducers. Once GPCRs are activated, as when catecholamines bind to adrenergic receptors, an intracellular, GDP-bound heterotrimeric G protein complex that is inactive separates into active Gα-GTP and Gβγ subunits. Guanidine nucleotide Exchange Factors (GEFs) and GTPase-Activating Proteins (GAPs) facilitate the cycle between GDP and GTP bound G proteins. Accompanying regulatory mechanisms of GPCRs involve a group of proteins called arrestins (55). This family of proteins binds to phosphorylated GPCRs, desensitizing the receptor, and is also key in facilitating signaling for receptor internalization, as arrestins have been shown to bind clathrin, a protein key in vesicle formation and cellular cargo sorting.

There are two classes of adrenergic receptors: alpha-adrenergic receptors (αAR), consisting of two subtypes, and three subtypes of beta-adrenergic receptors (βAR). These five subtypes are expressed across many different tissues. For example, smooth muscle cells express both α1ARs and α2ARs, while

platelets are positive for α2ARs. β1ARs are found on cardiac muscle and increase heart rate when activated (56-58). β2ARs regulate vasodilation in heart and lung, and control myeloid cell trafficking (45). Adipocytes are positive for β3ARs, and their activation leads to increased oxygen consumption and insulin secretion (59). Specifically discussing the β2AR, one of the focal points of this dissertation, this adrenergic receptor is rather ubiquitously expressed, detected in osteoblasts, and is known to regulate bone homeostasis (44, 46, 47). β2AR is coupled almost primarily to a $G\alpha_s$ family member, and $G\alpha_s$ signals through the secondary messengers adenylyl cyclase and cyclic AMP (cAMP). $G\alpha_s$ is described as activating because this G-protein member induces increases in intracellular cAMP, which further activates protein kinase A (PKA) through direct binding; PKA is an important negative regulator of the β2AR (54, 55). The cAMP arm of β2AR signaling further supports activation of RAF/MEK/ERK signaling pathway, a set of kinases that are highly associated with survival and proliferation of cancer cells (**Figure 2**).

As previously mentioned, stressful stimuli activate adrenergic receptors through the SNS arm of the nervous system. Short-term activation of the SNS is beneficial for survival; it is when this activation becomes chronic that pathologies arise. Autoimmune diseases as well as cardiovascular diseases have been linked to chronic stress (60). In regard to cancer, multiple tumor types have been shown to express adrenergic receptors, but the level of benefit from activation of these receptors varies by tumor type, suggesting a level of complexity regarding stress and its effects on cancer. Indeed, Schuller and colleagues in 1999 noted that β2ARs promote DNA synthesis in lung adenocarcinoma (61). Kasbohm and colleagues reported that βARs in prostate cancer could stimulate androgen receptors through increasing accrual of cAMP and PKA (62). Studies of ovarian cancer reveal that this tumor type also gains a survival benefit from adrenergic signaling through growth factor production and vascularization (63, 64). Furthermore, stromal cells associated with tumors such as bone marrow, endothelium, and

nerves, also express adrenergic receptors and can affect tumor progression through growth factor secretion and immune suppression (65).

Adrenergic Blockers in Clinical and Translational Cancer Studies

Many clinical cancer studies have elucidated advantageous actions of beta-blockers, a class of adrenergic receptor antagonist known to be effective at targeting arrhythmia and high blood pressure. Patients with breast cancer, malignant melanoma, and NSCLC were reported to have improved survival outcomes if their treatment regimen included a beta-blocker (66-68). One clinical study of CRC patients, however, showed no clinical benefit with beta-blocker treatment, highlighting the need for more scrutiny as to how beta-blockers affect the progression of multiple forms of cancer (69).

Translational studies have dissected many of the mechanisms behind how SNS activation promotes tumor progression and how beta-blockers negatively affect this progression. Researchers report direct effects on tumor growth and regulating tumor apoptosis of hemangiomas, ovarian cancer, breast cancer, and prostate cancer, showing that catecholamines can directly bind tumor cells and activate pro-survival pathways (48, 63, 64, 70). Effects of catecholamine signaling have also been shown to promote migratory and invasive behaviors. A study by Creed and colleagues reports that the TNBC cell line MDA-MB-231s exhibited increased invadopodia formation with ISO treatment. Moreover, use of a β2AR-specific inhibitor reduced that increase as well as the function of these invadopodia (71). Others report increases in the gelatinases MMP-2 and MMP-9, proteins that degrade the ECM and promote tumor cell invasion upon ISO treatment (72).

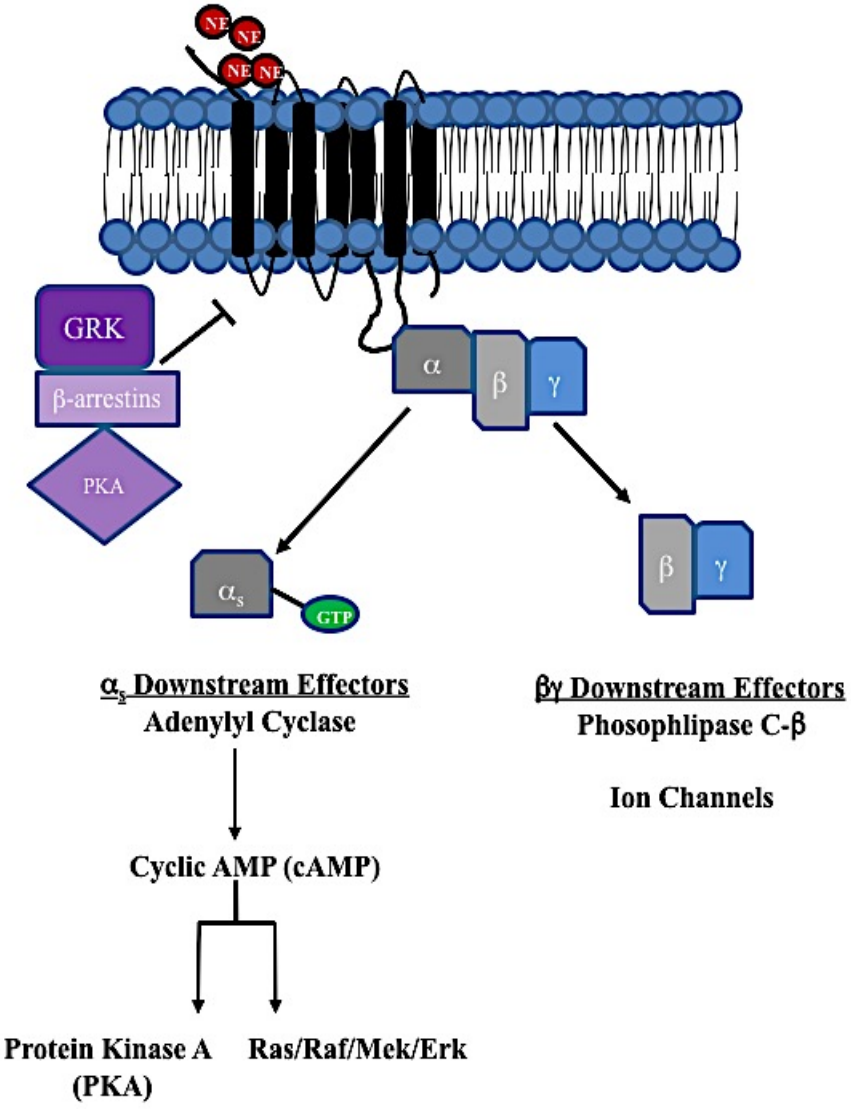

Figure 2: Simplified Schematic of β2AR signaling. Black cylinders represent α-helices of the β2AR. Norepinephrine (NE) binds extracellularlly, leading to activation of the heterotrimeric G-protein. $G\alpha_s$ then increases adenylyl cyclase activity, cAMP levels, and corresponding downstream targets. GRKs, β-arrestins, and PKA negatively regulate β2AR signaling.

Along with these direct effects on the tumors themselves, adrenergic signaling also changes stromal and immune cells that constitute the tumor microenvironment in ways that support tumor progression. NE and EPI have been shown to negatively alter levels of NK cells and macrophages in manners that promote prostate cancer growth (73, 74). Furthermore, Sloan *et al.* showed that stress-induced changes in the lung microenvironment via infiltration of tumor-promoting macrophages support breast cancer metastases to that specific site (75). Primary tumor angiogenesis was also negatively affected in models of ovarian cancer and neuroblastoma when beta-blockers were added to treatment regimens in the specific mouse models (63, 76).

Blood Vessel Formation, VEGF-A and Its Receptors, and Bone Vasculature

In addition to being innervated by sympathetic nerves, the bone is also highly vascularized. The formation of blood vessels can be categorized into two processes. Vasculogenesis is the *de novo* synthesis of blood vessels, which requires endothelial progenitor cells and angioblasts, as well as differentiation into functional endothelium. Angiogenesis, on the other hand, is the synthesis of blood vessels from existing vessels present in tissues. This developmental pathway involves tightly regulated schema of growth factors and developmental proteins. Vascular endothelial growth factor (VEGF) is essential for blood vessel formation, both in normal and tumor biology. This family of growth factors is transcribed by hypoxia-inducible factors (HIFs), has five members, and binds to three different VEGF receptors that belong to the receptor tyrosine kinase family (RTK) (77). VEGF-A, the isoform that is a main part of this dissertation work, is known to be alternatively spliced into as many as nine distinct isoforms and has been shown to bind VEGFR1 and VEGFR2. The VEGFA gene is comprised of eight exons and seven introns, which allows for the creation of multiple isoforms via alternative splicing. The four most common isoforms are $VEGF_{121}$, $VEGF_{165}$, $VEGF_{189}$, and $VEGF_{206}$. Where these proteins

differ most notably relates to properties involving binding affinity and localization. 121 is a diffusible protein, while the larger two isoforms, 189 and 206, are relegated to the extracellular matrix (ECM). 165, compared to the other three, is the most versatile isoform of VEGF-A; it is both secreted and bound to the ECM, and binds with high affinity to VEGF receptors and co-receptors. 121 and 165 are the most highly synthesized isoforms (78).

As previously stated, VEGF-A binds to two RTKs, VEGFR1 and VEGFR2. These RTKs are structured with an extracellular domain where the ligands bind, a single transmembrane region, a juxtacrine membrane domain, an interrupted kinase domain, and a C-terminal tail. Most commonly, these proteins form homodimers and are in part regulated by HIFs, similar to the VEGF-A ligand. When bound to VEGFR2, VEGF-A activates pro-angiogenic signaling and promotes migration and survival of endothelial cells; binding VEGFR1, however, activates anti-angiogenic signaling pathways and has been shown to negatively regulate VEGFR2 activity (79). This yin and yang relationship of VEGFR1 and R2 is key for normal vascular and organ system development, as genetic ablation of either receptor results in embryonic lethality (80). Furthermore, a secreted form of VEGFR1 (sVEGFR1) exists and plays a role in vessel formation and directed growth. There are scientific reports indicating that VEGFR1/R2 heterodimers exist, and that this specific receptor activates pro-angiogenic signaling.

Additionally, Notch signaling plays a role in dictating vessel sprouting and vessel structure. As the Notch pathway is the epitome of juxtacrine signaling in development, it is not surprising that it was discovered to be key in blood vessel formation (81). Communication between tip cells, which are at the leading edge of a new blood vessel, and neighboring stalk cells is heavily dependent on Notch. Elevated levels of VEGF that are sensed by the tip cell cause an increase in delta-like ligand 4 (Dll4); this ligand activates Notch in adjacent endothelial cells, which will eventually become the stalk cells. Subsequently, this leads to reductions in VEGFR2 and increases in sVEGFR1 (82). Furthermore, this increased

production of sVEGFR1 contributes to the proper production of blood vessels in a controlled, direct manner (83). Once the nascent vessel is formed, oxygen levels rise, reducing VEGF levels and ultimately halting angiogenesis.

Angiogenesis and Osteogenesis Are Coupled

Angiogenesis is tightly regulated in tandem with bone formation during endochondral bone development. After a cluster of condensed mesenchymal cells differentiate into chondrocytes, the center most group of this cell cluster stops proliferating and becomes hypertrophic (21, 84). Not only do these hypertrophic chondrocytes control mineralization of the surrounding tissue, they recruit endothelial progenitors and endothelial cells through the creation of a hypoxic environment and subsequent VEGF production in order to trigger the formation a blood vessel network (85). This complex network contains a central nutrient artery, epiphyseal and metaphyseal vessels, and periosteal vessels that supply each section of bone tissue, with the exception of the growth plate and articular cartilage. Osteoblast recruitment follows this vascular invasion and leads to the production of the primary spongiosa, providing structure for bone collar development and bone growth.

Importantly, osteoblasts are known sources of several pro-angiogenic growth factors, including VEGF-A. Many studies have shown that osteoblasts are an essential source of VEGF for normal bone homeostasis, and perturbations regarding this protein can lead to detrimental changes in bone. During development, hypertrophic chondrocytes instruct perichondral cells to become osteoblasts and recruit endothelial progenitor cells to the bone. These newly differentiated osteoblasts initiate formation of the bone collar and vascularization of the primary spongiosa through VEGF-A and other growth factor production (21, 86). Furthermore, Hu and Olsen elucidated multiple roles of osteoblastic VEGF-A in the context of bone repair in response to a monocortical osseous hole injury. These mice that lacked Vegf-a

specifically in osteoblasts via *OsxCre:Vegfaflox* system exhibited defects in macrophage recruitment and angiogenesis during the inflammatory phase of repair. Additionally, osteoclast formation was decreased during the remodeling stage of bone repair, illuminating a key role for VEGF-A in bone stromal cell communication (87). Manipulations of hypoxia-related genes specifically in osteoblasts can also cause changes in angiogenesis and osteogenesis. Overexpression or increased activation of hypoxia-inducible factor 1 (Hif-1) promotes both angiogenesis and osteogenesis, while silencing this pathway reduces blood vessel and bone formation (88). Factors such as BMPs, TGF-β, and vitamin D3 induce expression of VEGF in osteoblasts, linking the processes of osteogenesis and angiogenesis (85).

Bone Vascular Subsets

The structure and cellular involvement of blood vessels and the vascular system of each organ is unique. Bone vasculature has a sinusoidal layout that forms an open vascular bed. This configuration allows for greater entrance and exit of cells to and from the blood stream, specifically those of the hematopoietic lineage (89). Moreover, the bone is comprised of microvascular subsets that have distinct molecular characteristics. In depth analysis has revealed two subgroups of vessels that differ in expression patterns, locations, interaction with supporting stromal cells. They are designated Type H vessels and Type L vessels.

Type H vessels have high expression of the endothelial markers Cd31 and Endomucin. These cells comprise a small percentage of the total bone vessel vasculature and are located preferentially at the metaphysis near the growth plate and along the endosteum. Osterix-positive osteoprogenitor cells as well as PDGFRα and NG2+ pericytes were found to localize with Type H vessels via immunofluorescence (90). Interestingly, this subpopulation *in vivo* increases after an irradiation challenge and decreases with defective Hif1-α signaling. Old mice have a decreased amount of Type H

vessels, which correlates with lower Hif1-α signaling (88). In addition to Hif1-α signaling, Notch signaling plays a key role in Type H vessel biology. Mice lacking *Rbpj,* a protein that controls Notch-induced gene transcription, have lower BV/TV percentage and reduced Type H vessels. Conversely, endothelial ablation of *Fbxw7,* a protein that is part of an ubiquitin protein ligase complex that targets Notch, restores Type H vessel expansion (82).

The other subset of vessels described by the Adams group is Type L vessels. They have low expression of Cd31 and Endomucin and are located throughout the diaphysis of the long bones. Type L vessels are associated with the sinusoidal structures and can be derived from the Type H vessels. This group of vessels decreases upon irradiation, and seems to be replenished by the Type H vessels. CAR cells and LEPR+ cells have been found to interact with this vessel subtype (89). The percentage of type L vessels remains constant over time and is less metabolically active than their H vessel counterparts (89, 90).

Additionally, a range of perivascular cells is needed for support and function of bone vasculature. Pericytes, leptin receptor positive cells (LepR+), and CXCL12-abundant reticular cells (CAR) associate distinctly with Type H and L vessels and interact with the hematopoietic stem cells (HSC) niche in unique manners. Pericytes are a type of smooth muscle cell that surround small vessels and maintain their structure and function. Typically, these cells are both α-SMA and NG2 positive and localize to arteries. There is, however, an additional subset of PDGFRβ positive pericytes that associates with arterioles and Type H vessels. CAR cells function to maintain and regulate hematopoiesis through secretion of stem cell factor (SCF) and CXCL12 (82, 89). Using lineage tracing experiments, Zhou and colleagues showed that LepR+ cells found in the bone marrow microenvironment can differentiate into bone, cartilage, and adipose when exposed to different signals (91). Both CAR and LepR+ cells typically localize with Type L vessels. Little is known about how each of these vascular subsets might

affect breast cancer metastasis to bone, and how their functions may be altered in the presence of tumors. A key observation of bone physiology shows that the nerves of the SNS that innervate the bone run parallel to the bone vasculature on paths through both Haversian and Volkmann's canals and in compact as well as spongy bone (92). Research relating bone vasculature to SNS nerves and how they contribute to cancer progression is understudied and may lead to new and intriguing mechanisms of bone homeostasis and cancer metastasis to bone.

Targeting Vasculature in Cancer

The vasculature is a common target of many therapies in the cancer field, as tumors that become vascularized can grow exponentially and tend to be more aggressive. Additionally, the vascular network of the tumor is a series of conduits for metastatic cells to intravasate and initiate metastasis. Therefore, targeting tumor vascular networks by either inhibiting vessel recruitment and formation or normalization of tumor vessels to enable enhanced drug delivery became an important area of cancer research involving the stroma.

Bevacizumab is a humanized monoclonal antibody that targets VEGF-A, preventing its binding to both VEGFR1 and R2 (93). This treatment is currently approved for multiple cancers, like non-small cell lung cancer (NSCLC), breast cancer, and colorectal cancer. The clinical benefits, however, are reported to be moderate for breast cancer and pancreatic cancer, and side effects such as hypertension, proteinuria, and hemorrhage were reported (94). When combined with chemotherapy, Bevacizumab exhibits its beneficial effect and prolongs progression free survival of cancer patients with metastatic breast cancer by approximately 3 months (95). The suggested mechanism of action related to the clinical benefit of the Bevacizumab/ chemotherapy combination is that the anti-VEGF-A antibody normalizes and improves the integrity of tumor blood vessels, which are known to be leaky and corrupt. With the

vessels more structured, delivery of chemotherapies is now more efficient, targeting more of the tumor mass and killing more of the cancerous cells (96).

Small molecule inhibitors (SMIs) of VEGFR2 like Sunitinib and Sorafenib are approved for treatment multiple tumor types yet also cause multiple off-target effects: fatigue, hypertension, and skin rashes being the most common (97). This is partially due to the fact that these SMIs are multi-targeted kinase inhibitors; along with VEGFR2, these drugs inhibit c-KIT, PDGFRβ, and FLT3, each of which in its own right is linked to cancer pathology (98). Currently, according to the National Cancer Institute, sorafenib is FDA approved for treating renal cell carcinoma (RCC), differentiated thyroid carcinoma, and hepatocellular carcinoma; sunitinib is approved for Gastro-intestinal stromal tumor (GIST), pancreatic neuroendocrine tumors (pNET), and RCC.

Clinical results have shown that there is synergy between VEGF/R inhibitors with anti-metabolite and platinum-based chemotherapies, suggesting that targeting angiogenic signaling in cancer biology is efficacious (99). One way that these treatments could be improved is through more direct and specific delivery methods, both site as well as tumor specific targeting. Many of the current anti-angiogenic therapies target multiple arms of VEGF signaling, both pro and anti-angiogenic, or other RTK family members. More research is needed to understand if this multi-targeted approach is always beneficial, or whether more selective drugs that target one aspect of angiogenic signaling could be more efficacious in treating cancer. Moreover, stromal vasculature and the changes that can occur in the tumor microenvironment must be considered and studied in the context of cancer metastasis and disease progression (**Figure 3**).

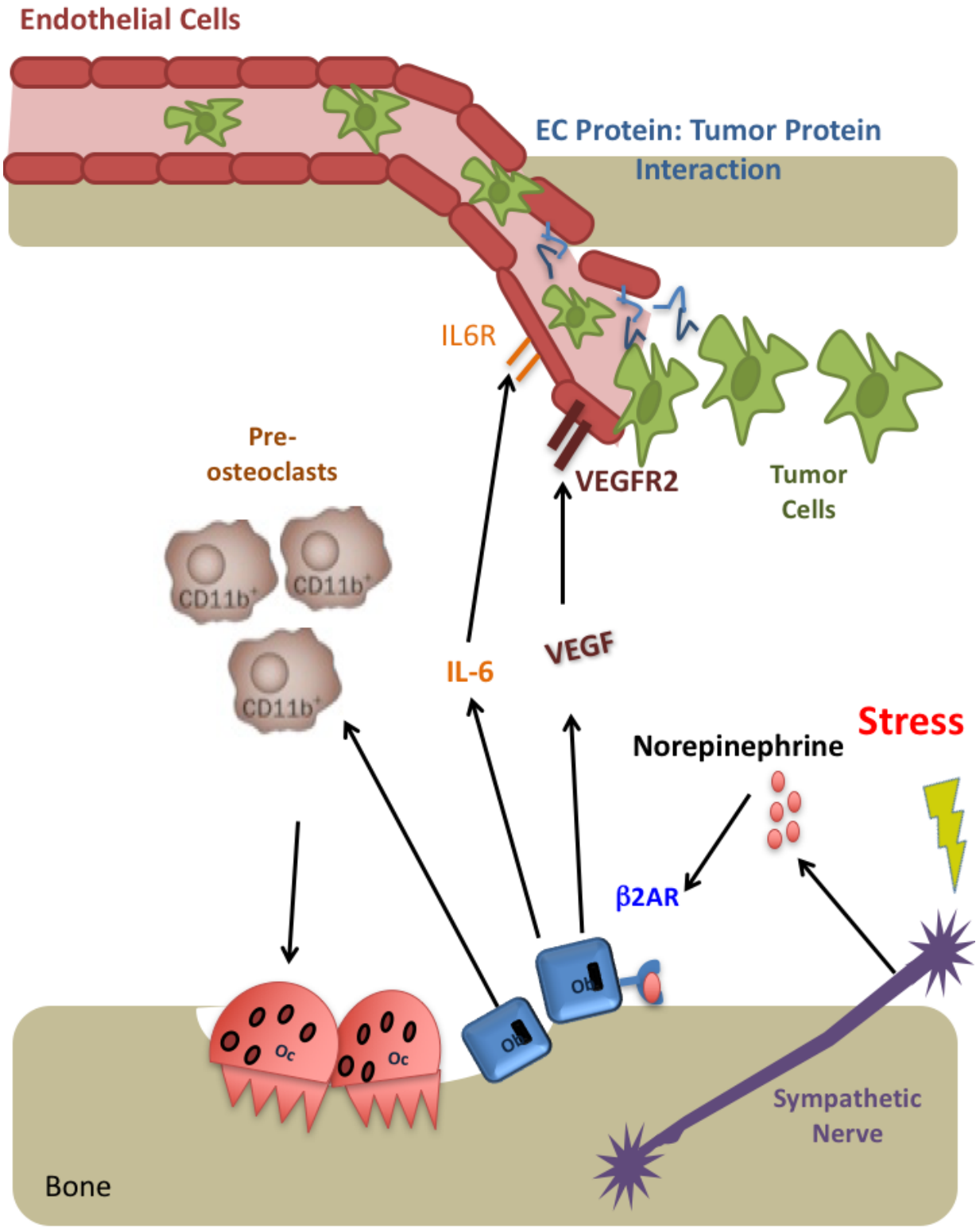

Figure 3. Graphical Abstract of the Influence of Stress on Bone Vasculature and Breast Cancer Bone Metastasis.

CHAPTER II

Skeletal Colonization by Breast Cancer Cells is Stimulated by an Osteoblast and β2AR-dependent Neo-angiogenic Switch

The data presented in this chapter are published in the *Journal of Bone & Mineral Research* under the same title. Some words and figures have been edited for this dissertation.

Introduction

According to the American Cancer Society, ~250,000 US women are diagnosed with breast cancer each year, and around 41,000 will ultimately succumb to the disease (100). Up to 75% of breast cancer patients with diffuse metastatic disease will develop a bone lesion (13). Bony metastases lead to hypercalcemia, intractable bone pain, bone destruction, and fracture. Although treatments are now available to limit bone destruction when skeletal metastases are detected, the clinical management of breast cancer patients remains palliative, and life expectancy is still limited (13). Uncovering the major determinants controlling the nesting of metastatic cancer cells within the skeleton, at early stage of the disease, is necessary to design new strategies to treat bone metastases and prevent the complications associated with these lesions.

Clues about the conditions driving the osteotropism of metastatic cancer cells can be obtained from retrospective studies, in which factors associated with reduced survival are identified. In that regard, chronic emotional stress has been linked to higher breast cancer recurrence, reduced survival, and poor prognosis, and β-blockers were associated with prolonged survival in breast cancer patients when treatment was initiated at time of diagnosis (48-51, 101-104). A common factor between these

studies is the activity of the sympathetic nervous system (SNS) that is stimulated by chronic psychosocial stress and whose action is antagonized by β-blockers.

The skeleton is richly vascularized, with arterial vessels dividing within the marrow into arterioles and capillaries that span throughout the bone marrow and supply sinusoids. An interesting observation is that this vascular network is closely associated with nerves, including sympathetic dopamine β-hydroxylase-positive fibers that have a circumferential perivascular distribution in bone but also branching varicosities in proximity with bone trabeculae (43). Although the influence of this neurovascular network on bone metastasis is unknown, previous studies provided evidence that sympathetic outflow increases cell proliferation as well as vascular endothelial growth factor (VEGF) levels and vascular density in primary tumors (63, 104). While these studies focused on the effect of sympathetic nerves in tumors, the same scrutiny has not been given to the different microenvironments to which breast cancer cells spread.

Severe emotional stress stimulates the Hypothalamic-Pituitary Axis (HPA) and sympathetic outflow, causing the release of peripheral catecholamines that stimulate post-synaptic β-adrenergic receptors (βARs) (105-107). Osteoblasts mainly express the β2AR and respond to βAR agonists by an increase in Receptor Activator of Nf-κB ligand (RANKL), a key cytokine involved in the maturation of osteoclasts and bone turnover (22). Our group and others have shown that high sympathetic outflow and HPA activation triggered by chronic immobilization stress promotes breast cancer homing to lungs and bone, implicating macrophages and RANK/RANKL signaling, respectively (51, 75). Daily administration with the non-selective β1/β2AR agonist, isoproterenol (ISO), triggered the same effects, validating this approach to mimic an increase in sympathetic nerve outflow without overt effect on the HPA axis. However, a retrospective study by Santini *et al*. showed that a large proportion of bone lesions in breast cancer patients contained RANK-negative cells, suggesting that additional mechanisms

might be at play for sympathetic nerves signals to influence the homing of metastatic cancer cells into the skeleton (30).

In this study, we show that βAR stimulation in mice promotes the expansion of the post-natal bone vascular network via an osteoblastic βAR- and VEGF-dependent mechanism, and that this stromal, neo-angiogenic switch contributes to the colonization of the bone marrow environment by breast cancer cells.

Materials & Methods

In Vivo Drug Treatments

The Institutional Animal Care and Use Committee at Vanderbilt University Medical Center approved all procedures. All mice used for *in vivo* studies were female. Mice were housed 2-5 per cage, and any mice on the Rag2-/- background were housed in sterile cages, also 2-5 per cage. The β-agonist Isoproterenol (ISO, Sigma #I6504-1G) was injected intraperitoneally each day for 6 weeks at a dose of 3mg/kg in 100 μL of sterile PBS. For the tumor and vessel characterization studies, 200 μg mcr84 (kindly shared by Dr. Brekken) or control IgG2 antibodies (generated by the Vanderbilt University Antibody and Protein Core) were injected intraperitoneally twice a week for 6 weeks. The mcr84antibody is a mouse chimeric IgG2, monoclonal antibody that targets VEGF-A specifically and prevents it from binding to VEGFR2 (80, 98, 108).

Generation of Rag2-/-; Adrβ2$^{flox/flox}$; Col1-Cre Mice

β2AR$_{ob}$KO mice (*Adrβ2*$^{flox/flox}$; *mouse 2.3kb Col1-cre* on the C57BL/6 background) were generated by crossing the mouse 2.3kb *α1(1)-collagen-cre* transgenic line with the *Adrβ2*$^{flox/flox}$ mutant mouse line expressing a floxed allele of *Adrβ2*, kindly shared by Dr. Karsenty. For tumor studies

utilizing human MDA-MB-231 cells, β2AR$_{ob}$KO mice were bred with immunodeficient *Rag2-/-* mice to allow human-derived tumor take in the resulting double KO mice (109, 110). *Rag2*-/-; *Adrβ2*$^{flox/flox}$; *2.3kbCol1-cre*-positive mice are herein called *Rag/β2AR$_{ob}$KO*, and control littermates (*Rag2*-/-; *Adrβ2*$^{flox/flox}$, *2.3kbCol1-cre*-negative mice) are herein called *Rag/WT*. These immune-compromised mice have experimental advantages and limitations. They allow the use of human cancer cells in a genetically modified murine host and to exclude the potential contribution of βAR-expressing immune cells when interpreting results, thus reducing complexity of the experimental system. However, the age of these mice and their immune-compromised status is not clinically relevant, hence the relevance of these findings will need to be further addressed in immune-competent models and in humans.

Intracardiac Injection of Cancer Cells

For all experiments requiring tumor cells, a bone metastatic clonal variant of the human triple negative breast cancer cell line MDA-MB-231 was used (111). This variant was established by serial *in vivo* passage of parental MDA-MB-231 cells (ATCC) that metastasized to bone following intracardiac injection. These osteotropic MDA-MB-231 cells were cultured in 10% DMEM (Gibco) containing 10% fetal bovine serum and 1% penicillin/streptomycin, trypsinized at 70% confluence, and re-suspended in cold PBS at 10^6 cells/ml. Six-week old, *Rag/WT* or *Rag/β2AR$_{ob}$KO* female mice were anesthetized with isoflurane and injected in the left cardiac ventricle with 100 μL of cell suspension (a total of 10^5 cells) as previously described (101).

Imaging Analysis

Bone metastases were assessed via a Faxitron digital x-ray imaging system. Osteolytic lesions were quantified in the hind limbs and the forelimbs at end point (28 days) from Faxitron images by ROI

analysis using MetaMorph software (Molecular Devices, Inc.). Measurements were performed blinded from treatment/genotype and by three persons. Presence of bone tumors was confirmed by histology. Lesion number was calculated as total number of hind limb and forelimb osteotropic lesions per mouse. Lesion area was analyzed from the hind limb and forelimb lesions present by x-ray and calculated by pixel area using the MetaMorph Software.

Microcomputed Tomography (μCT) Analysis

Hind limbs from each mouse were dissected, cleaned, and fixed for 48 h in 10% formalin/PBS and move to 70% EtOH. Femurs were then loaded into 12.3-mm-diameter scanning tubes for imaging (μCT 40; Scanco Medical, Bassersdorf, Switzerland). Tubes were able to house one to four femurs. The scans were converted to three-dimensional (3-D) voxel images for analysis. A Gaussian filter (sigma=0.8, support=1) was used to reduce signal noise, and a threshold of 300 was applied to all analyzed scans. Scans were done at 12 μm resolution (E=55 kVp, I=145 μA). Two hundred transverse slices of the distal femur were taken from the growth plate and extended away from the distal growth plate. All femoral measurements were made by manual determination of appropriate slices and automated contouring, using voxel counting and sphere-filling distance transformation indices.

Histomorphometry

For histological analyses, hind limbs were dissected and immediately placed into neutral buffered formalin for 48 hours at 4°C on a plate shaker. The bones were then transferred to 20% EDTA for 5 days at 4°C for decalcification. Following this step, the bones were processed for paraffin sectioning according to standard protocols. Samples were mounted in wax blocks and sectioned at 6 μm. Sections were stained for Vegf- a, Endomucin, or CD31 according to the manufacturers' instructions (Primary- Abcam #46154 (5μg/mL), Santa Cruz sc-65495 (1:100) or Abcam #56299 (1:100);

Secondary- Santa Cruz sc-2005 (1:500)). A 20 μg/mL proteinase K solution (Roche #03115828001) was applied for 20 minutes to sections for antigen retrieval. Signal was detected by immunohistochemistry using the NOVA Red Kit (Vector Laboratories, #SK-4800) or immunofluorescence (Primary- Santa Cruz sc-65495 (1:100); Secondary- Thermo Fisher Alex Fluor 647 A-21247 (1:500) (112).

Osteoclast and osteoblast number and size were assessed using the Osteomeasure imaging software (OsteoMetrics, Decatur, GA). Hind limb sections were analyzed for osteoclasts by counting tartrate resistant acid phosphatase (TRAP)-positive cells with 3 or more nuclei along the bone surface. Sections were counterstained with hematoxylin. Osteoblasts were counted based on morphology, contact with bone tissue, and a series of at least 3 similar cells. Immunohistochemistry images were captured using an Olympus BX41 Microscope, and immunofluorescence results were analyzed using a laser-scanning microscope (510/Meta/FCS Carl Zeiss, Inc.) with 10x and 20x objectives using 0.7x zoom.

Mouse Metatarsal Assay

Two day-old C57BL/6 pups were sacrificed, and their hind limb metatarsals were dissected as previously described (113). Metatarsals were cultured in α-MEM medium (Gibco) containing 10% fetal bovine serum (hereby 10% α-MEM) and 1% penicillin/streptomycin in a 24-well plate for 14 days. For conditioned media (CM), MC3T3 mouse osteoblasts were cultured in 10% α-MEM and passaged in a 1:3 ratio. Once cells became 70% confluent, cells were treated with PBS or drug overnight (18 hours) in 10% α-MEM. The following morning, CM was collected. After 3 days in 10% α-MEM, metatarsals were treated with one of the following: unconditioned 10% α-MEM or the CM of PBS, 10 μM norepinephrine (NE), or 10 μM isoproterenol (ISO)-treated osteoblasts. After 4 CM treatments over the 2-week experimental time course, metatarsals were fixed with 10% Zinc formalin and stained for CD31 (Primary- BD Pharmingen #553370 (1:100), Secondary- Santa Cruz sc-2005 (1:500)). The number of

vessels sprouting from the bones was calculated. Measurements were performed blinded from treatment by three persons.

Primary Mouse Bone Marrow Stromal Cell (BMSCs) and Mouse Bone Marrow Endothelial Cell (BMECs) Cultures

Hind limbs from WT C57BL/6 mice were used to prepare primary mouse bone marrow stromal cells (BMSCs). Femur and tibia were stripped of skin and muscles, distal and proximal epiphyses were cut off, and each bone was inserted into a punctured 0.5mL tube placed into a 1.5mL tube containing 1mL of 10% α-MEM. Tubes were centrifuged for 2 mins at 13.2x1000 rpm at 4°C. Resulting pellets were resuspended in 10% α-MEM, and cells were plated. Cultures were grown in 10% α-MEM for 4 days, and then switched to an osteogenic medium (10% α-MEM containing 50ug/mL ascorbic acid (Sigma, #A-5950) and 5 mM beta-glycerophosphate (Sigma, #G9891-25G)) for 8-14 days.

Primary mouse bone marrow endothelial cells (BMEC) were harvested as previously described (114). Mouse hind limb bone marrow was flushed and centrifuged in Complete Endothelial Cell Growth Media (ScienCell #1001). Cells were plated on tissue culture dishes or in tissue culture flasks coated with 4 μg/mL fibronectin (Gibco #33016015) in Complete Endothelial Cell Growth Media. After 7 days, cells were used for experiments.

Tube Formation Assay

Twenty-four well plates were coated with 200 μL of growth factor reduced matrigel (Corning #354230) for 45 mins at 37°C before 30,000 HUVECs (Gibco #C0035C), or BMECs from wild-type C57BL/6 mice were plated and cultured in 500 μL of Basal Endothelial Cell Growth Media (ScienCell #1001). Cells were then treated with human (10ng/mL) or mouse (50ng/mL) rVEGF (R&D Biosystems #293-VE, #493-MV), PBS, or 10 μM ISO. For conditioned media treatments, mouse MC3T3 osteoblasts

were treated with PBS or 10 μM ISO for 24 hours in 10% FBS αMEM. Media was collected, and a total 500 μLs of media were added in the wells. For blocking experiments, mcr84 or a control IgG antibody was added at 100 μg/mL to conditioned media. The experiments were run at 37°C for 12hrs, and pictures were taken under 4x and 10x objectives on an Olympus CKX41 Microscope. Total tube length was analyzed using MetaMorph software. Measurements were performed blinded from treatment/genotype by three persons.

Mouse Vegf-a ELISA

An ELISA for mouse Vegf-a was run per manufacturer's instructions (R&D Systems, #MMV00). Media used for this assay was collected from primary BMSCs after 24 hours of either PBS or 10 μM ISO treatment.

Quantitative PCR

Mouse tissues were snap frozen in liquid nitrogen immediately following mouse sacrifice and stored at -80°C. Tissue samples were pulverized with liquid nitrogen-cold mortar and pestle into powder. RNA extraction for both tissues and cells was performed using TRIzol (Life Technologies #15596018). cDNA for qRT-PCR experiments was synthesized using the High Capacity cDNA Reverse Transcription Kit from ABI Applied Biosystems (#1502205). Taqman probes were used to amplify the following genes: Murine *Vegf-a* (Mm00437304), Murine *Hprt* (Mm01545399), Murine *18s (*4333760T), Human *VEGFA* (Hs00900055), and Human *HPRT* (Hs02800695). Expression was analyzed by the ΔΔCt method.

Statistics

All data are presented as means ± the standard error mean (SEM). For experiments comparing two groups, a standard two-tailed student's *t* test was used unless otherwise stated in the figure legend. For experiments comparing more than 2 groups, one-way ANOVA was used with a Newman-Keuls post-hoc test unless specifically stated in the figure legend. For all tests, a *p value* less than or equal to .05 was considered significant.

Results

βAR Stimulation Increases Blood Vessel Formation in Post-natal Mouse Bones.

During our previous studies, we noticed the presence of a high number of vascular structures in hind limb sections of mice subjected to daily βAR stimulation by ISO, in which erythrocytes were stained bright red by H&E (51). Because such treatment and chronic stress have been linked to vascular changes in normal physiology and cancer (115-117), we asked whether an increase in sympathetic outflow, typically caused by chronic stress, could alter the vasculature of the adult skeleton and contribute to the efficiency of cancer cells colonization into the skeleton.

To address this question, we reanalyzed the hind limbs of 6 week-old nude mice subjected to a chronic immobilization stress (CIS) protocol (51, 102) that was aimed at stimulating an endogenous stress response. We also analyzed the hind limbs of 6 week-old nude mice treated for 6 weeks daily with the non-selective β1/β2AR agonist isoproterenol (ISO, 3mg/kg ip), used to mimic an increase in sympathetic outflow without stimulating the HPA axis or raising glucocorticoids levels. At endpoint in both models, we measured a 25 to 50% higher vessel area and vessel number per bone marrow area in the treated groups (ISO or CIS) compared to the control groups (**Figure 4A, B**). We then used an *ex vivo* tube formation assay to further define the angiogenic properties associated with ISO treatment and

relevant mode of action. In this experiment, HUVECs as well as CD31-positive, tube-forming primary mouse bone marrow endothelial cells (BMECs) prepared from WT mice were seeded on growth factor-reduced matrigel in 0% serum endothelial cell growth medium, and treated with PBS or ISO (10μM) (114). Direct treatment of these endothelial cell cultures with ISO did not significantly increase tube length, suggesting that ISO acts indirectly to stimulate bone vessel formation *in vivo* (**Figure 5A-C**). Therefore, to address the contribution of a putative bone-derived factor to the increase in bone vascular density in response to βAR stimulation, the 24hr-conditioned medium (CM) from PBS or ISO-treated mouse MC3T3 osteoblasts was compared in two independent angiogenesis assays. We first treated HUVEC and BMEC cultures with the CM from PBS or ISO-treated mouse MC3T3 osteoblasts. In both endothelial cell cultures, the CM from ISO-treated osteoblasts increased tube length compared to PBS control (**Figure 4C, D**), suggesting that osteoblasts secrete pro-angiogenic factor(s) in response to βAR stimulation. We also cultured metatarsal bone explants from 2 day-old mouse pups in the CM from MC3T3 cultures treated by PBS, ISO (10μM), or the natural βAR ligand norepinephrine (NE, 10 μM) (**Figure 4E**). Following 2 weeks, outgrowing blood vessels were labeled by CD31 staining, and vessel sprouting was quantified. We observed that the CM from both NE and ISO-treated osteoblasts caused a significant 80% increase in the number of sprouting parental vessels compared to PBS controls, to a level equal or higher to the one induced by recombinant VEGF, a major angiogenic factor used here as positive control (**Figure 4E, F**).

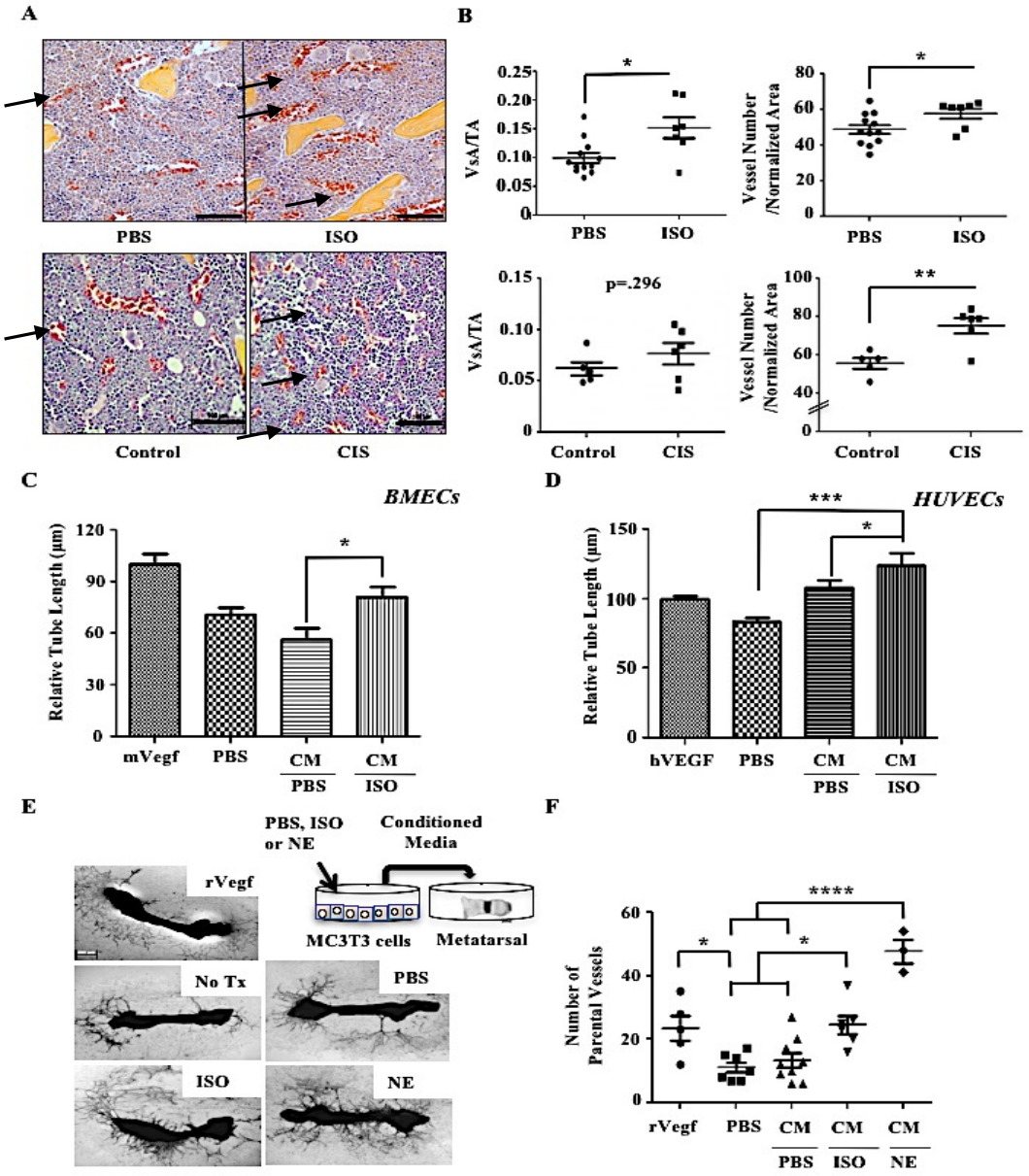

Figure 4. Isoproterenol Treatment Increases Skeletal Blood Vessel Area and Number *In Vivo* via Bone-derived Factors: A) Representative 40x H&E images of hind limb bone sections from athymic nude mice treated with PBS, 3mg/kg Isoproterenol (ISO), or Chronic Immobilization Stress (CIS). Arrows indicate blood vessels (red). Bar=100µm B) Quantification of vessel area (VsA) and vessel number normalized by tissue area (TA) in mice that received PBS (N=12) or ISO (N=7) (p=.009 and p=.037), as well as PBS (N=5) or CIS (N=6) (p=.296 and p=.004). C) Quantification of primary mouse BMEC tube length (P<.001) (*=<.05, N=3). D) Quantification of HUVECs tube length (P<.001) (*=<.05, ***=<.001, N=6). E) A schematic of the metatarsal assay and representative 4x Images of metatarsals according to each treatment. After 2 weeks of culture, mouse explants were stained for the endothelial cell marker CD31. F) Quantification of the number of CD31+ parental vessels sprouting from the metatarsal bones (P<.001) (*=<.05, ****=<.0001 N≥3).

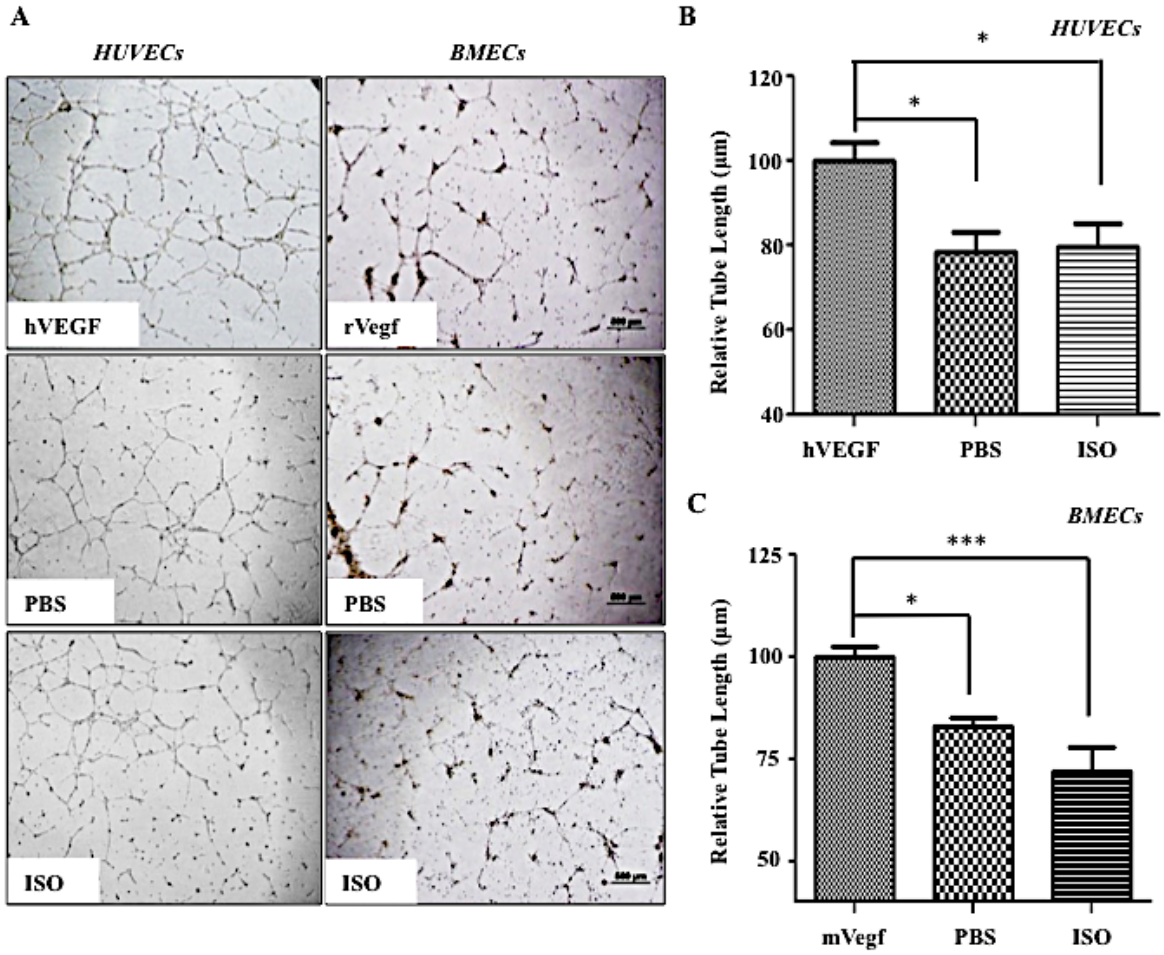

Figure 5. Direct Isoproterenol Treatment of Endothelial Cells Does Not Induce Tube Formation: A) 4x Images of both HUVECs and BMECs treated with PBS or ISO (10µM). VEGF treatment (positive control: 10ng/mL hVEGF, 50ng/mL mVegfa) increases tube length as compared to PBS or ISO. B) & C) Quantification of tube length for HUVECs (B) and mouse BMECs (C), respectively, following treatment (*=<.05, ***=<.001, N=3 for both data).

βAR Stimulation in Osteoblasts Increases *Vegf-a* Expression and Bone Angiogenesis.

VEGF-A is a well-known pro-angiogenic growth factor. Consistent with the observed increase in blood vessel formation in ISO and CIS-treated mice, its expression level in long bones from mice treated with ISO was 50% higher than in bones from PBS control mice (**Figure 6A**). Multiple cell types within the bone microenvironment, including osteoblasts, express the β2AR and could be the source of the increased *Vegf-a* levels measured in bone following ISO treatment (44). To determine if the osteoblast lineage was one of the principal sources of bone *Vegf-a* secreted in response to βAR agonists, a series of *in vitro* and *in vivo* experiments were performed. First, MC3T3 osteoblast cultures, which represent a pure culture of osteoblastic cells, as well as adherent primary mouse bone marrow stromal cells (BMSCs), were treated with PBS or ISO (10μM). After 2hrs of ISO treatment, *Vegf-a* expression increased 10-fold in MC3T3 cells, and returned to normal levels within 24 hours (**Figure 6B**). Similar results were observed with BMSCs treated with ISO, although the response was of lesser intensity, which most likely reflects the more heterogeneous nature of this type of culture (**Figure 6C**). *Vegf-a* expression was not increased in ISO-treated BMSCs prepared from β2AR-deficient mice, indicating that in osteoblasts, the β2AR specifically controls *Vegf-a* expression (**Figure 6D**). The increase in *Vegf-a* mRNA expression in BMSCs was associated with a 3-fold increase in VEGF protein expression, measured by ELISA (**Figure 6E**). Expression of additional angiogenic genes, including other *Vegf* isoforms, *Vegfr2, Ang-2, Fgf2,* and *Pdgfa* in BMSCs was not affected by ISO treatment (**Figure 7A-H**).

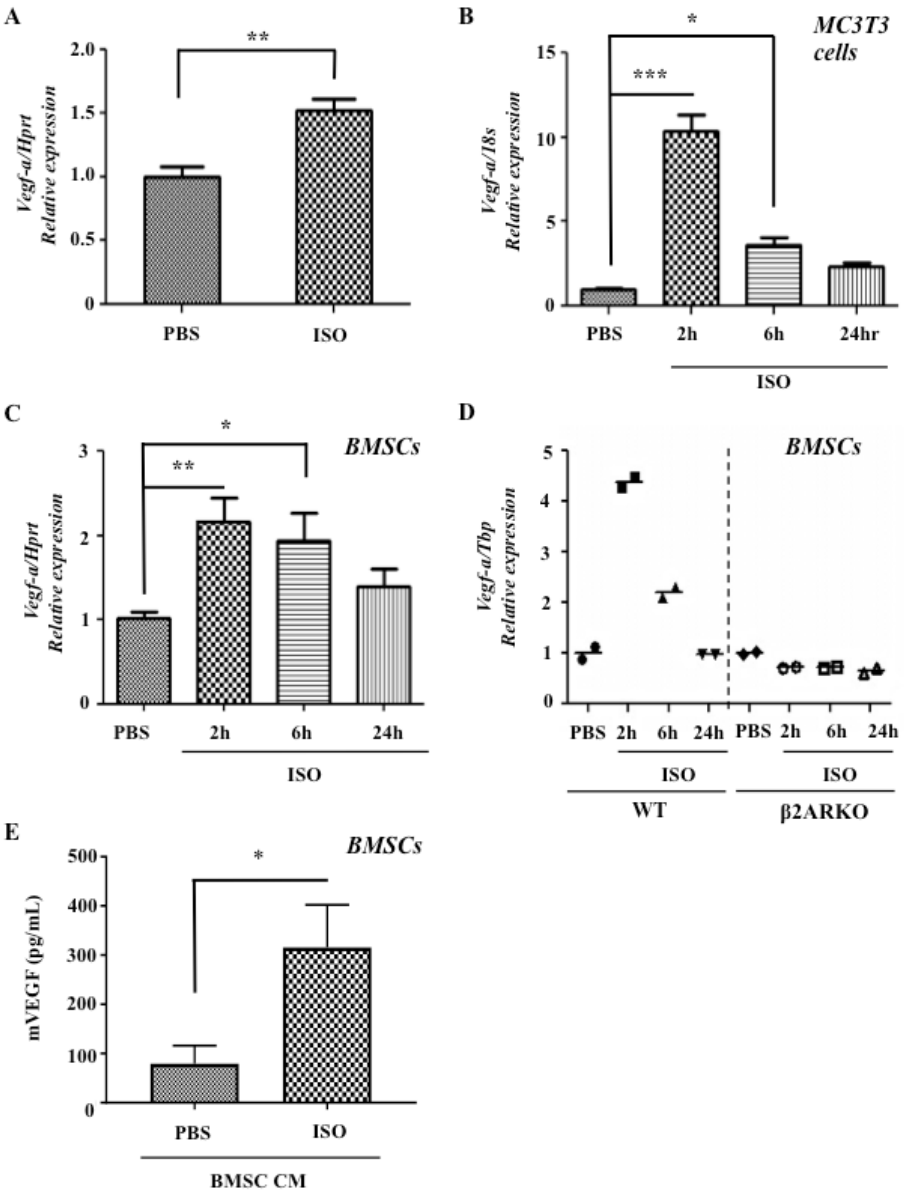

Figure 6. ISO Increases Vegf-a Bone Levels both *In Vivo* and *In Vitro*: A) ISO (2 hrs, 3mg/kg, IP) increases *Vegf-a* expression significantly in whole mouse bone, P=.0064 (qPCR, N=3 for ISO, N=5 for PBS). B) ISO increases expression of *Vegf-a* in MC3T3 mouse osteoblasts, P<.001 (qPCR, N=3). C) ISO increases expression of *Vegf-a* in primary mouse BMSCs, P=.012 (qPCR, N=6). D) *Vegf-a* expression does not increase upon ISO treatment in β2ARKO BMSCs (qPCR, N=2). E) ISO-treated CM from BMSC contains higher amounts of mVegf (N=5, p=.0159 via Mann Whitney U Test, *P=<.05, **P=<.01, ***P=<.001).

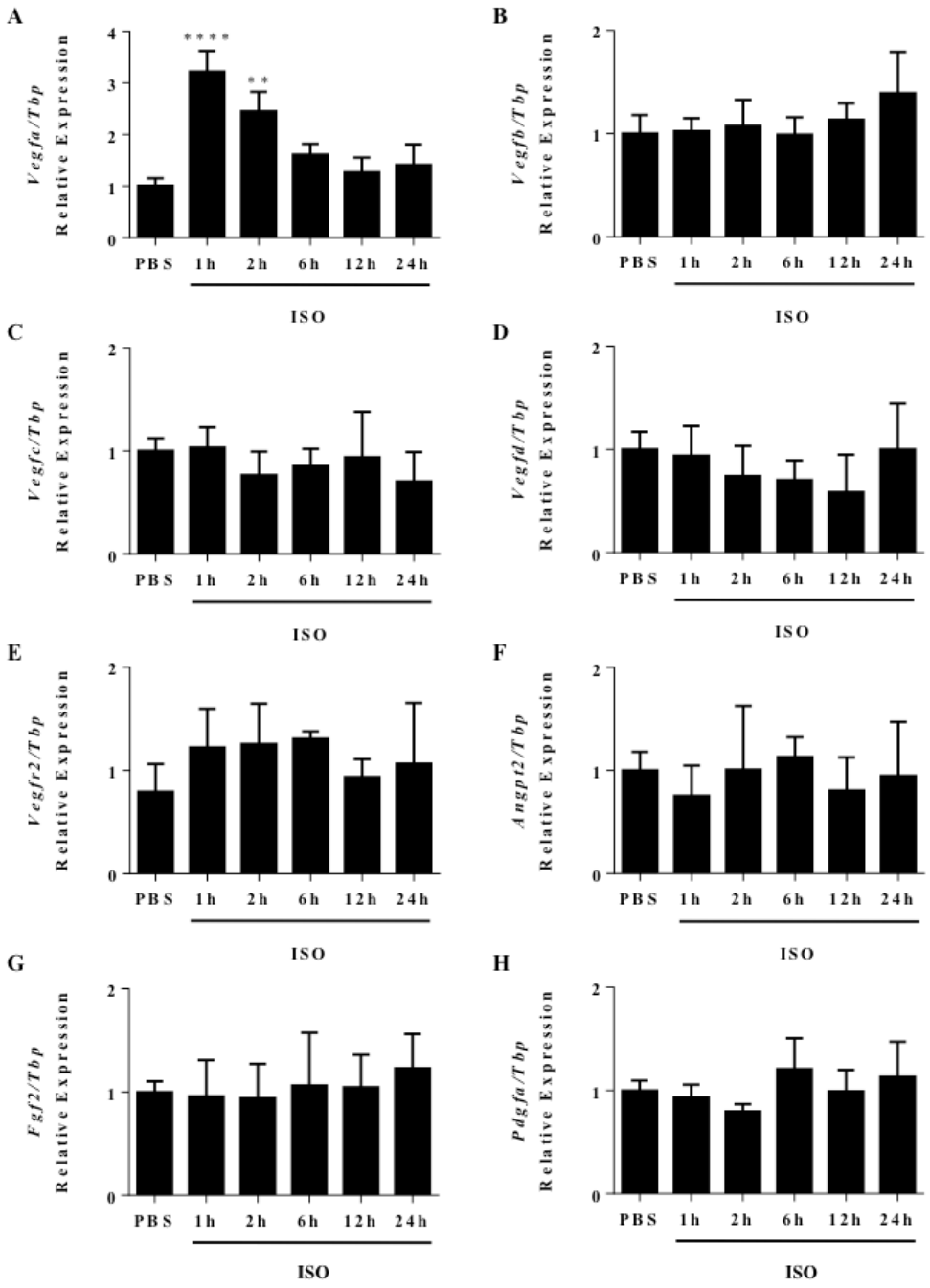

Figure 7. Isoproterenol Treatment Increases *Vegf-a* Expression but Not Other Angiogenic Genes: A) ISO increases expression of *Vegf-a* in primary mouse BMSCs. B-H) ISO treatment does not increase *Vegf-b*, *Vegf-c*, *Vegf-d*, *Vegfr2*, *Angpt2*, *Fgf2,* or *Pdgfa* (qPCR, N=4, Kruskal-Wallis test, **=<.01, ****=<.001).

To determine whether osteoblasts are the source of the increased *Vegf-a* expression in response to ISO treatment *in vivo* and whether the β2AR mediates this effect, ISO (3mg/kg) or PBS (control) were administered to mice lacking the β2AR in type I collagen-expressing osteoblasts (*Adrβ2*$^{flox/flox}$; *mouse 2.3kb Col1-cre*, called herein β2AR$_{ob}$KO) or WT mice (*Adrβ2*$^{flox/flox}$, called herein WT) for 6 weeks. At endpoint, femoral vessel density was quantified by measuring the number of endomucin-positive vessels. β2AR$_{ob}$KO mice showed a blunted response to ISO treatment compared to WT mice, as measured by a significant reduction in the number of endomucin-positive vessels compared to ISO-treated WT mice (**Figure 8A-C)**, and this phenotype was accompanied by a reduction in the number of Vegf-positive osteoblasts (**Figure 9A, B**). Similar results were obtained with mice globally deficient for the β2AR (**Figure 10)**.

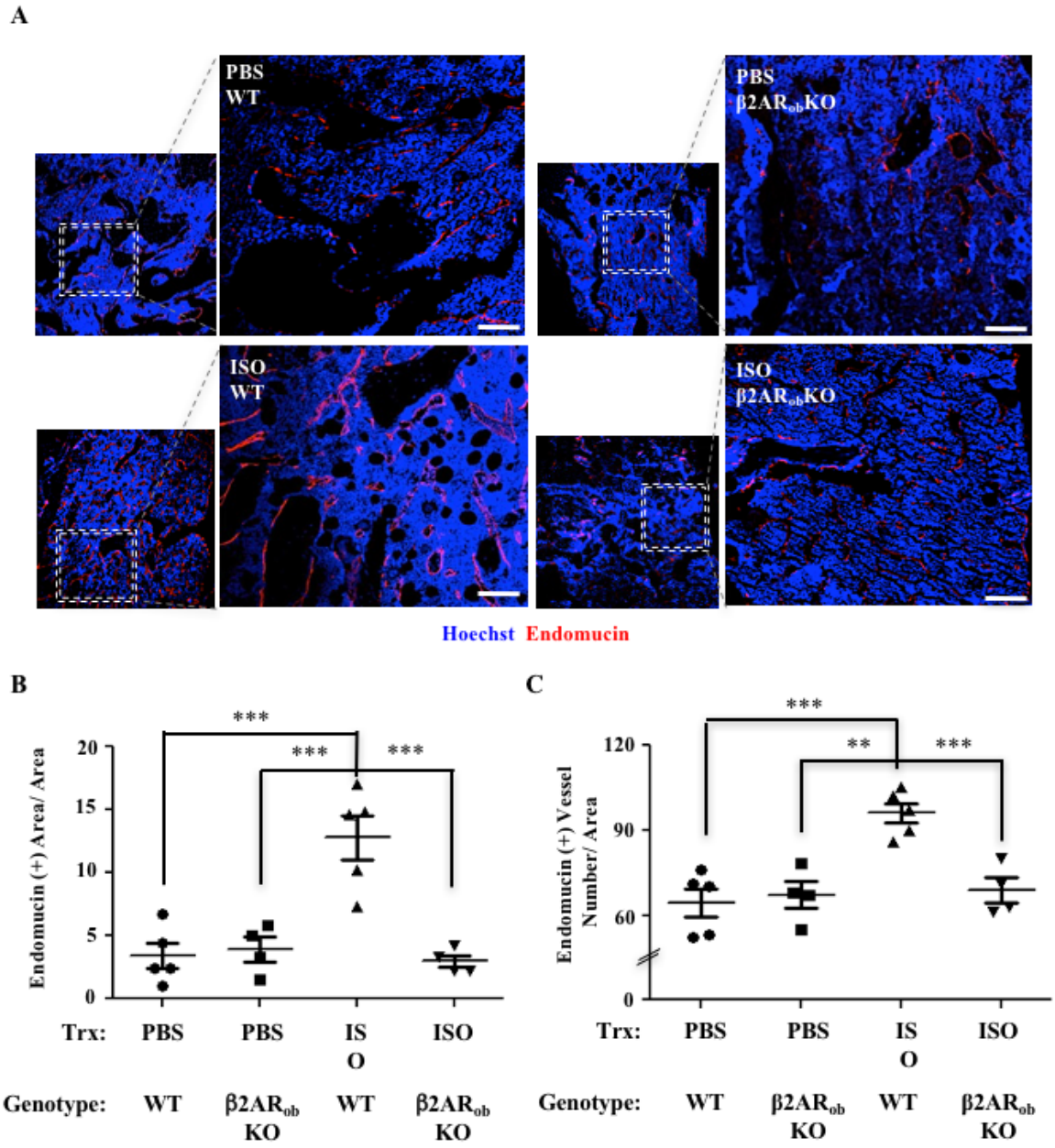

Figure 8. Genetic Loss of β2AR in Osteoblasts Prevents ISO-induced Vascular Increase *In Vivo*: A) Representative 10x and 20x confocal images of hind limb bone sections from WT and β2AR$_{ob}$KO mice treated with PBS or ISO for 6 weeks. Bar: 100µm. Hoechst= Blue, Endomucin= Red. B) Quantification of Endomucin (+) Area/ Total Area in WT and β2AR$_{ob}$KO mice receiving PBS or ISO (P<.001) (N=4-5). C) Quantification of the number of Endomucin (+) Vessels/ Area (N=4-5) (P<.001) (*=<.05, **=<.01 ***=<.001).

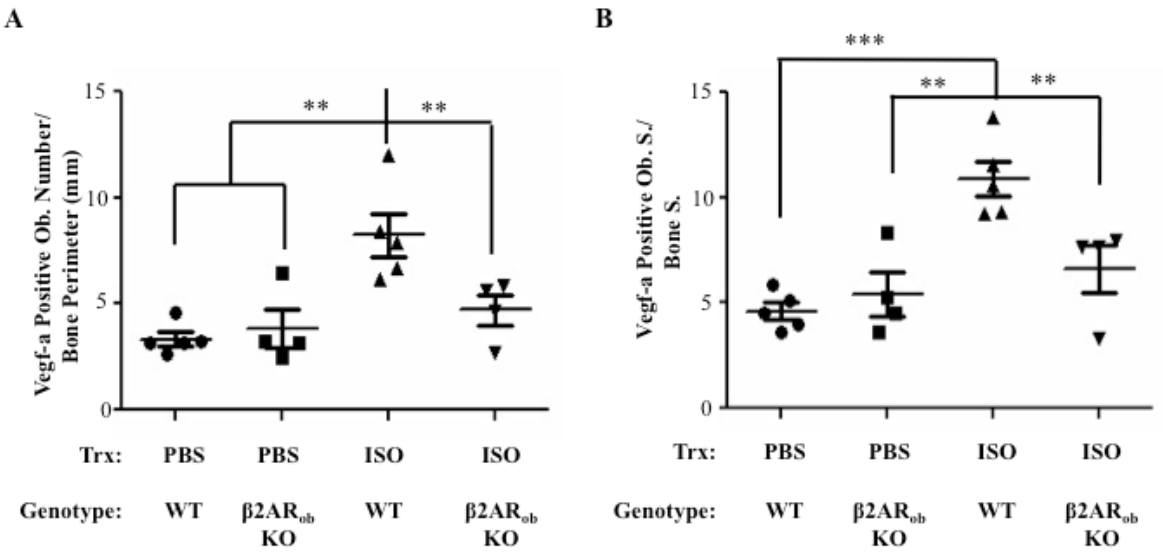

Figure 9. ISO Treatment Does Not Increase Vegf-a Positive Osteoblasts in Hind Limbs of β2ARobKO Mice: A) Vegf-a positive osteoblasts were counted using 40x images of hind limbs. Cells were designated osteoblasts based on cell shape, contact with secondary spongiosa, and a series of at least 3 similar cells. (P=.0018, **=<.01, N=4-5 mice per group) B) Vegf-a positive osteoblasts surface over bone surface as a representation of osteoblast size was measured using Osteomeasure software. (P=.0004, **=<.01,***= <.001, N=4-5 mice per group)

Osteoblast-derived VEGF-A Promotes Bone Angiogenesis in Response to β2AR Stimulation.

To confirm that the pro-angiogenic effect induced by β2AR stimulation in osteoblasts was mediated by VEGF-A, we used an antibody (mcr84) that specifically perturbs VEGF-A:VEGFR2 signaling in a tube formation assay with BMECs (118, 119). Upon addition of mcr84 (100μg/mL), the pro-angiogenic effect of the CM from ISO-treated BMSC cultures was significantly attenuated compared to addition of a non-immune IgG. Total tube area and tube length were reduced, and the complexity of the vascular network (average branching points) was lost upon treatment with mcr84 in the presence of CM from ISO-treated osteoblasts (**Figure 11A-D**).

The VEGF-A:VEGFR2 blocking properties of mcr84 were then tested *in vivo* to determine if the observed increase in bone blood vessel formation upon β2AR stimulation was mediated by an increase in *Vegf-a* expression. For that purpose, WT C57BL/6 female mice were injected for 6 weeks with either PBS or 3mg/kg ISO daily, along with mcr84 (200 μgs/ inj.) or a control IgG antibody twice per week (98). Quantitative analysis of femoral bone sections via immunofluorescence confirmed a 70% increase in endomucin-positive vessel area in the ISO group versus PBS group, and a significant reduction in endomucin-positive vessel area and number in the ISO, mcr84 group compared to the ISO, IgG group (**Figure 12A-C**). ISO increased osteoclast number per bone perimeter, as expected from our previous studies, but this osteoclastogenic effect was not affected by mcr84 treatment, suggesting that VEGF-A is not involved in the osteoclastogenic effect of ISO (**Figure 13).**

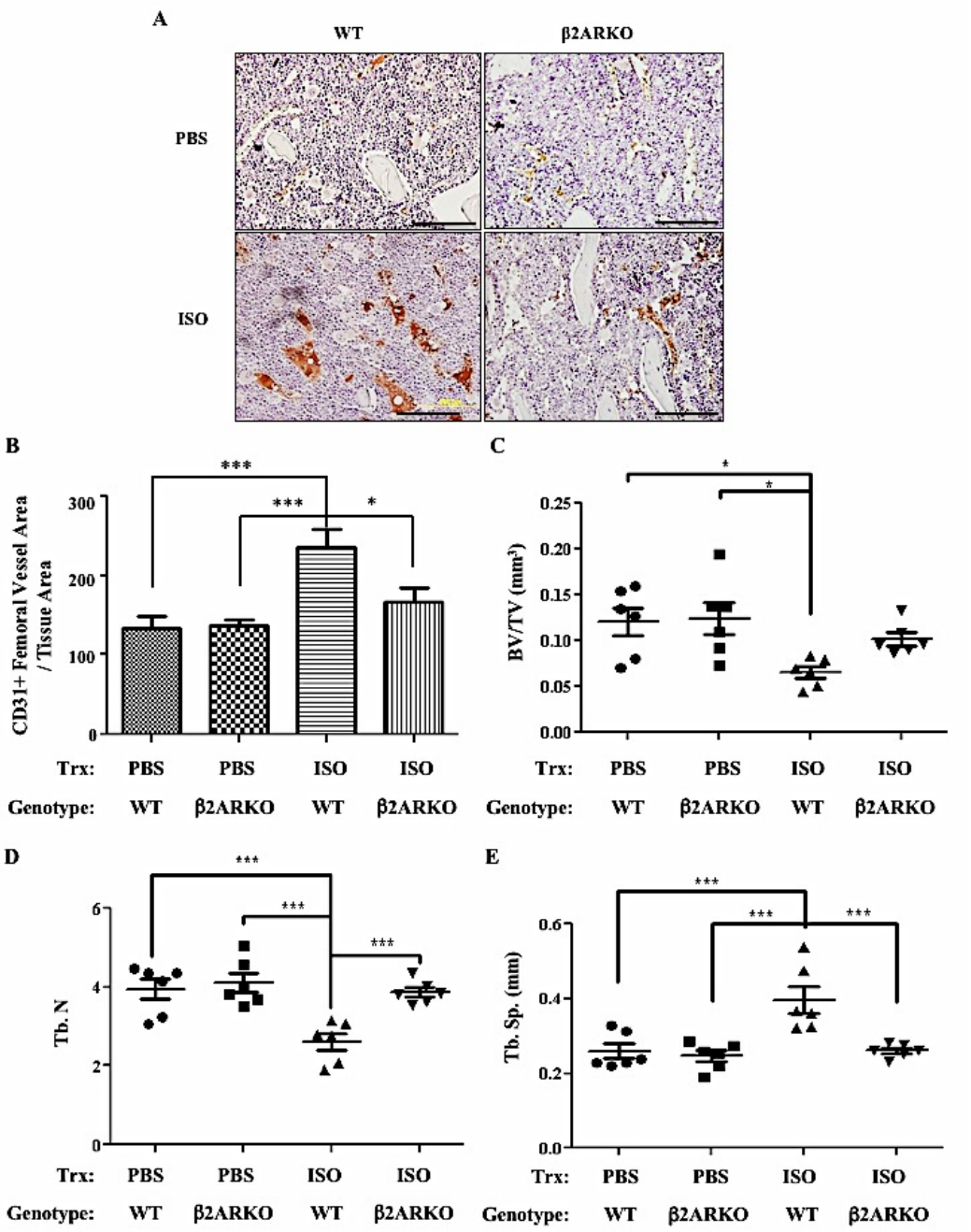

Figure 10. Global Loss of β2AR in Mice Receiving ISO Nullifies the Increase in Bone Vascular Density and Blunts ISO-induced Changes in Bone Turnover: A) Representative 20x Images of femurs for each group. Red indicates CD31+ cells. Bar =100μm B) Quantification of CD31 positive vessel area/tissue area in the femurs of WT and β2KO mice (N=6-7 mice/group, P=.0003, *=<.05, ***=<.001, N=6-7). C) BV/TV, D) Trabecular Number, and E) Trabecular Spacing of tibiae all reveal that ISO is ineffective in stimulating bone turnover in β2ARKO mice. (N=6 mice/group, P=.0127, <.001, and <.001 for C, D, and E respectively).

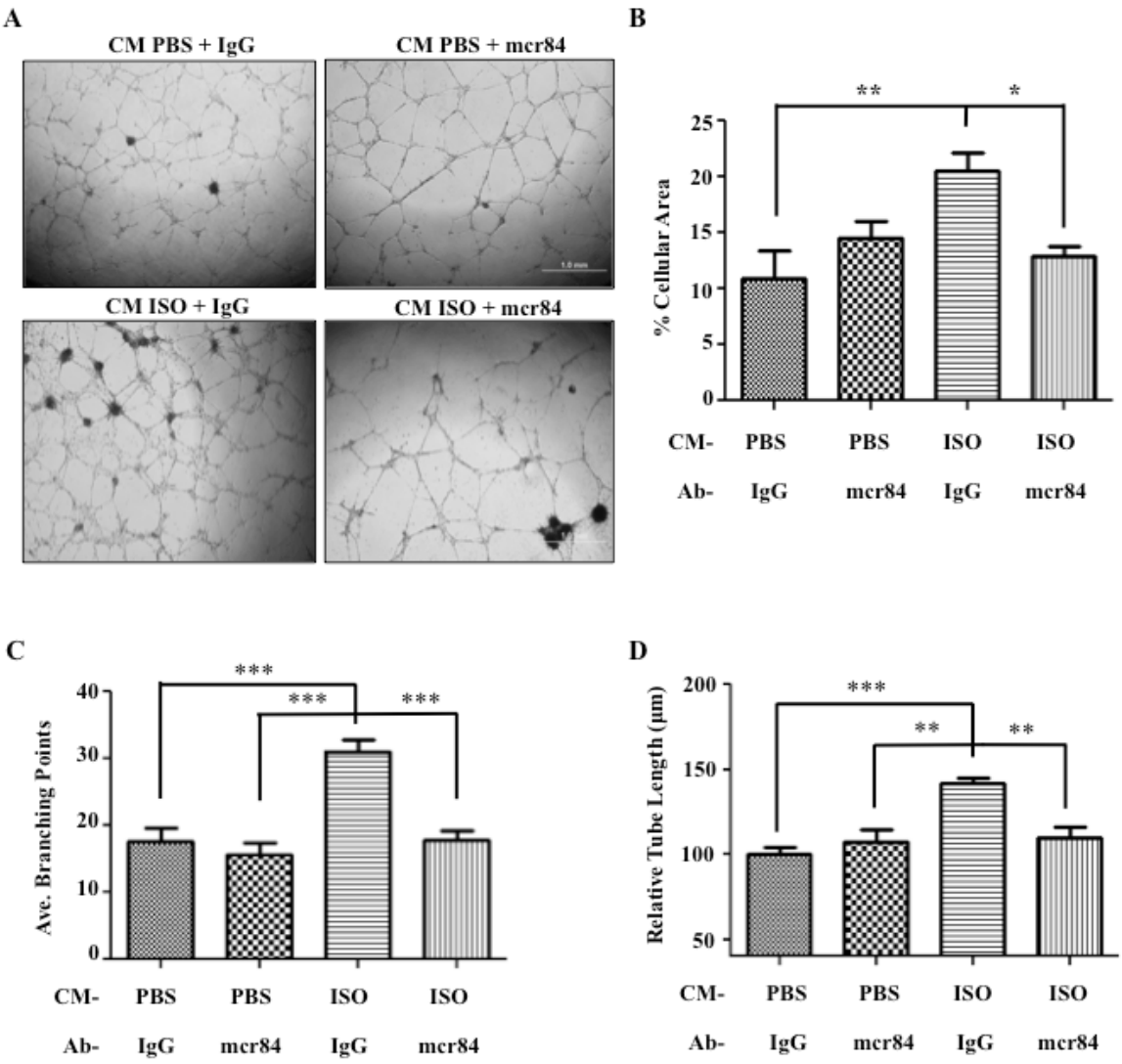

Figure 11. Blocking Vegf-a:Vegfr2 Signaling Diminishes the Effects of Conditioned Media from ISO-treated BMSCs on Primary Endothelial Tube Formation *in vitro:* A) 4x phase contrast images of mouse BMECs differentiated on Matrigel and receiving the conditioned media from BMSCs treated with either PBS or ISO, and with either mcr84 (100ugs/mL) or IgG2a control antibody for 12 hrs. B) Quantification of the percentage of GFP-positive cellular area used as an assessment of tube formation after 12 hours. (P=.003) C) Tube length was also used to assess tube formation. (P<.001) D) Average Branching Points were assessed via bright field images (P<.001) (*=<*.05,* **=<*.01,* ***=<*.001,* N=6 for each analysis).

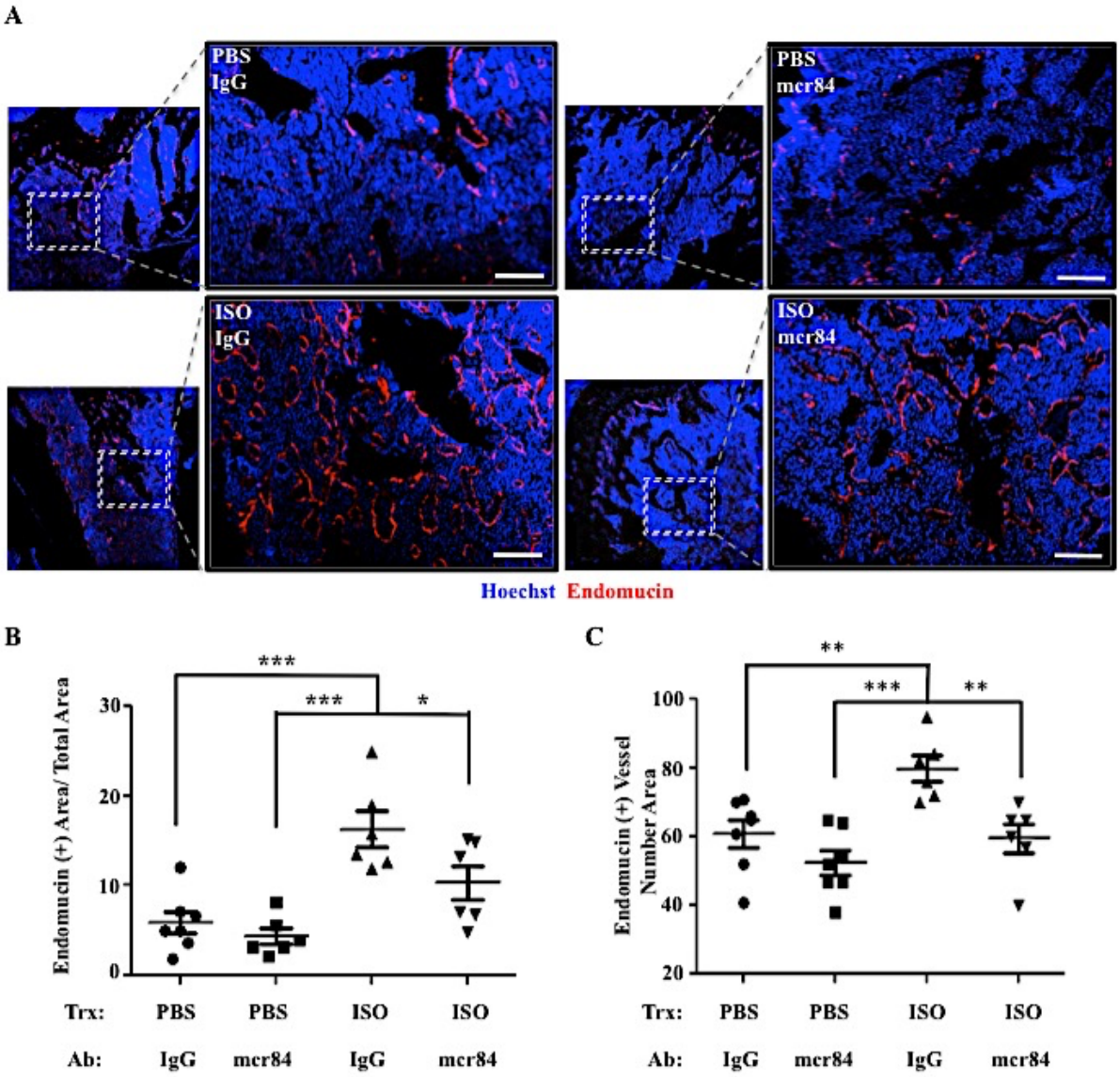

Figure 12. Blocking the Interaction Between Vegfa and Vegfr2 Diminishes the Increase in Bone Vascular Density Caused by ISO Administration: A) Representative 10x and 20x confocal images of hind limb paraffin sections from mice treated with either PBS or ISO, and with either mcr84 or IgG2a control antibody for 6 wks. Hoechst= Blue, Endomucin= Red. Bar: 100μm. B) Quantification of the Endomucin-positive Area/ Total Area. C) Quantification of the number of Endomucin (+) Vessels/ Area (*=<.05, **=<.01, ***=<.001, N=6-7).

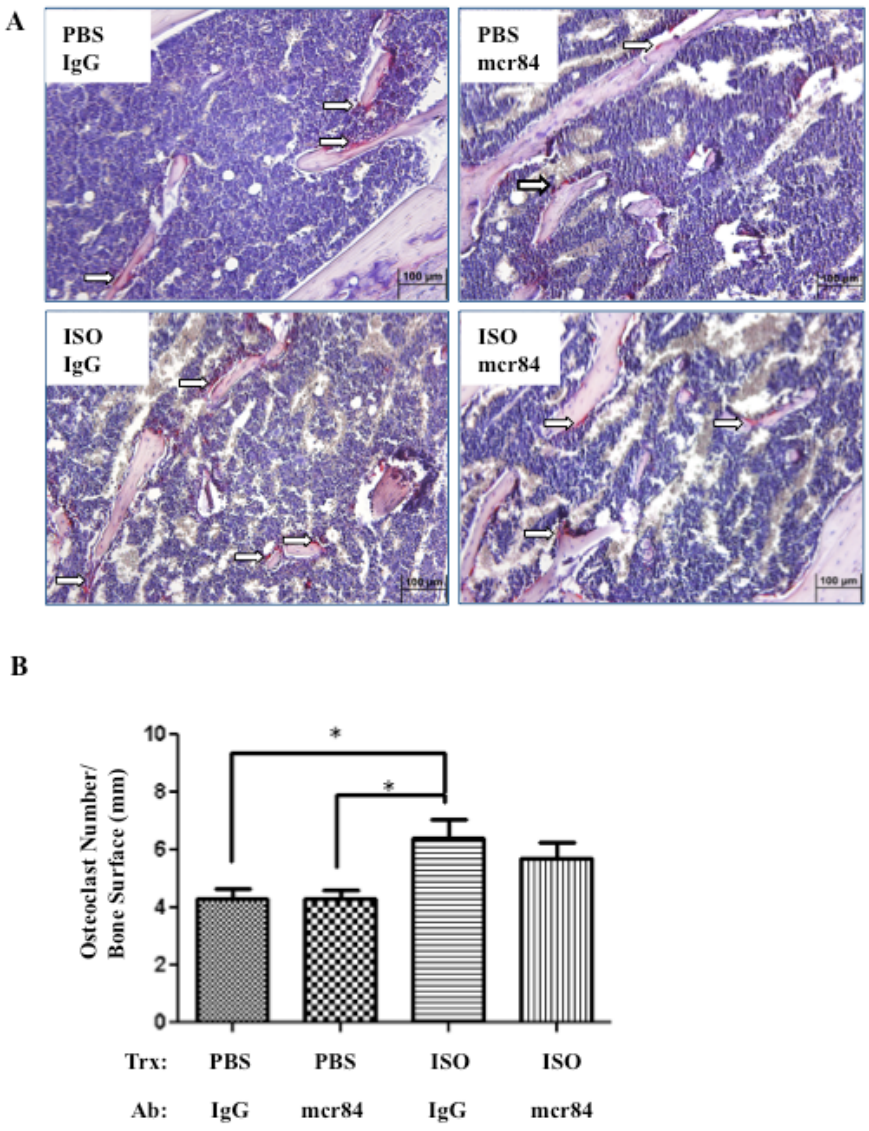

Figure 13. Mcr84 Does Not Alter Osteoclast Number in Mouse Hind Limbs: A) Representative 20x images. TRAP+ osteoclasts are stained red and have ≥3 nuclei. Arrows indicate osteoclasts. B) Osteoclast number per bone surface in mouse hind limbs after 6 weeks of listed treatments. (*=<.05, N=5-7)

The Increase in Bone Vascular Density Caused by Osteoblastic βAR Stimulation Promotes the Colonization of Breast Cancer Cells in Bone.

Since blood vessels act as conduits through which disseminating tumor cells travel to distant organs, we posited that the stimulatory effects of ISO on osteoblasts, VEGF-A expression, and bone vascular density could contribute to the successful establishment of circulating metastatic cells into the skeleton. This question was addressed experimentally by measuring the bone homing efficiency of bone metastatic triple negative MDA-MB-231 breast cancer cells in response to ISO treatment, in absence of either the β2AR in osteoblasts or VEGF-A: VEGFR2 interaction.

Four week-old female Rag/β2AR$_{ob}$KO or control littermates, Rag/WT, were given PBS or ISO (3mg/kg) ip injections for 3 weeks, a dosing and time frame verified to allow a significant increase in long bone blood vessel density (**Figure 14**). The day following the last injection, 10^5 osteotropic MDA-MB-231 breast cancer cells were inoculated into the left cardiac ventricle. We used this model of cancer cell inoculation to specifically focus on the late phase of the metastatic process, excluding confounding factors related to a possible effect of ISO on the primary tumor. The skeletal colonization of metastatic MDA-MB-231 cells was assessed 4 weeks later by radiographic and histological analyses. Confirming our previous results in nude mice (51), we observed that the area and number of long bone metastatic osteolytic lesions on X-rays was more than 50% higher in ISO-treated WT mice compared to PBS-treated WT mice (**Figure 15A-C**). Importantly, lack of the β2AR in Rag/β2AR$_{ob}$KO mice blunted the stimulatory effect of ISO on bone lesion area and number. X-rays lesions were verified by the presence of cancer cells at sites of lesion by histology (**Figure 15D**).

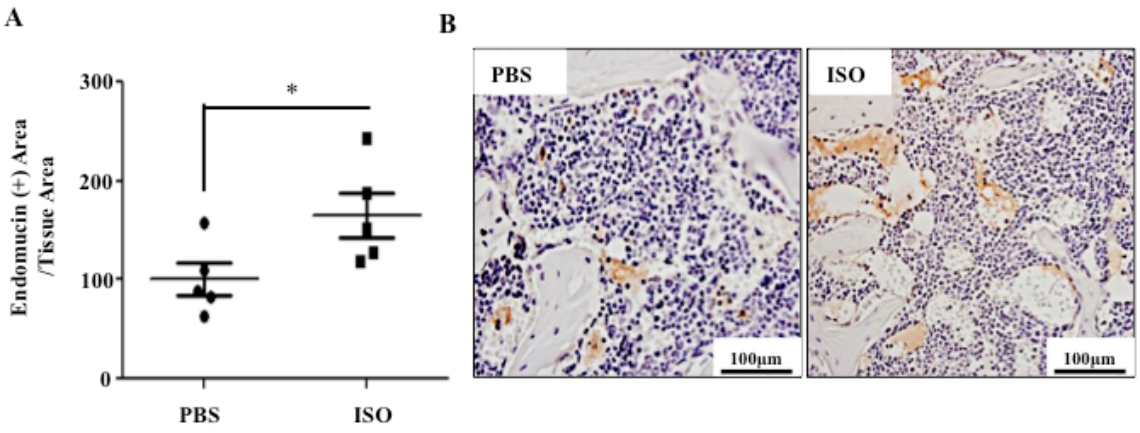

Figure 14. Femoral Vessel Density Increases after 3 weeks of ISO Treatment: A) Endomucin-positive vessels in mouse femurs increase after 3 weeks of daily ISO IP injections. Counts were normalized by tissue area (p=.048, N=5). B) Representative 40x images of mouse femurs stained for endomucin (brown).

In a second experiment, four week-old *Rag2*/WT mice were treated with PBS or ISO as above for 3 weeks, in combination with the VEGF-blocking antibody, mcr84 (200 μgs/inj., twice per week), or a control IgG2 antibody. The day following the last injection, 10^5 osteotropic MDA-MB-231 breast cancer cells were inoculated via the intracardiac route, and mice were sacrificed 4 weeks later. Radiographic and histological analyses again confirmed an increase in bone colonization upon ISO treatment (**Figure 16A-D**), and similarly to the lack of β2AR, mcr84 treatment significantly reduced the number and area of bone lesions compared to ISO and IgG-treated mice. Confirming our previous results, we found that average total bone tumor area was increased in ISO-treated mice, but the average area of each bone tumor foci was unchanged, suggesting that the action of ISO on the bone microenvironment mainly affects the colonization efficiency of metastatic cancer cells, and not their growth in bone (**Figure 17**). Together with the β2AR-dependent increase in bone blood vessel number induced by ISO treatment shown above, these results support a model in which increased sympathetic outflow in mice triggers a VEGF-dependent neo-angiogenic switch in the bone microenvironment, via stimulation of the β2AR in osteoblasts, favoring the early skeletal establishment of metastatic cancer cells.

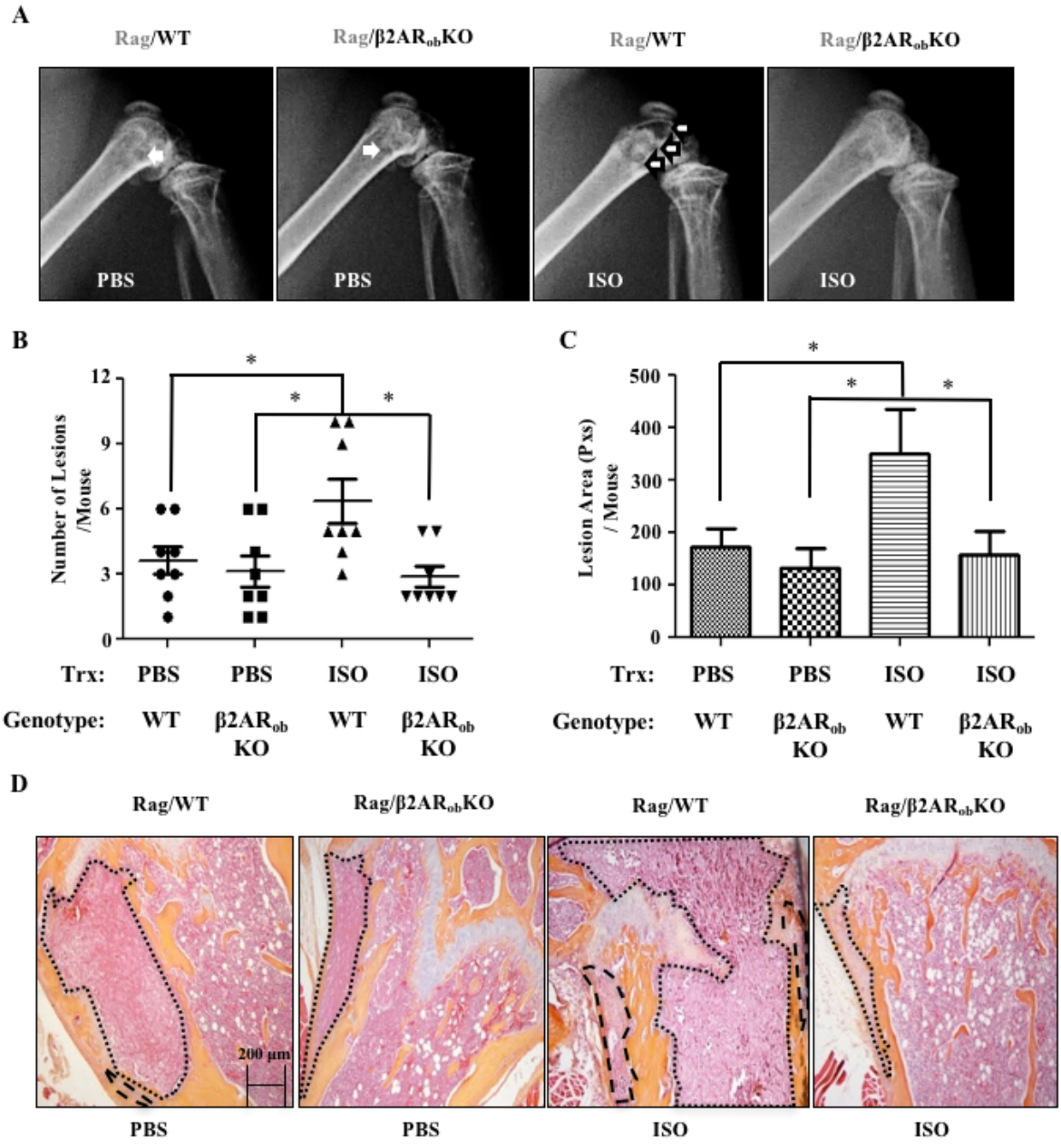

Figure 15. Absence of β2AR in Osteoblasts Abrogates the Stimulatory Effect of ISO on Osteotropic MDA-MB-231s Seeding in Long Bones: A) Representative X-rays of hind limbs 28 days following intracardiac inoculation of osteotropic MDA-MB-231 breast cancer cells in Rag/WT and Rag/β2AR$_{ob}$KO mice that received PBS or ISO for 3 weeks prior to cancer cell inoculation. B) Quantification of lesions in the forelimbs and hind limbs of mice detected by full-body X-ray at day 28 post IC injection. (*=<.05, N=8). C) Total lesion area in each group of mice, calculated from the same X-ray images. (*=<.05, N=8). D) 20x H&E Images of mouse femurs. Lesions are outlined in black.

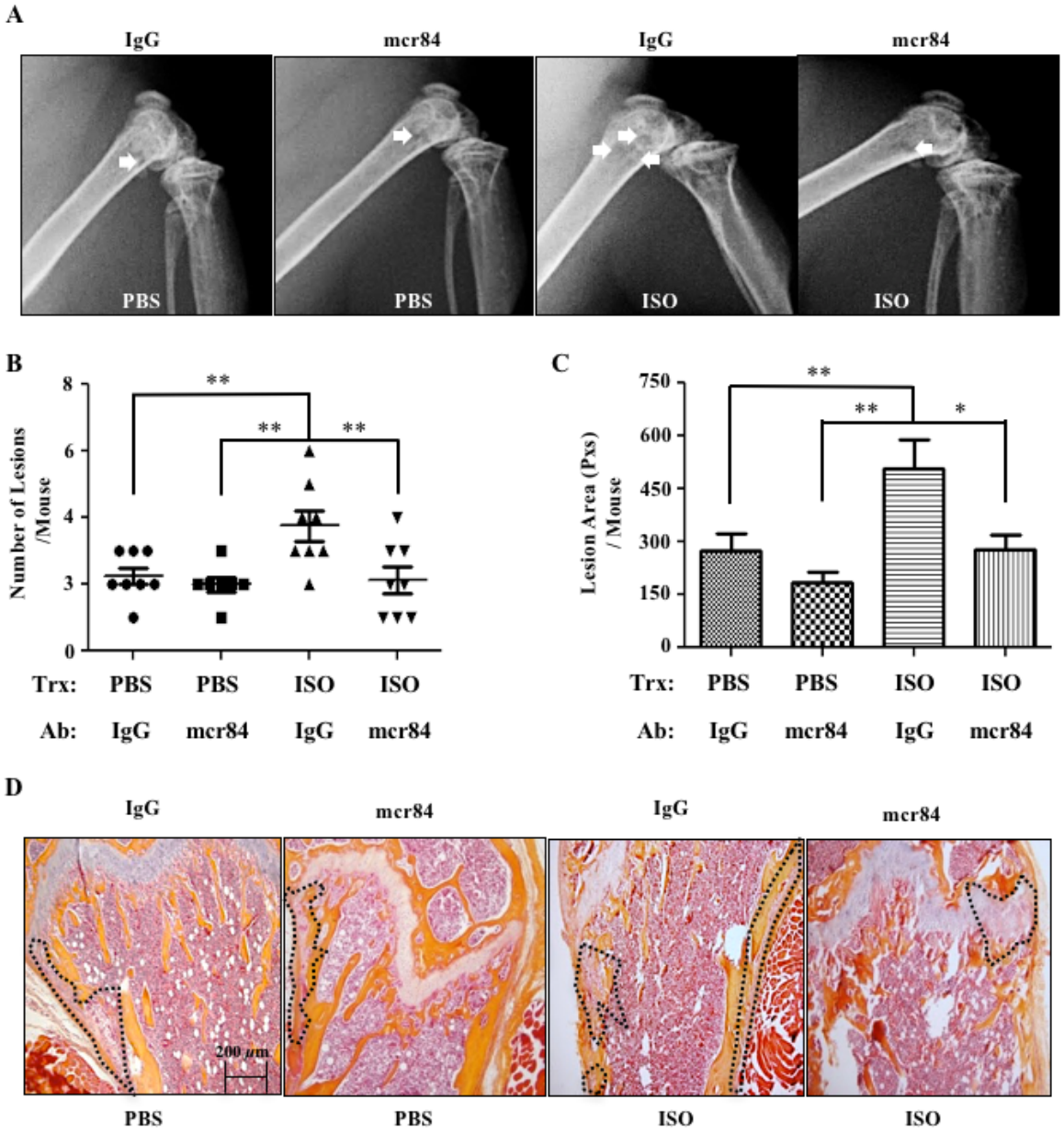

Figure 16. Blocking the Interaction Between Vegf-A and Vegfr2 Prevents the Stimulatory Effect of ISO on Osteotropic MDA-MB-231 Seeding in Long Bones: A) Representative X-rays of hind limbs 28 days following intracardiac inoculation of osteotropic MDA-MB-231 breast cancer cells in *Rag2*-/- mice treated with PBS or ISO, and with either mcr84 or an IgG2a control antibody. B) Quantification of lesions in the forelimbs and hind limbs of mice detected by full-body X-ray at day 28 post IC injection (**<.01, N=7-8). C) Total lesion area in each group of mice, calculated from the same X-ray images (*=<.05, **=<.01, N=7-8). D) 20x H&E Images of mouse femurs. Lesions are outlined in black.

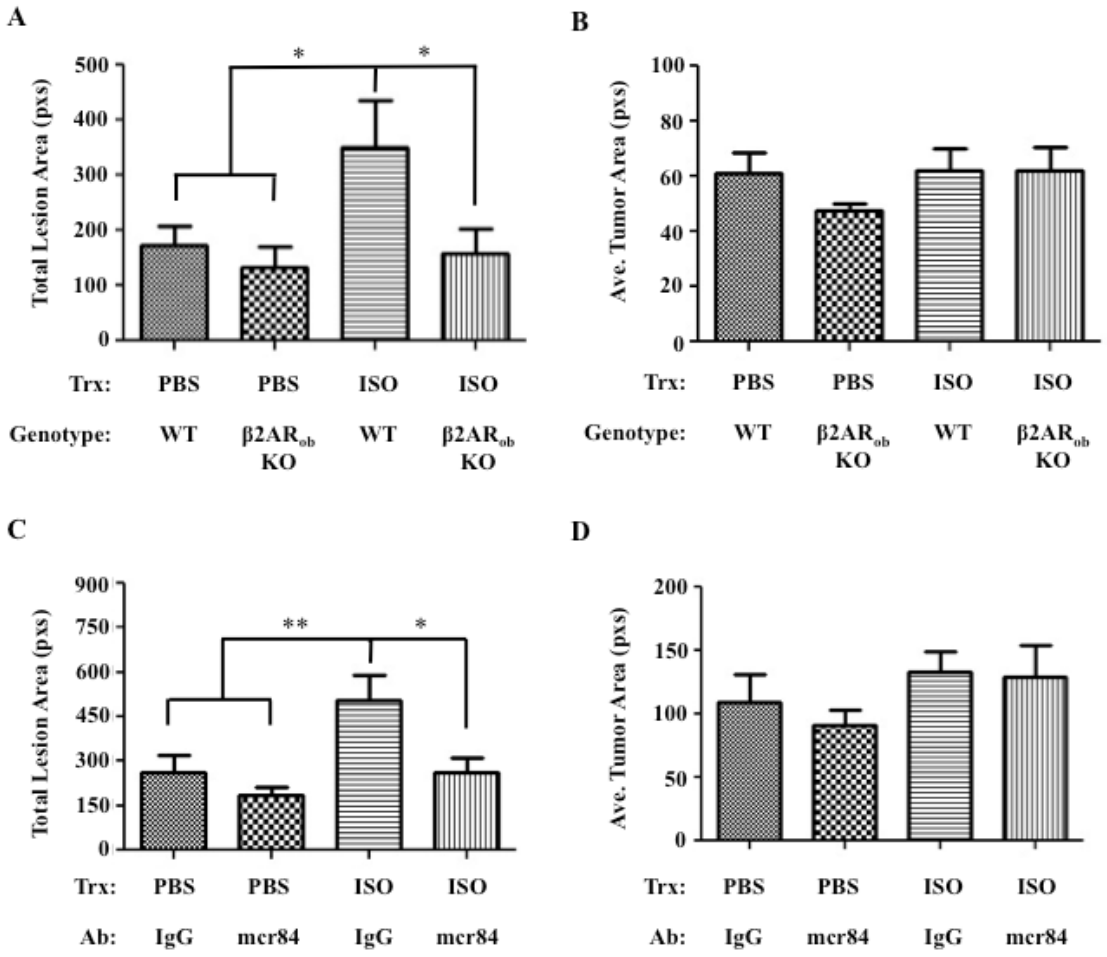

Figure 17. Total Tumor Area, but Not Average Tumor Size, Is Affected by Absence of β2AR or mcr84 Treatment in Mouse Models of ISO-induced Stress: A) Total lesion area in each group of mice. (*=<.05, N=8). Average size of individual tumors does not differ between Rag/WT and Rag/β2AR$_{ob}$KO treatment groups. (P=0.411). C) Totla lesion area in each group of mice. (*=<.05, **=<.01, N=7-8). D) Average size of individual tumors does not differ among treatment groups. (P=0.449)

Discussion

The vasculature is essential for tumor growth and escape of metastatic cells from the primary tumor, and pro-angiogenic pathways became and still are a major target of many cancer therapeutic drugs (49, 50, 106, 117-123). We show here that an increase in vascular density can be induced in the mouse bone microenvironment following stimulation of the β2AR by ISO treatment, which mimics a state of high sympathetic outflow. Through *in vitro* and *in vivo* loss-of-function approaches, we show that these changes in bone vascular density are mediated in part by an increase in Vegf-a expression and the β2AR expressed in osteoblasts. We also provide experimental evidence that this increase in bone vascular density favors the colonization of bone metastatic MDA-MB-231 cells in the skeleton. Together, these results strengthen the importance of sympathetic nerves and chronic SNS activation in the process of metastatic bone colonization, and implicate neo-angiogenesis in this process.

The effect of stress on sympathetic nerve activity has beneficial consequences in the short term (fight-or-flight response), but can lead to a wide range of pathologies if it becomes chronic, as the SNS regulates the homeostasis of many peripheral organs (115). We have previously shown that bone remodeling and the expression of RANKL by osteoblasts are under the control of sympathetic nerves (51, 102). RANKL is well known for its osteoclastogenic properties, and its pro-migratory effects on metastatic cancer cells have been more recently demonstrated (14, 17, 124). In the specific context of breast cancer, we have shown that ISO treatment leads to increased number of bone metastatic tumors following intracardiac injection of MDA-MB-231 breast cancer cells (51). An increase in the size of osteolytic lesions in these conditions was expected as ISO treatment increases RANKL, osteoclastogenesis, and bone resorption, thus feeding the osteolytic bone destruction associated with the presence of breast cancer cells in bone (71). However, the observed increase in the number of metastatic foci and bone osteolytic lesions suggested a specific effect on cancer cell colonization. This was

demonstrated in this model by restricting ISO treatment prior to cancer cell inoculation, in order to affect the bone microenvironment without directly impacting the behavior of metastatic cancer cells. In this experiment, bone colonization by cancer cells was still increased, confirming a major effect of ISO on the bone microenvironment, and likely via osteoblasts. Additional *in vitro* and *in vivo* experiments demonstrated the contribution of RANKL to the bone homing response observed in these conditions that mimic chronic SNS activation (51). Our new findings related to the effect of ISO on bone vascularity thus suggest that the activity of sympathetic nerves in the bone microenvironment can influence the pre-metastatic niche via at least two mechanisms: 1) by increasing the likelihood of bone colonization through a higher density of blood vessels, and 2) by promoting the migration of breast cancer cells after extravasation into the bone marrow toward the RANKL-secreting osteoblastic niche. Of note, the effect of increased sympathetic outflow on vascular structures in the context of metastasis is not limited to the bone microenvironment, as chronic stress also promotes breast cancer cell intravasation into lymphatic vessels in mice, via a Vegf-c:Cox-2 mechanism (125). In addition, the increased number of tumor-induced bone lesions in ISO-pretreated mice was interpreted to reflect increased tumor cell colonization of the skeleton, but one cannot exclude an effect on blood and nutrient supply leading to increased tumor growth after cells have reached the bone microenvironment, even if initial tumor bone colonization was equivalent in control and ISO-treated groups. However, the observation that the average size of single bone tumors per mouse was not significantly different between groups does not support the latter mechanism.

It has been shown that multiple tumor types express adrenergic receptors and benefit from their activation in term of growth or survival (126-128). Our experimental set up of a 3-week ISO pre-treatment, prior to MDA-MB-231 inoculation, however exposes tumor cells to negligible levels of ISO, thus supporting the key role of the stroma in the higher bone colonization efficiency observed following

β2AR stimulation. The fact that ablation of the β2AR in osteoblasts blunted the average number of Vegf-a-positive osteoblasts and the increase in blood vessel density following ISO treatment brings further evidence that the osteoblast is one of the main cell responsive to sympathetic nerves in bone.

The molecular mechanism whereby β2AR stimulation in osteoblasts leads to increased Vegf-a expression remains to be identified. The contribution of HIF-1α or HIF-2α to a β2AR-dependent increase in VEGF-A expression needs to be addressed, as expression of HIF-1α or HIF-2α can be controlled in a hypoxia-independent manner (129, 130). In addition, the bone vasculature is composed of different types of endothelial cells that respond to different signaling pathways (82, 90). Which specific population of endothelial cells engaged in the ISO-induced neo-angiogenesis reported here needs to be further defined. Lastly, it can be noticed that the inhibitory effect of Vegf-a blockade on ISO-induced angiogenesis was partial. Although a suboptimal dose or treatment regimen could explain this observation, it cannot be excluded that other angiogenic factors than Vegf, Fgf2, Angpt2 and Pdgfa are involved.

From a therapeutic point of view, angiogenesis, being a normal physiological process, imposes limitations and difficulties as a therapeutic target for cancer treatments. This partially explains why the clinical use of VEGF inhibitors, although beneficial in certain cancers, is still limited by adverse effects, toxicity, and acquired drug resistance (131). Contrastingly, the use of β-blockers as adjuvant therapy in patients diagnosed with breast cancer may have several therapeutic advantages. If both Vegf-a and Rankl are β2AR target genes and critical mediators of bone resorption, angiogenesis and metastatic cancer cell colonization of bone, the use of a single drug with β-blockade activity has the potential of reducing bone resorption, angiogenesis, and bone tumor establishment in at-risk patients (132). These properties could make β-blockers particularly efficacious in preventing disseminated cancer cells from reaching the safe haven of the bone microenvironment and may expose these cells more readily to

chemotherapy or actions of the immune system. In that regard, several preclinical and clinical studies have shown a benefit from β-blocker use on survival in patients with triple negative breast cancer, non-small cell lung cancer, hemangiomas, and ovarian cancer (63, 70, 98, 104, 117, 133). Whether this protective effect is mediated through a reduction in cancer cell growth, bone metastasis, or other mechanism(s) remains unknown.

In conclusion, this work supports the importance of sympathetic nerve activation on breast cancer bone colonization and identifies an osteoblastic, β2AR- and VEGF-A-dependent neo-angiogenic switch mechanism contributing to this effect. It provides suggestive preclinical evidence in mice that targeted therapies that prevent these vascular changes could improve treatment outcomes for women diagnosed with breast cancer; especially for women subjected to chronic stress, such as those with poor socioeconomic status or facing challenging familial situations. These preclinical findings need to be further investigated clinically.

CHAPTER III

Sympathetic Activation Increases Il-6 in Osteoblasts and Promotes Breast Cancer Cell Adhesion to Bone Marrow-derived Endothelial Cells In Vitro

Introduction

A majority of cancer patients die due to diffuse metastatic disease. Breast cancer, the most common cancer diagnosed among women, routinely metastasizes to bone, causing severe pain, decreased quality of life, and death. Moreover, current treatments for bone lesions are palliative, requiring more research to understand the mechanisms responsible for bone metastases and how to specifically and successfully treat them in patients. Recent studies have shown that stress can exacerbate cancer progression in many tumor types (62-64, 108, 132-136). Furthermore, clinical studies reveal that certain cancer patients, including those with triple-negative breast cancer (TNBC), have increased survival metrics when the treatment regimen includes a beta-blocker such as propranolol (66).

Stress activates the Sympathetic Nervous System (SNS) via release of NE from nerves, which then bind adrenergic receptors present throughout the body. Regarding the immune system, adrenergic activation stimulates B-cell activation, IgE production, and acute phase protein synthesis (137). In the context of bone biology, osteoblasts express the β2AR and are known to respond to signals from the SNS (44). Previous research has shown that chronic activation of the SNS can promote primary tumor growth and metastasis via changes in stromal homeostasis, an influx of pro-inflammatory macrophages, and increases in primary tumor vasculature (63, 75). While these results implicate stress signaling in cancer progression, the concept needs to be explored further in the many cells that comprise the different microenvironments to which tumors spread.

The vasculature is a crucial component of the metastatic process. Interactions with endothelial cells must occur in order for tumor cells to extravasate from circulation and establish at a secondary site (138, 139). The bone is a highly vascularized tissue, and osteoblasts, the bone-forming cells, are known producers of proteins, such as Vegf-a and RANKL, that regulate angiogenesis and bone remodeling (85, 87). Similar to the diapedesis of immune cells, tumor cells are recruited in secondary sites by chemotactic gradients of cytokines and growth factors. Pro-inflammatory cytokines, such as Interleukin 6 (IL-6) IL-1β, and TNF-α, have been show to support cancer cell interactions with endothelial cells by altering the levels of adhesion proteins present on the endothelium. Elevated production of the aforementioned cytokines are known to increase protein levels of adhesion molecules such as VCAM1, E-Selectin, and multiple β-integrins, all of which facilitate extravasation of metastatic breast and prostate tumor cells into bone (137-142). However, it is unknown how chronic SNS signaling, which regulates bone homeostasis, affects adhesion proteins on bone marrow endothelium that mediate breast cancer bone metastases.

In this chapter, it is reported that osteoblast-derived Interleukin 6 (Il-6) supports breast cancer cell interaction with BMECs *in vitro*.

Materials & Methods

Primary Mouse Bone Marrow Endothelial Cells

Primary mouse bone marrow endothelial cells (BMEC) were harvested as previously described from with WT or Il6KO mice (114). Mouse hind limb bone marrow was flushed and centrifuged in Complete Endothelial Cell Growth Media (ECM) (ScienCell #1001). Cells were plated on tissue culture dishes or in tissue culture flasks coated with 4μg/mL fibronectin (Gibco #33016015) in Complete

Endothelial Cell Growth Media. After 7 days, cells were used for experiments with both human MDA-MB-231 breast cancer cells and 4T1 mouse mammary tumor cells.

BMEC and Tumor Cell Co-Culture Experiments

BMECs were grown on fibronectin-coated 4-well chamber slides for 7 days in Complete ECM (ScienCell). The next day, media were changed to 0% FBS ECM or BMSC conditioned media, and BMECs were treated with varying stimuli for 24 hours. Then, 30,000 GFP-labeled MDA-MB-231s or 4T1s were added to the chambers; after 3.5 hours, chamber slides were fixed and processed for fluorescent imaging. DAPI (1:4000) was used to mark nuclei of all cells, and pictures were taken at 4x and 10x objectives on an Olympus BX41 upright microscope.

Mouse Il-6 and an anti-mIl6 antibody were purchased from R&D Biosystems (406-ML-005, MAB406) and used at 50ng/mL and 200ng/mL concentrations, respectively. Conditioned media were harvested from WT as well as Il6KO primary mouse bone marrow stromal cells (BMSCs) after 24hours of treatment with PBS or 10μM ISO.

Quantitative PCR

Mouse hind limbs, lungs, heart, and spleen were snap frozen in liquid nitrogen immediately following mouse sacrifice and stored at -80°C. Bone samples were pulverized with liquid nitrogen-cold mortar and pestle into powder. RNA extraction for cells and mouse tissue was performed using TRIzol (Life Technologies #15596018). cDNA for qRT-PCR experiments was synthesized using the High Capacity cDNA Reverse Transcription Kit from ABI Applied Biosystems (#1502205). Taqman probes were used to amplify the following genes: Murine *Il-6* (Mm00437304), Murine *Hprt* (Mm01545399), Murine *18s (*4333760T). Expression was analyzed by the ΔΔCt method.

The RT^2 Profiler qPCR array targeting mouse adhesion and extracellular matrix genes was performed per manufacturer's instructions (QIAGEN #PAMM-013ZA). RNA from BMECs treated with PBS or 50ng/mL mIl-6 was harvested after 24 hours using QIAGEN Shredder technology, and online software was used to produce a heat map that visually represents the data from the array. (www.SABiosciences.com/pcrarrayanalysis.php)

Mouse Il-6 ELISA

An ELISA for mouse Il-6 was run per manufacturer's instructions (R&D Systems, #M6000B). Media used for this assay were collected from either WT or IL6KO BMSCs after 24 hour treatment of either PBS or 10 μM ISO.

Statistics

All data are presented as means ± the standard error mean (SEM). For experiments comparing two groups, a standard two-tailed student's *t* test was used unless otherwise stated in the figure legend. For experiments comparing more than 2 groups, one-way ANOVA was used with a Newman-Keuls post-hoc test unless stated specifically in the figure legend. For all tests, a *p value* less that .05 was considered significant. All data are an average of at least 3 individual experiments.

Results

Conditioned Media (CM) from ISO-treated BMSCs Promotes Tumor:Endothelial Interaction *In Vitro*

In order for tumor cells to successfully seed in a secondary organ, they must interact with the endothelium and traverse into a separate tissue. Regarding the bone microenvironment, osteoblasts have

been shown to produce many tumor-promoting proteins, some of which can affect the vascular density of adult bones (Chapter II). Following up on these results, we asked whether these proteins could also impact the function of bone endothelial cells in a way that could promote tumor metastasis. To address this question, we assessed whether the conditioned media from ISO-treated primary osteoblasts could promote tumor cell interaction with BMECs. Conditioned media (CM) from primary BMSCs treated with ISO for 24 hours increased the number of both human MDA-MB-231s breast cancer cells that interacted with the BMECs after 3.5 hours *in vitro,* compared to PBS-treated BMSC CM. Similar results were obtained with murine 4T1s mammary cancer cells (**Figure 18A, B**). These results indicated that activation of the β2AR in osteoblasts leads to the secretion of proteins that promote tumor cell interaction with bone marrow endothelium *in vitro*.

ISO Treatment Increases Il-6 Expression *In Vitro* and *In Vivo*

Due to the interaction observed between tumor cells and BMECs, we investigated proteins produced by osteoblasts that could alter adhesion proteins in endothelial cells. Il-6 has been shown to change levels of several adhesion proteins in both untransformed cells and tumor cells, and is produced by osteoblasts for normal bone homeostasis (142). Upon ISO treatment, MC3T3 osteoblasts and primary BMSCs displayed an immediate and short term induction of Il-6 mRNA after 2 hours (**Figure 19B, C**). To corroborate this finding *in vivo*, Il-6 expression in whole mouse bone was measured. Similar to the *in vitro* results, whole mouse femurs exhibited an increase in Il-6 expression, showing that beta-adrenergic signaling in bone increases in Il-6 (**Figure 19A**). Furthermore, Il-6 ELISA data indicated that WT BMSCs treated with ISO secrete nearly 10-fold more Il-6 than WT BMSCs treated with PBS; Il6KO BMSCs, regardless of treatment, secreted no Il-6 (**Figure 19D**).

A

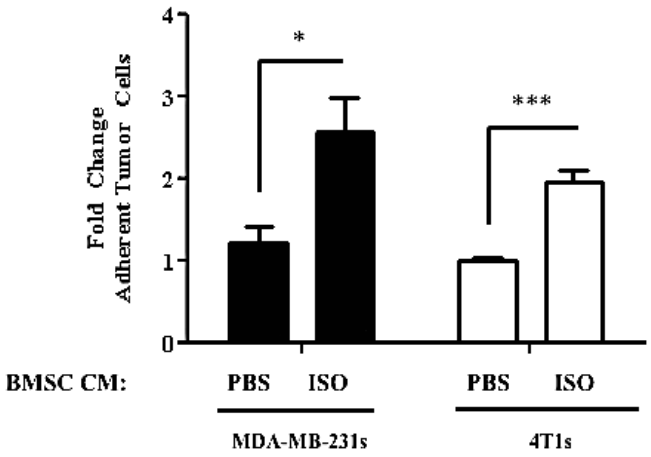

B

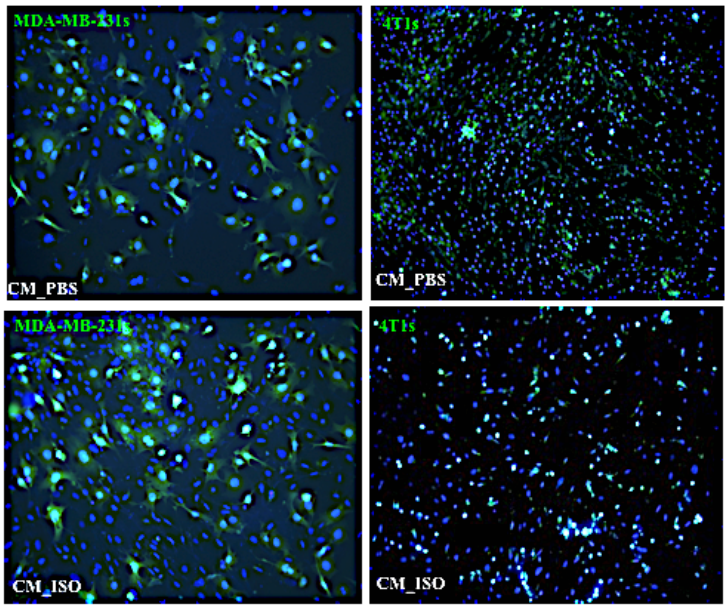

Figure 18. Conditioned Media from Isoproterenol-treated BMSCs Increases Mammary Tumor Binding Capacity to BMECs: A) Primary mouse BMECs were treated for 24hours with CM_PBS or CM_ISO prior to addition of MDA-MB-231s or 4T1 cells. Quantification of adherent tumor cells was calculated by fluorescence microscopy and graphed as fold change relative to CM_PBS. (N=4 *=p<.05, ***=p<.001) B) Representative 20x images of co-cultures. Blue-DAPI, Green-Tumor Cells

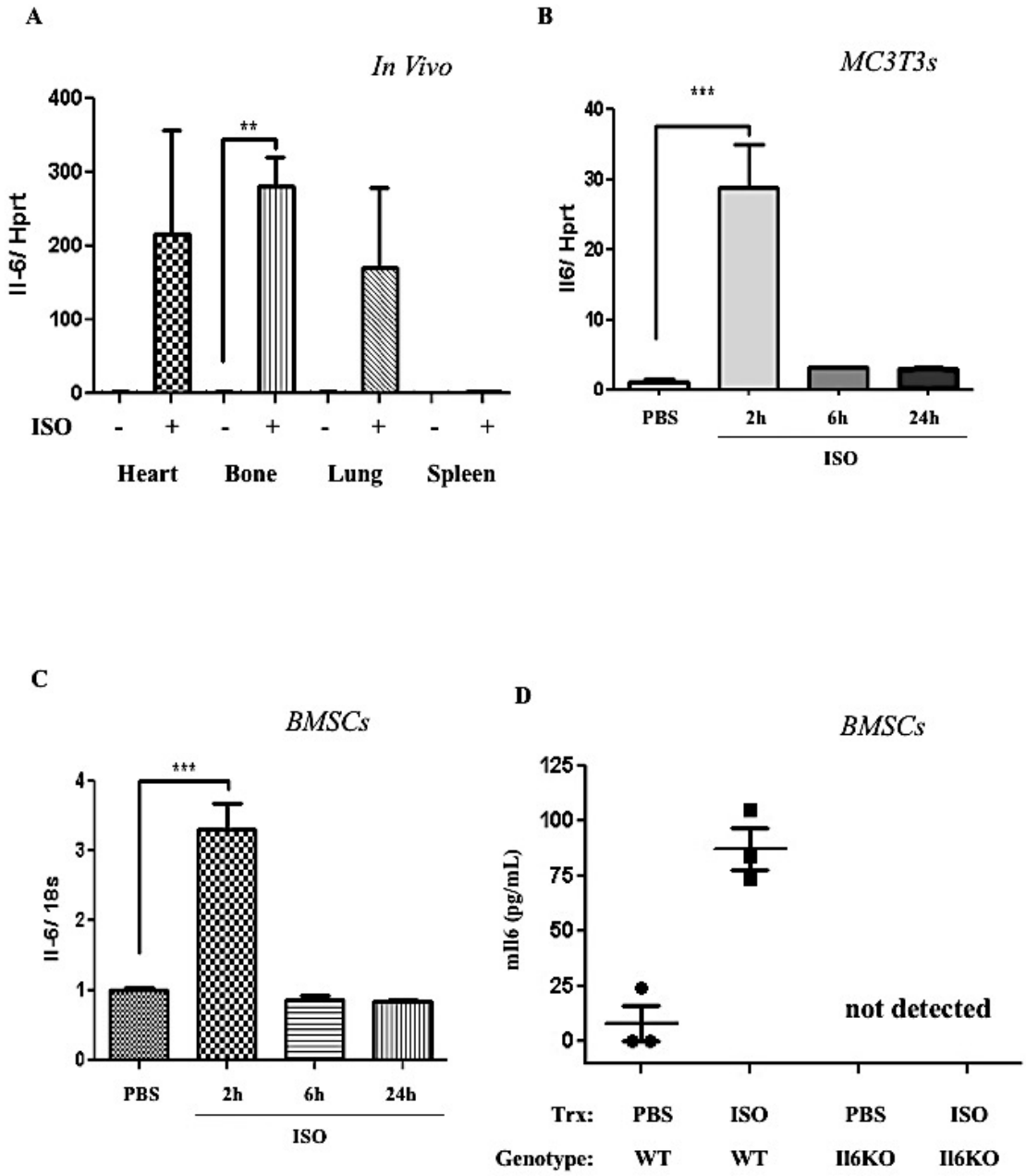

Figure 19. Isoproterenol Treatment Increases Murine Il-6 Expression *in vivo* and *in vitro*: A) ISO (3mg/kg) increases Il-6 expression in whole mouse bone in vivo after 2 hours of treatment. (N=3, **=p<.01) B) 10 μM ISO increases expression of Il-6 in MC3T3 mouse osteoblast cell line after 2 hours. (N=3, ***=p<.001 C) 10 μM ISO increases Il-6 expression in primary mouse BMSCs after 2 hours. (N=3, ***=p<.001) D) Il-6 ELISA data reveal that BMSCs treated with ISO secreted more Il-6 than PBS-treated. Il6 KO BMSCs were used as a negative control.

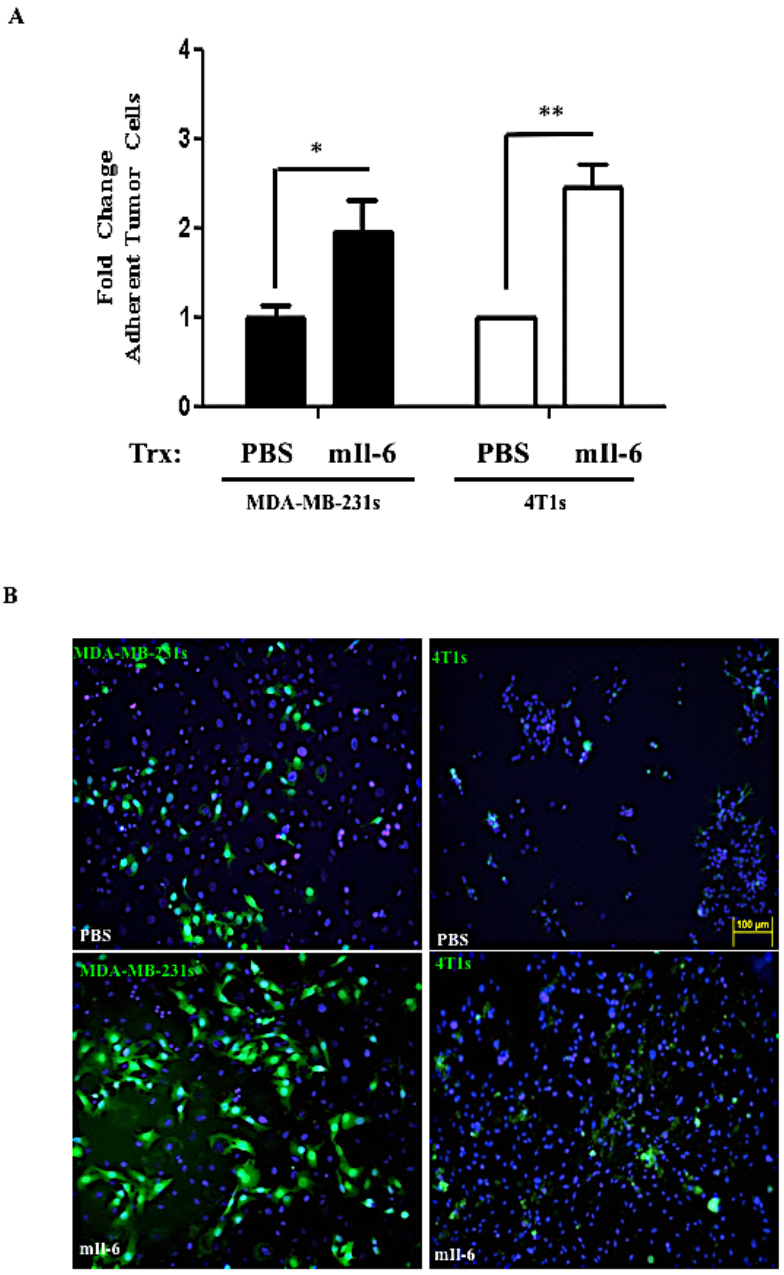

Figure 20. Mouse Il-6 Increases Mammary Tumor Binding Capacity to mBMECs: A) Primary BMECs were treated with mouse recombinant IL6 (50nM) for 24hrs prior to addition of MDA-GFPs or 4T1-GFPs for 3.5hrs. Number of adherent tumor cells was calculated using fluorescence microscopy and graphed as fold change relative to PBS group. (N=3-4, *=p<.05, **=p<.01) B) All images are 20x; Blue=DAPI, Green=Tumor Cells.

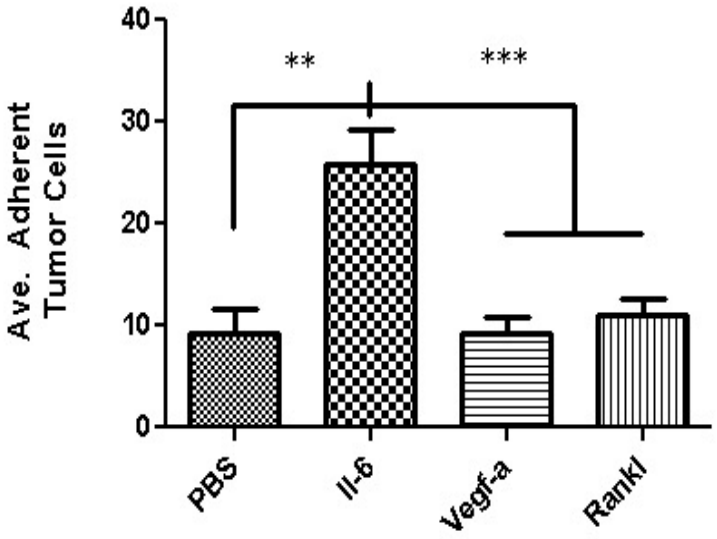

Figure 21. Other Osteoblastic Proteins Induced by ISO Treatment Do Not Promote Adhesion of MDA-MB-231s to BMECs. Treatment of BMECs with murine Vegf-a or RANKL does not increase adhesion compared to mIl-6. (N=4, **=p<.01, ***=p<.001)

To test the functionality of Il-6 in the adhesion assay, we repeated the tumor cell-BMEC co-culture experiment with direct treatment of mouse Il-6. After a 24-hour treatment of BMECs with this cytokine, an increase in the attachment of tumor cells was observed for both tumor cell lines tested, compared to PBS treatment (**Figure 20A, B**). Importantly, mouse Il-6 cannot bind the human IL-6R, reinforcing the notion that this endothelial-tumor cell interaction is in part mediated by action of stromal-derived IL6. Moreover, treating the BMEC monolayer with Rankl or Vegf-a, two other ISO-induced osteoblastic proteins, did not promote cancer cell adhesion in the co-culture experiment (**Figure 21**).

Loss of Il-6 Signaling Reduces Tumor Cell Adhesion to BMECs

In order to strengthen the claim that stromal Il-6 is key for breast cancer cell adhesion to BMECs, we performed co-culture experiments with MDA-MB-231s and 4T1s in two systems of Il-6 inhibition. In the first system, the CM from WT BMSCs and Il6KO BMSCs was added to the BMEC co-cultures. Both breast cancer cell lines adhered to BMECs in the presence of WT-ISO CM in greater numbers compared to WT BMSCs treated with PBS, and IL6 deficiency prevented this increase induced by ISO (**Figure 22A-D**).

Secondly, an Il-6 neutralizing antibody or an IgG control antibody was added to the conditioned media co-culture experiment. The results reveal that the Il-6 neutralizing antibody, when added to the CM-ISO group, reduced the number of adherent MDA-MB-231 cells compared to CM-ISO plus the IgG antibody (**Figure 23A, B**). These results infer that stromal Il-6 stimulates tumor and endothelial interaction *in vitro*.

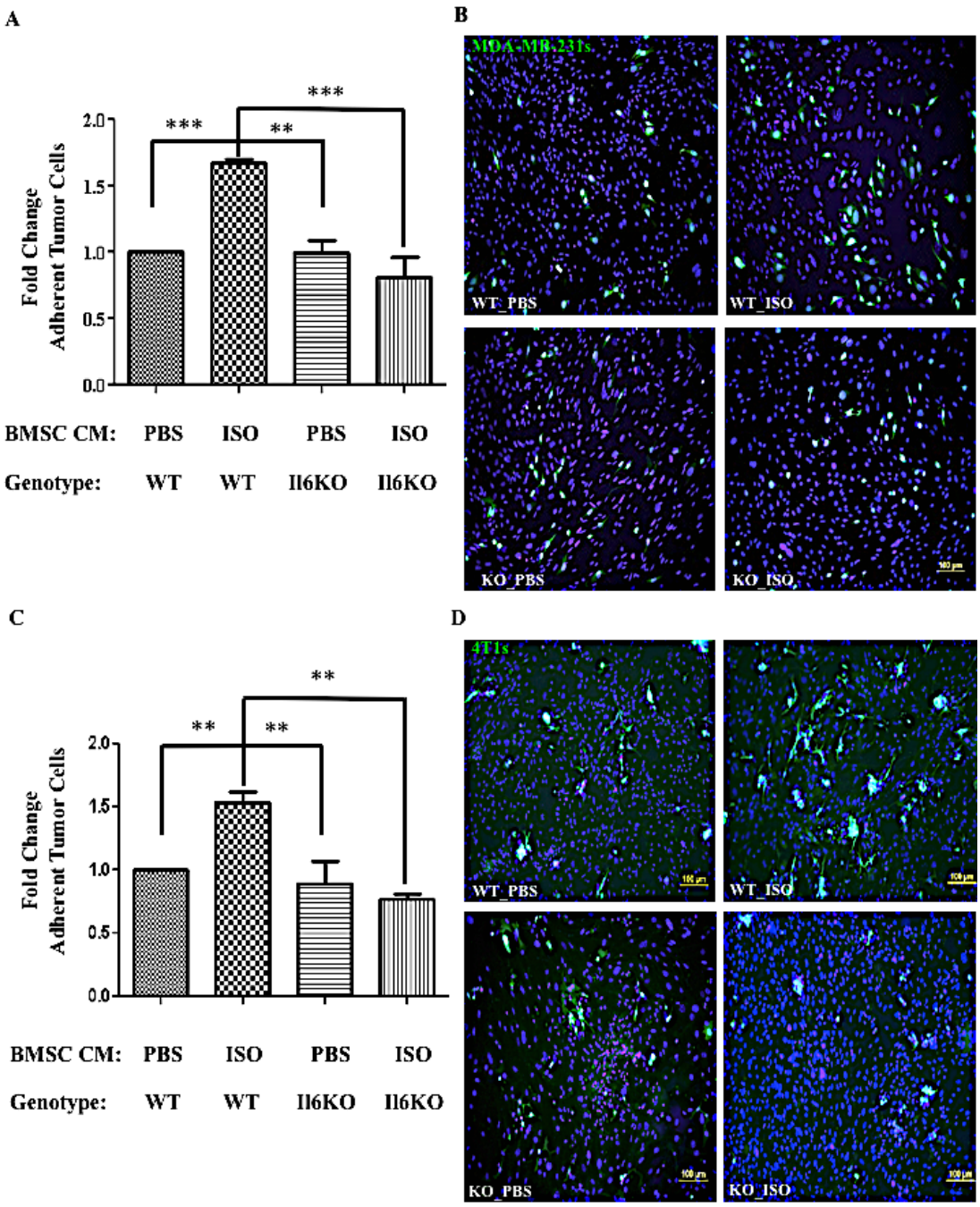

Figure 22. Conditioned Media from Il6KO BMSCs Does Not Promote Tumor Cell Interaction with BMECs: A) Fold change of GFP-positive MDA-MB-231 cells that adhered to BMECs treated with varying BMSC conditioned media. B) Representative 20x images (Blue=DAPI, Green=MDA-GFPs, N=3). C) Fold change of GFP-positive 4T1s that adhered to BMECs treated with varying BMSC conditioned media. D) Representative 20x images (Blue=DAPI, Green=4T1s, N=3, P=.0027).

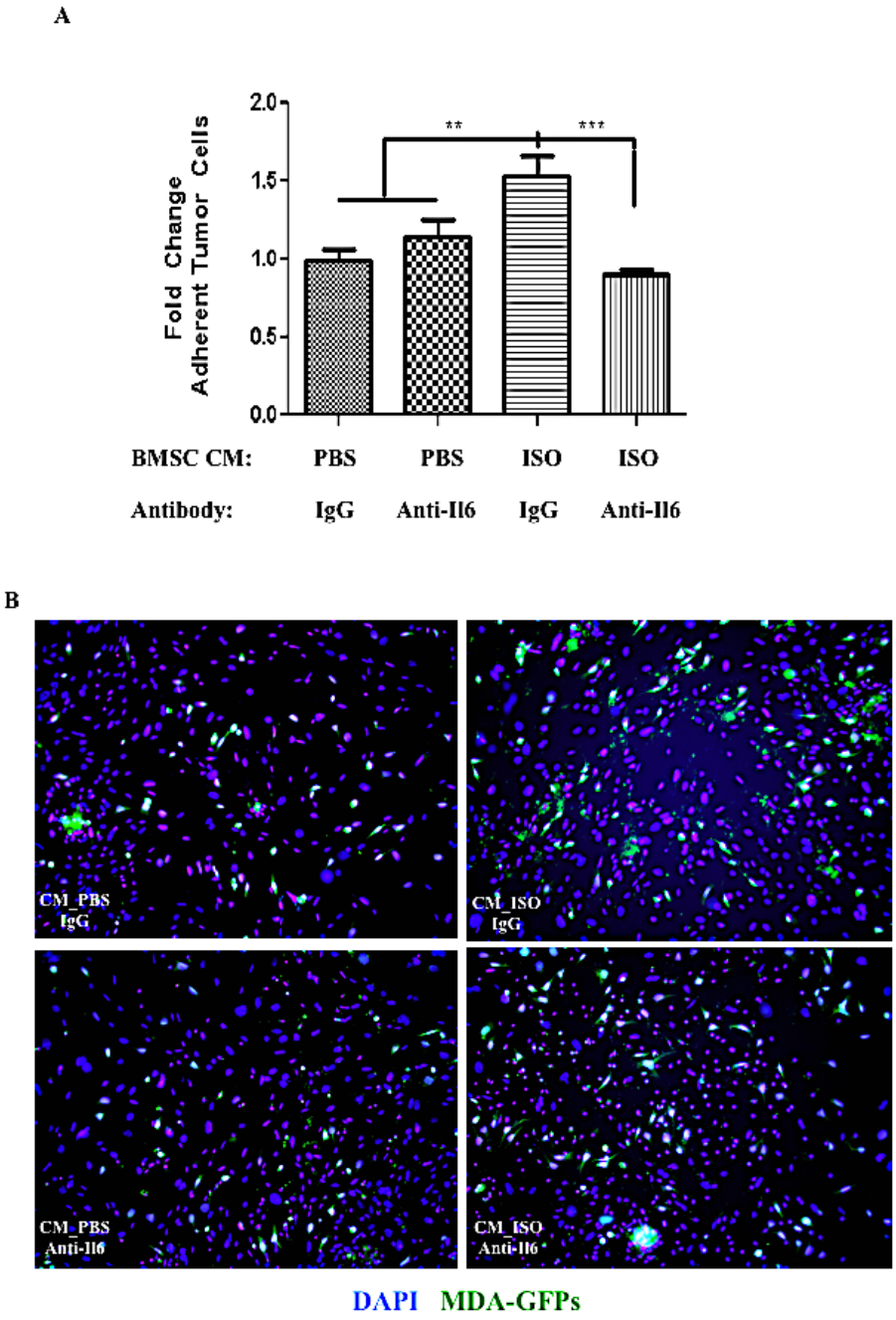

Figure 23: Addition of a Neutralizing Mouse Il-6 Antibody Reduces MDA-MB-231 Adhesion to mBMECs Caused by ISO-treated BMSC Conditioned Media. A) Primary BMECs were treated for 24hrs prior to addition of MDA-GFPs. Number of adherent tumor cells was calculated using fluorescent microscopy and graphed as fold change relative to PBS group. (N=6, **<.01, ***<.001) B) All images are 20x; Blue=DAPI, Green=Tumor Cells, Red=Cell Membrane Dye.

Neither Direct Treatment of BMECs with ISO nor Endothelial Il-6 Is Required for Breast Cancer Cell Adhesion *In Vitro*

It is reported that endothelial cells express α1ARs and β2ARs that control vasodilation and vasoconstriction, and in turn alter vascular biology (70, 137). Therefore, to investigate whether endothelial adrenergic signaling could promote interactions with breast cancer cells, BMEC monolayers were treated with Il-6, PBS, or ISO prior to addition of MDA-MB-231-GFPs or 4T1-GFPs. Regarding both cell lines, Il-6 caused the greatest amount of tumor cell interaction with BMEC monolayers, confirming previous results (**Figure 24A, B**). ISO treatment yielded a moderate increase in adherent MDA-GFPs compared to the PBS group.

To study whether endothelial Il-6 may be partially responsible for this result, we repeated this co-culture experiment with BMECs derived from the bone marrow of Il6KO mice. Both the MDA-GFPs and 4T1-GFPs exhibited adhesion to the Il6KO BMECs upon Il-6 treatment in a similar manner observed with WT BMECs. Neither PBS nor ISO promoted tumor/ BMEC interaction, a pattern mimicked in WT BMECs (**Figure 24A, B**). This result was also reflected when the total number of each tumor cell line was analyzed (**Figure 25A, B**). These findings suggest that endothelial Il-6 is not required for tumor cell interactions, and that β adrenergic signaling in the BMECs does not promote their adhesion to the tumor cells in static culture.

qPCR Array Data Reveal Multiple Adhesion Proteins of Interest

Due to the enhanced interactions between tumor cells and BMECs in both the Il-6 and ISO-CM co-culture systems, we were interested in examining proteins that could mediate this phenotype. A non-candidate approach was used via a qPCR array consisting of genes related to adhesion and extracellular matrix (ECM). BMECs treated with murine Il-6 for 24 hours showed that each isoform of the anti-

A

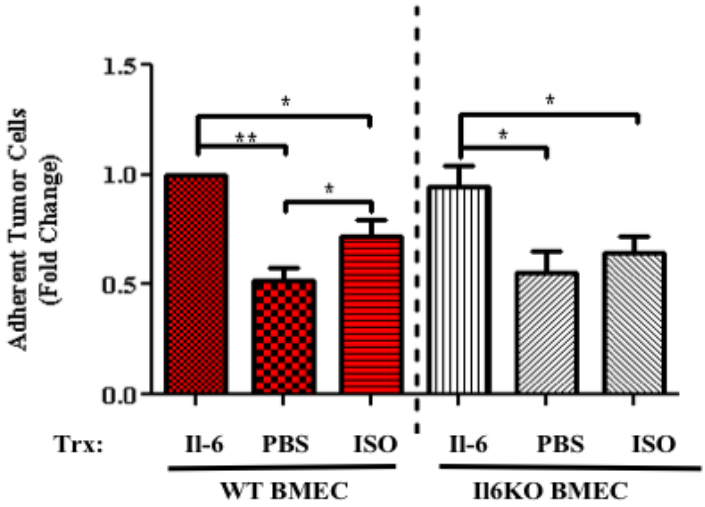

B

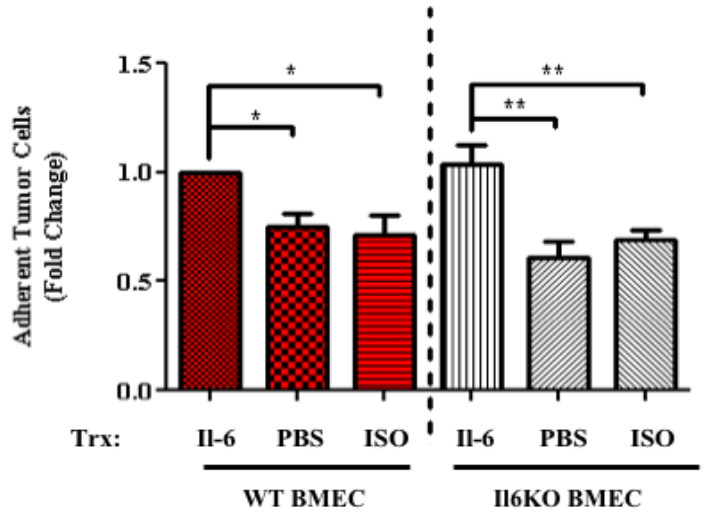

Figure 24. MDA-GFPs and 4T1-GFPs Adhere to Il6KO BMECs with Il-6 Treatment: A) MDA-231-GFP adhere to WT and Il6KO BMECs treated with Il-6. B) 4T1-GFPs adhere to WT and Il6KO BMECs treated with Il-6. Direct ISO treatment does not support tumor/endothelial interaction compared to Il-6 treatment. (N=3-4)

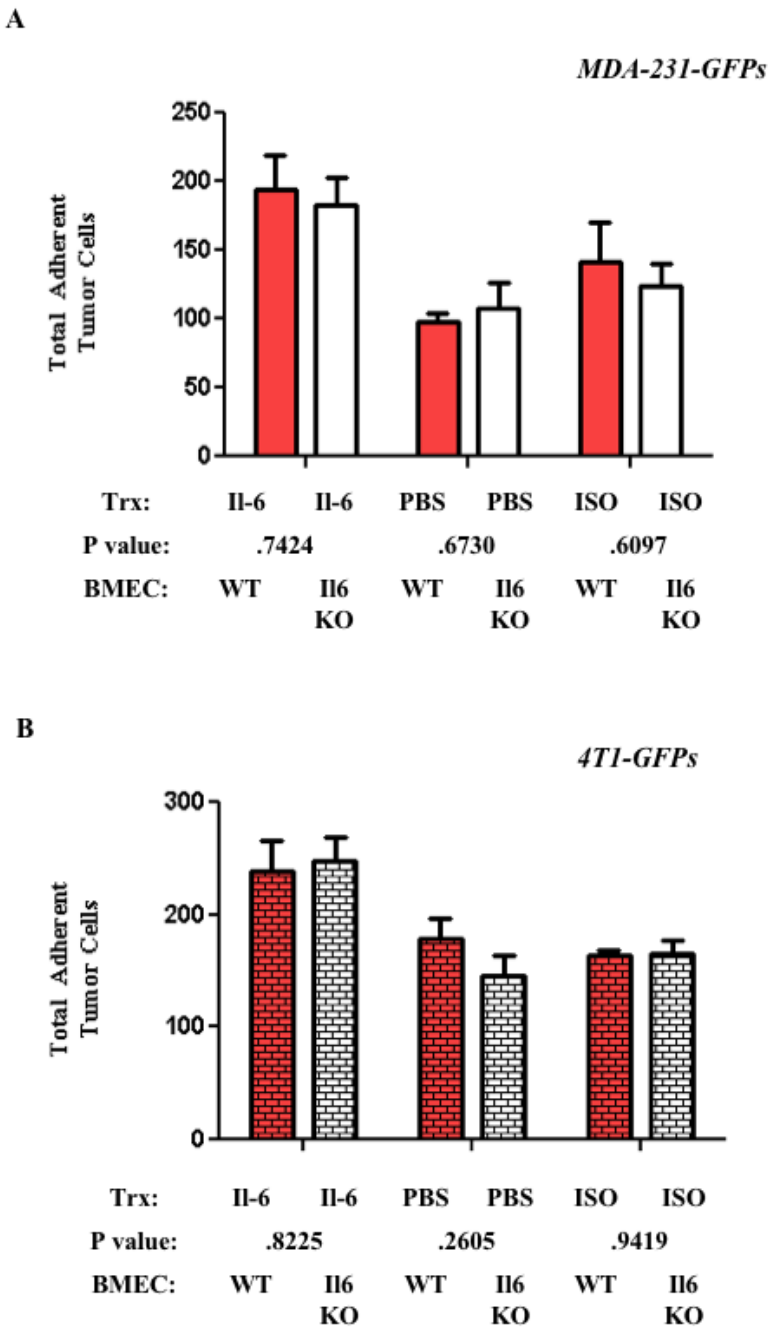

Figure 25: Endothelial Il-6 Is Not Required for Tumor/ BMEC Interaction *In Vitro*. A) Average Total MDA-231-GFP adhering to WT and Il6KO BMECs. B) Average Total 4T1-GFP adhering to WT and Il6KO BMECs. (N=3-4)

A

	1	2	3	4	5	6	7	8	9	10	11	12
A	Adamts1	Adamts2	Adamts5	Adamts8	Cd44	Cdh1	Cdh2	Cdh3	Cdh4	Cntn1	Col1a1	Col2a1
B	Col3a1	Col4a1	Col4a2	Col4a3	Col5a1	Col6a1	Ctgf	Ctnna1	Ctnna2	Ctnnb1	Ecm1	Emilin1
C	Entpd1	Fbln1	Fn1	Hapln1	Hc	Icam1	Itga2	Itga3	Itga4	Itga5	Itgae	Itgal
D	Itgam	Itgav	Itgax	Itgb1	Itgb2	Itgb3	Itgb4	Lama1	Lama2	Lama3	Lamb2	Lamb3
E	Lamc1	Mmp10	Mmp11	Mmp12	Mmp13	Mmp14	Mmp15	Mmp1a	Mmp2	Mmp3	Mmp7	Mmp8
F	Mmp9	Ncam1	Ncam2	Pecam1	Postn	Sele	Sell	Selp	Sgce	Sparc	Spock1	Spp1
G	Syt1	Tgfbi	Thbs1	Thbs2	Thbs3	Timp1	Timp2	Timp3	Tnc	Vcam1	Vcan	Vtn

B

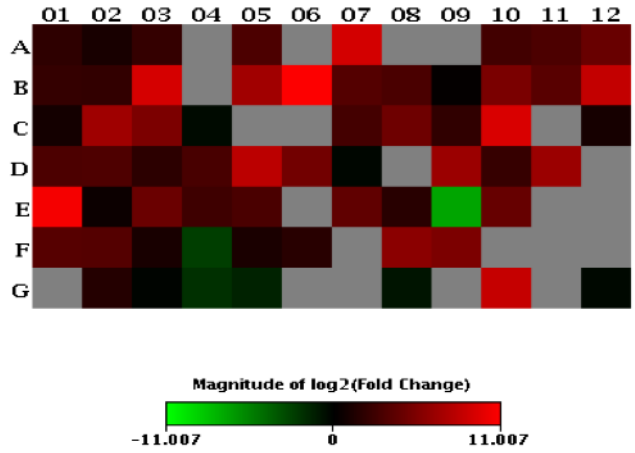

C

Upregulated Genes	Downregulated Genes	HKG
E-Selectin	*Mmp2*	*Gusb*
P-Selectin	*Pecam1*	
Emilin-1	*Thbs1*	
Integrins B1, B2, B3	*Thbs2*	
Sarcoglycan-ε	*Thbs3*	
Vcam1		

Figure 26: qPCR Array of Mouse Adhesion and ECM Genes Reveals Increased Expression of Multiple Adhesion Proteins in Primary BMECs upon Il-6 Treatment. A) Table of genes tested in the array. B) Heat Map reveals expression fold changes in array. cDNA was prepared from RNA of primary mouse endothelial cells cultured on fibronectin-coated tissue plastic for 7 days and treated with either PBS or 50ng/mL mIl-6 for 24 hours on day 7. C) Selected genes of interest that were upregulated or downregulated. *Gusb* was used at the housekeeping gene (HKG).

angiogenic protein thrombospondin was decreased upon Il-6 treatment, suggesting that Il-6 activates BMECs to a pro-angiogenic state (**Figure 26**). Many genes of interest were increased with the Il-6 treatment, warranting verification and further scientific investigation. Five such genes were chosen due to their studied roles in tumor metastasis, bone biology, and endothelial biology: Integrin β1, Integrin β3, Vcam1, E-selectin, and P-selectin.

Integrin β1 and β3, and Vcam1 Expression Do Not Increase in Il-6 Treated BMEC Cultures *In Vitro*

Integrins are a set of proteins that form heterodimeric complexes and are involved in cellular signaling regarding the surrounding environment. These complexes facilitate cell adhesion to the ECM, leading to clustering of actin filaments, stress fibers, and signaling through focal adhesion kinase (FAK). Integrins β1 (*ITGB1*) and β3 (*ITGB3*) have been implicated in cancer progression, particularly to the bone (143-148). Although an increase was observed in these two proteins in the qPCR array, verification studies *in vitro* showed no increase in mRNA expression of either family member upon treatment of BMEC monolayers with Il-6 (**Figure 27A, B**).

Next, vascular cell adhesion molecule 1 (*VCAM1*) expression was measured in BMECs *in vitro*. This protein belongs to the transmembrane immunoglobulin superfamily. Multiple reports indicate that VCAM1 levels are increased in renal cell carcinoma, breast cancer, gastric cancer, and breast cancer bone metastases, strongly implicating this protein in tumor progression (149-151). BMECs treated with Il-6 *in vitro*, however, exhibited a 40% reduction in *Vcam1* expression (**Figure 27C**).

Expression Levels of Both E-Selectin and P-Selectin Increase in BMEC Cultures *in Vitro*

The next two adhesion proteins selected for verification were E-Selectin (*SELE*) and P-selectin (*SELP*). These glycoproteins are cell adhesion molecules known to be expressed by endothelial cells and facilitate interactions with platelets, leukocytes, and endothelial progenitors (153). Additionally, *SELE* and *SELP* have been implicated in the progression of various tumor types including breast, pancreatic, and prostate cancer (154-161). Treatment of BMECs with Il-6 *in vitro* caused a 3 and 7-fold increase in expression of *Sele* and *Selp*, respectively, confirming the array data (**Figure 28A, B**). Connecting these results to clinical data, information from Kaplan Meier (KM) Plot show that breast cancer patients whose tumors expressed high levels of E-Selectin Ligand 1, a ligand for *SELE* and *SELP*, had reduced distant metastasis free survival (DMFS), suggesting that targeting these proteins may be beneficial for breast cancer patients with metastatic disease (162) (**Figure 29**).

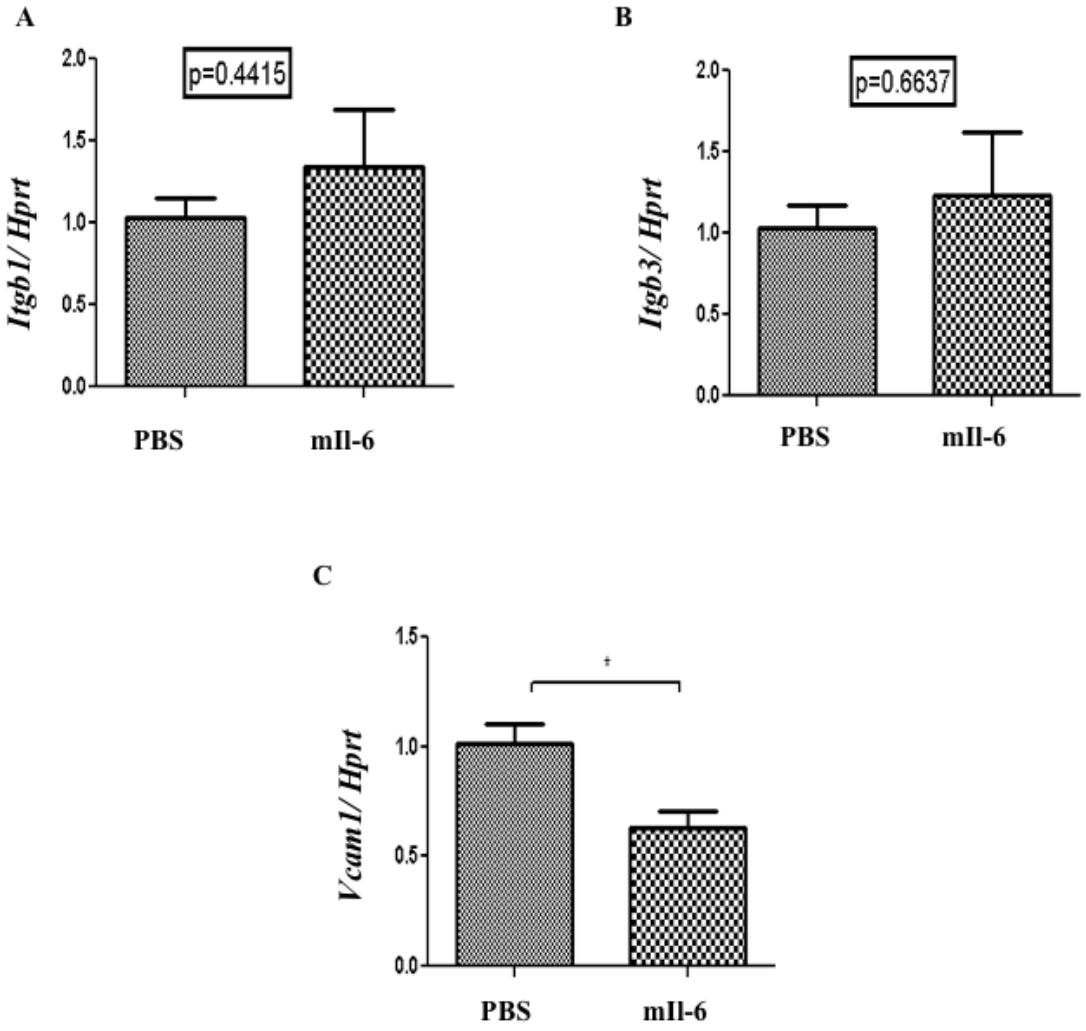

Figure 27: Expression of Integrin Beta1 and Beta3 Do Not Change, while Vcam1 Expression Decreases with Il-6 Treatment in BMECs. A) Integrin Beta1 expression and B) Integrin Beta3 expression do not change significantly with Il-6 treatment. C) VCAM1 levels decrease by 40% in BMECs with Il-6 treatment. N=3 for each analysis. (*=p<.05)

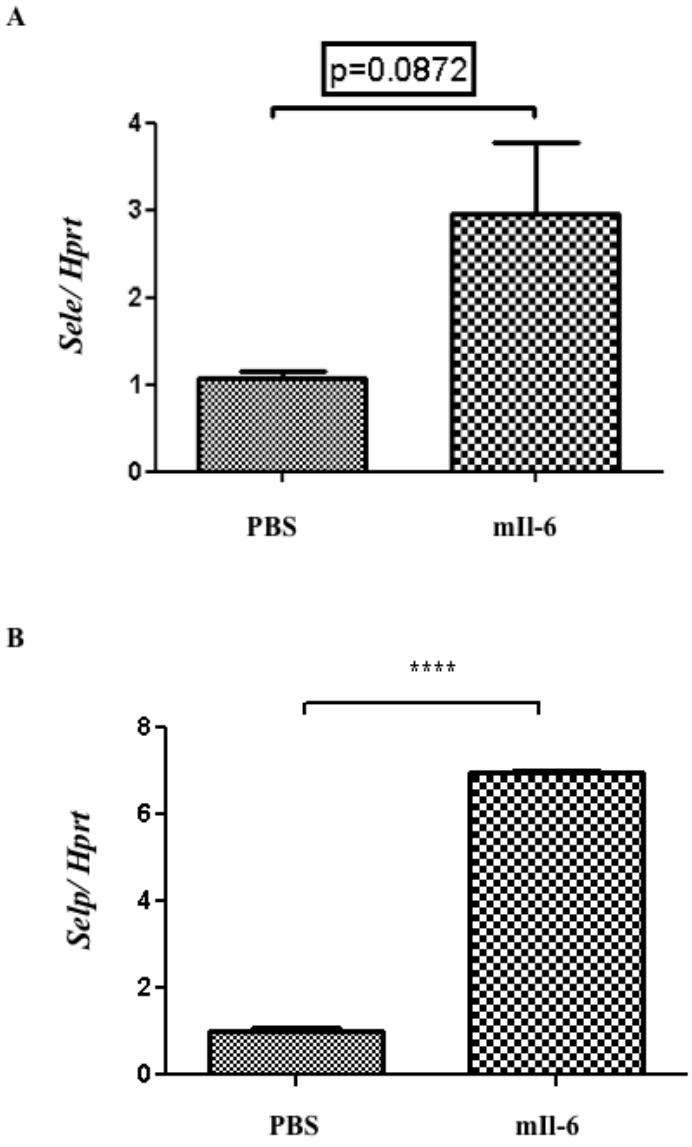

Figure 28: Il-6 Increases Expression of E-Selectin and P-Selectin in primary BMECs *in vitro*. A) E-Selectin levels increase in BMECs treated with 50ng/mL Il-6 for 24 hours. B) P-Selectin levels are significantly increased with this treatment as well (N=3, ****= p<.0001).

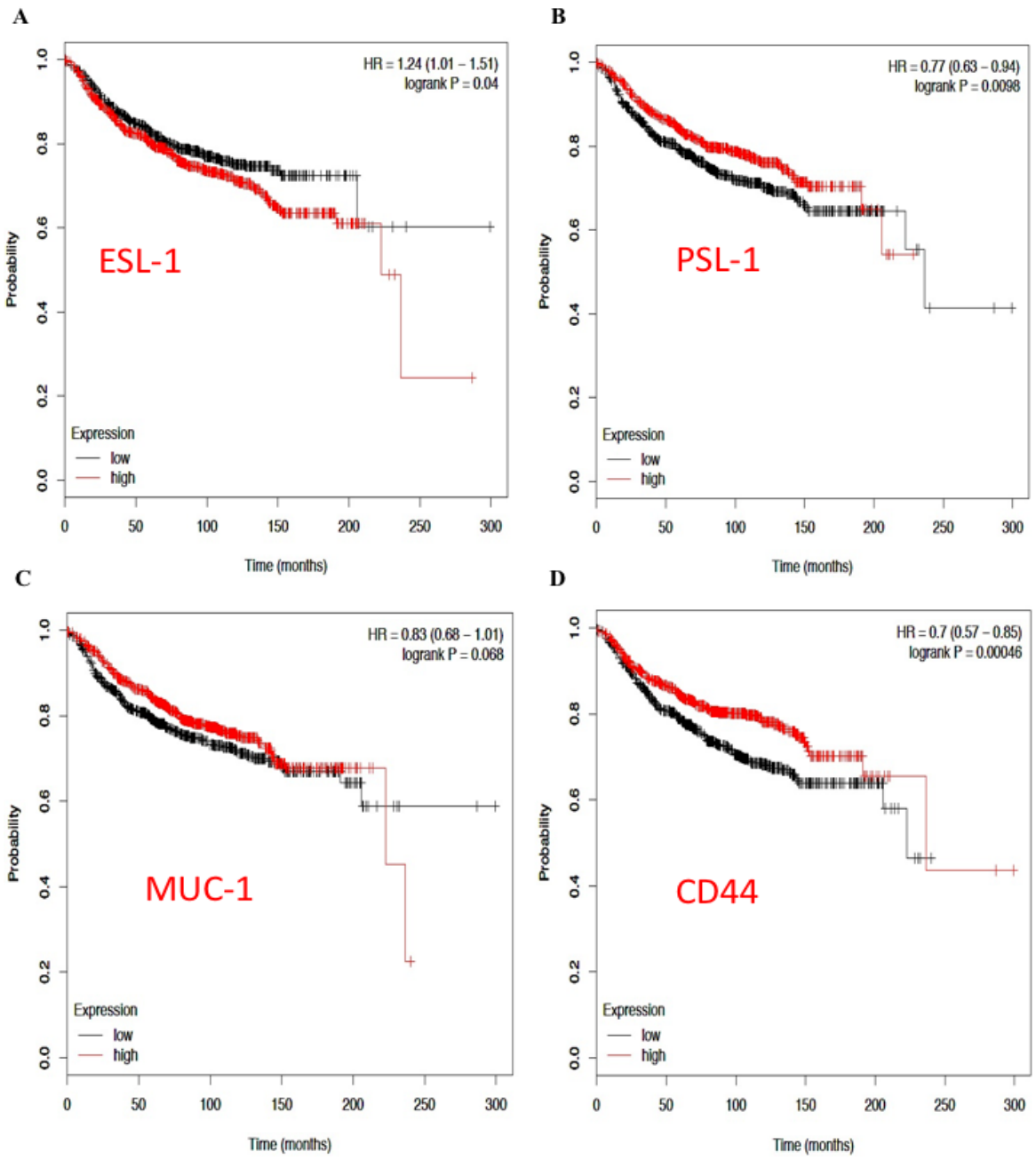

Figure 29: Certain Adhesion Proteins Are Linked to Worse Distant Metastasis-Free Survival in Breast Cancer Patients. Low levels of A) *ESL1* show a better prognosis for DMFS. C) Low levels of *MUC-1* trend toward significance regarding DMFS, while elevated B) *PSL1* and D) *CD44* levels suggest a better prognosis. Source of Data is KM Plot.

Discussion

Breast cancer commonly metastasizes to bone, and in order for the metastatic cells to successfully colonize that secondary site, they must extravasate from circulation by interacting with the bone vasculature. In this chapter, I showed that stromal Il-6 produced by osteoblasts following stimulation of beta-adrenergic receptor signaling promotes the interaction between MDA-MB-231 and 4T1 tumor cells with primary mouse BMECs *in vitro*. Furthermore, I showed that endothelial-derived Il-6 is not required for tumor cell interaction with BMECs, as both tumor cells tested adhered equally to WT and Il6KO BMECs stimulated by the CM of ISO treated BMSCs. Additionally, we further examined expression levels of five proteins known to play roles in cell adhesion and tumor progression. Il-6 treatment increased expression of E-Selectin and P-Selectin in BMEC cultures, but not Integrin β1, Integrin β3, or Vcam1.

IL-6 is a pro-inflammatory cytokine that is synthesized by many different cell types, including macrophages and osteoblasts. In osteoblasts, IL-6 increases the production of RANKL, thus promoting osteoclastogenesis and bone turnover. However, osteotropic tumor cells can also produce this cytokine, leading to tumor survival and progression through propagation of the "vicious cycle "by activating osteoblasts and enhancing bone turnover (14, 33). There are many drugs that target this cytokine, as well as components of the IL-6 receptor, and its specific downstream pathways (39, 163, 164). Regarding breast cancer, IL-6 can induce migration and promote resistance to apoptosis (40, 164). In addition, activation of IL-6 receptor has been linked to both *de novo* and acquired Trastuzumab resistance in HER2+ breast cancer; knocking down this cytokine in MDA-MB-231 cells caused a reduction in bone lesion area in a mouse model of metastatic breast cancer (41, 165). IL-6 has also been reported to affect multiple steps of the metastatic cascade, such as invasion and extravasation: Geng and colleagues report that IL-6 and TNF-α are able to induce an aggregation phenotype in breast cancer cells and promote

invasiveness of MDA-MB-231s *in vitro* (139). Circulating tumor cells express myriad of adhesion proteins that allow them to roll along the endothelium, interacting with corresponding binding partners present on the blood vessels. Regarding bone metastases, certain proteins have been shown to correlate with disease severity and progression (166). Indeed, Yasmin-Karim and colleagues report that prostate cancer cells which express high levels of the E-selectin (*SELE*) binding protein ESL-1 are more aggressive and more likely to metastasize to bone (167). This implicates a direct interaction with bone vasculature for prostate cancer cells, as SELE is an endothelial-specific surface protein.

Of the five genes selected from the qPCR array for verification, E-selecin (Sele) and P-selectin (Selp) expression levels were increased in BMECs treated with Il-6 *in vitro*. These cell adhesion molecules contain an extracellular N-terminus, a calcium-dependent lectin domain, an EGF-like domain, a single transmembrane domain, and an intracellular C-terminal tail (153, 154). SELE is found exclusively on endothelial cells, and *SELP* is expressed by endothelial cells and platelets. It has been known that the vasculature of the bone marrow, spleen, and liver constitutively express *SELE*. Schweitzer *et al.* revealed that *Sele* expression was increased by many different cytokines in mice, such as IL-1β, TNF-α, lipopolysaccharides, and IL-3 (155). In the context of bone homeostasis, Yang and colleagues reported that Esl-1KO mice have severe osteopenia due to decreased mineralization by osteoblasts and increased number, size, and activity of osteoclasts. Intriguingly, treating these genetically altered mice with 1D11, a pan-TGF-β inhibitor, rescues their osteopenia phenotype, linking these two pathways (156). P-selectin (*SELP*) is important for inflammatory responses as well. This adhesion protein, when found on endothelium, promotes leukocyte binding via interactions with P-selectin Ligand 1 (*PSGL-1*). Platelet and monocyte interactions are dependent on SELP-PSGL-1 binding, leading to further inflammatory signals and thrombosis. Additionally, eosinophils and neutrophils are recruited to sites of inflammation via SELP-dependent mechanisms (157).

Various cancers are able to commandeer the biological pathways associated with both SELE and SELP in order to survive and progress. Tremblay and associates reported that SELE is required for HT-29 colorectal cancer (CRC) cell rolling and extravasation through an endothelial monolayer. HT-29s exhibited this SELE-dependent extravasation in both static and dynamic culture systems (159). Moreover, patient data regarding prostate cancer show that metastatic tumors have higher gene expression of ESL-1, a common SELE binding partner, compared to either primary prostate tumors or normal prostate tissue (167). Podocalyxin, another SELE binding partner, was shown to be expressed by metastatic pancreatic cancer and localize mostly to the invasive fronts in histological sections (158). Pertaining to SELP, Coupland *et al.* revealed that endothelial Selp was necessary for B16F1 melanoma metastases to the liver in mice (160). Nasti and colleagues further explored the role of Selp on mammary tumor progression and metastasis. Along with confirming a protective effect against primary mammary tumor growth in SelpKO mice, their study showed that SelpKO mice exhibited reduced lung metastases (161). Interestingly, this effect was due in part to a reduction in CD4+ Foxp3+ regulatory T-cells and elevated levels of interferon gamma (IFNγ). It is unknown whether chronic adrenergic signaling is linked to altered E-selectin and P-selectin activity in the bone microenvironment as it pertains to extravasation and establishment of breast cancer bone lesions. The expression results we obtained need to be further explored *in vivo* and in metastatic mouse models of bone metastases.

One limitation of the co-culture model presented in this chapter is its static nature. Tumor metastasis is a dynamic process affected by blood flow and 3-dimensonal, physical stressors, The use of a parallel plate flow chamber or bioreactor to create a controlled, dynamic model of tumor-bone endothelium will be a useful tool to more accurately assess the effects of stress-induced Il-6 on breast cancer cell extravasation.

Adrenergic signaling is also known to regulate aspects of vascular biology and cardiac function through recruitment of endothelial progenitor cells, increased eNOS expression, and Nf-kB signaling (168, 169). Ciccarelli *et al.* demonstrated that global β2ARKO mice have defects in responding to multiple angiogenic stimuli when subjected to femoral artery resection (170). While we report no direct effect of βAR stimulation with Isoproterenol on BMECs in the context of increased tumor cell interaction in an *in vitro* co-culture system, this relationship should be further explored in an *in vivo* model.

Research documented in this chapter shows that chronic activation of the SNS can affect tumor-to-endothelial interaction via osteoblasts production of IL-6. This cytokine is known to regulate the expression of multiple adhesion proteins, which was reflected in the qPCR array results. Future intentions aim to explore the biological relevance of these stromal-dependent tumor-to-endothelial interactions in murine tumor studies focused on disruption of Il-6 signaling, as well as potentially inhibiting contact between certain adhesion protein pairs, specifically those involving E-Selectin or P-selectin.

CHAPTER IV

Conclusions and Future Directions

Summary of Studies

Tumor metastasis to bone remains a clinical challenge for physicians and a life-threatening phenomenon for patients diagnosed with cancer. The research documented in this dissertation demonstrates that chronic SNS activation alters the bone vasculature in manners that promote tumor establishment in the bone microenvironment in mice, and suggests that βAR stimulation in osteoblasts enhances interaction between breast cancer cells and primary bone marrow endothelial cells (BMECs).

The osteoblasts, which express β2ARs, respond to SNS activation through adrenergic receptor signaling and amplify production of VEGF-A and IL-6 at both the RNA and protein levels. Elevated osteoblastic VEGF-A increases bone vascular density in both mouse metatarsal and endothelial tube formation assays, as well as in mouse models of chronic stress. Disruption of SNS-VEGF-A signaling, either through genetic ablation of the β2AR in osteoblasts, or treating mice with the anti-VEGF-A antibody mcr84, reduces the vascular density expansion caused by SNS activation. Importantly, loss of β2AR as well as mcr84 treatment hinder the ability of MBA-MB-231s, a triple negative breast cancer cell line, to colonization the bone in the context of chronic SNS activation. Upregulated osteoblastic IL-6 promotes physical interaction between breast cancer tumor cells and BMECs *in vitro*, as conditioned media from SNS-activated osteoblasts promotes tumor-endothelial interaction. However, conditioned media from IL6KO osteoblasts, or the addition of an IL-6 blocking antibody, diminishes that tumor-endothelial interaction in culture. These results may be related to adhesion proteins, as IL-6 treatment increases expression of E-selectin and P-selectin in primary BMECs.

Because targeting VEGF-A and/or β2ARs in the bone reduces the effects of chronic stress on breast cancer colonization of bone, these aspects of bone biology warrant further study and could be key for improving treatments in the clinic for patients with osteotropic breast cancer lesions. Currently, bisphosphonates like Zoledronic Acid (ZA), and Denosumab, a neutralizing antibody against RANKL, are the most commonly used regimens for osteolytic lesions caused by breast cancer and multiple myeloma bone lesions. Denosumab has also shown efficacy regarding prostate cancer bone lesions that tend to manifest as both osteolytic and osteosclerotic (171). Although both of these treatments reduce bone pain and improve patients' quality of life, these drugs do not improve survival nor target the tumors directly; they are palliative in nature. Therefore, new therapeutic options must be researched and tested.

Chronic activation of the SNS due to stress and depression are linked to a wide range of pathologies, and creation of pre-metastatic niches is also one of the biological effects of chronic stress. It is estimated that approximately 25% of cancer patients are clinically depressed, and these patients could be at a higher risk of developing a metastatic lesion (172). Palesh *et al*. report that breast cancer patients that experienced a traumatic event had their tumors recur the fastest compared to other patients. Furthermore, the percentage of bone lesions was highest in these "traumatic" patients (50). The work documented in this dissertation, as well as many of the clinical studies cited throughout it, would strongly suggest that addition of either an anti-angiogenic drug or a beta blocker in the early stages of breast cancer development would have a beneficial effect on reducing the likelihood of bone lesions through preventing vascular changes and expression of pro-migratory and inflammatory factors in the bone microenvironment, ultimately increasing survival metrics of patients.

While effects of adrenergic signaling have been documented to affect tumor growth, tumor vasculature, and tumor survival, its effects on the stromal cell compartments in the context of metastasis

have been understudied, especially regarding bone metastasis. The novelty of the research detailed in this dissertation is that a relationship between osteoblastic adrenergic signaling and the exacerbation of breast cancer bone metastasis was experimentally linked to bone vascular changes. Communication between osteoblasts and endothelium is essential for bone development, bone turnover, and bone repair. Chronic SNS signaling in adult mice alters the bone vasculature by increasing its density and elevating expression of endothelial adhesion proteins shown to be involved in successful bone metastasis. Tumors that metastasize to bone benefit from these stress-induced changes, as expansion of the bone vascular network and increased levels of endothelial adhesion proteins in bone endothelium induced by SNS activation increase the likelihood of tumor cells migrating to, docking, and extravasating into bone tissue while in circulation. Furthermore, the proteins responsible for these vascular changes and migratory behavior, namely Vegf-a, Rankl, and Il-6, all promote tumor growth in the bone microenvironment and are all increased by chronic SNS signaling.. These studies highlight bone vasculature as a key component of tumor induced bone disease (TIBD) and emphasize the importance of osteoblast-endothelial cell communication in breast cancer progression, an understudied concept in cancer and bone biology. Further exploration of the mechanisms involved in osteoblast-endothelial cell communication during disease states of bone could lead to effective therapies for patients with bone metastatic lesions.

Vascular Therapies for Metastatic Bone Lesions

The addition of drugs early in treatment regimens that target angiogenesis and blood vessels may prove to be beneficial for patients that present with malignant tumors. Targeting angiogenesis has been explored for decades, and there are multiple types of these drugs used to treat several cancers. Bevacizumab, a monoclonal antibody that targets human VEGF-A, is one of the most well-known anti-

angiogenics. It was approved in 2010 by the FDA for the treatment of breast cancer and exhibited beneficial effects on progression-free survival and overall response rate in multiple clinical trails. However, due to minimal significant effect on overall survival and causing a multitude of side effects, such as hypertension, proteinuria, and congestive heart failure, this drug is now used in very controlled drug regimens for certain breast cancer pathologies (173). Even though these clinical results were disappointing, angiogenesis, notwithstanding, is a hallmark of cancer progression, and current research still suggests benefits from anti-angiogenic drugs. Our research, as well as others, imply that therapies more specifically targeted to VEGF-A:VEGFR2 that are given to patients early in their regimens would be beneficial in treating metastatic bone lesions by possibly preventing vascular expansions in the bone and commandeering of the vascular network by the tumor mass.

Bachelier and colleagues highlighted the importance of tumor VEGF signaling of bone-tropic MDA-MB-231s via shRNA technology. Tumor cells with shVEGF-A had reduced vascularity and were smaller *in vivo* compared to their control counterparts. Furthermore, treatment of mice with both Bevacizumab and the anti-angiogenic small molecule inhibitor (SMI) Vatalanib caused severe reduction in bone lesions caused by the bone-tropic MDAs (174). Cabozantinib, an SMI that targets c-MET and VEGFR2, has been shown to alter the bone microenvironment and affect metastatic bone lesions. This drug caused an increase in osteoblast number, a decrease in osteoclast number, and a modest increase in BV/TV (175). Varkaris *et al.* show that Cabozantinib is effective in the treatment of both primary prostate cancer and lesions present in bone. Further dissection of the mechanism behind this effect revealed that the targeting of VEGFR2 was most effective, and that this anti-angiogenic means of action not only promoted tumor cell death but also decreased vascularity of the tumor mass (176). One could infer from these studies, as well as the information presented in this dissertation, that drugs that prevent

angiogenesis could be used to counter the effects that stress and chronic SNS signaling have on both the tumor itself and the surrounding stroma.

Along with treatments that prevent angiogenesis, drugs that promote vessel normalization have been proposed as a methodology to treat tumors. The vasculature of tumors is leaky and structurally unsound due to constant stimuli that affect vessel establishment and development. As a result, blood flow is compromised, and drug delivery is inefficient. Correcting these structural issues regarding tumor vasculature could lead to improved delivery and potentially tumor static effects. Schadler and colleagues were able to show that aerobic exercise was effective at increasing the delivery of gemcitabine and doxorubicin to PDAC and melanoma tumors, respectively (177). Moreover, these increases in delivery and subsequent tumor cell apoptosis were linked to increased NFAT signaling and elevated levels of endothelial Tsp-1, an anti-angiogenic protein, in both primary tumor cites and the lungs. These data link back to a study by Ghajar *et al.* referenced earlier in this dissertation, which shows that increased Tsp-1 levels are protective against the growth of breast cancer bone lesions (178). Perhaps increased levels of anti-angiogenic proteins restore balance regarding vascular signaling, therefore impeding the commandeering of host biology by tumors. Glycolysis inhibitors have also been proposed to normalize vasculature, as active and sprouting endothelium favor glycolysis over oxidative phosphorylation in manners that are similar to tumor cells (179). The importance of the vasculature cannot be overlooked moving forward regarding therapies for bone metastatic lesions.

Effects of SNS on the Signaling that Regulates VEGF-A Expression in Bone

There remain many unanswered questions pertaining to the SNS-induced increase in VEGF-A seen in these studies. Even though our results show that SNS activity can promote breast cancer bone metastasis through bone vascular changes, the specific mechanisms responsible for these changes need

to be elucidated. Two plausible next areas of research should focus on transcription factors as well as signaling and processing proteins that could be responsible for the elevated levels of this growth factor. The literature revealed that hypoxia-inducible factor 1 (Hif1-α) can induce the expression of pro-angiogenic genes like VEGF-A. Furthermore, S-Y Park *et al.* show that treatment with NE *in vitro* is linked to elevated Hif1-α protein and activity in MDA-MB-231 breast cancer cells, PC-3 prostate cancer cells, and SK-Hep1 hepatocellular carcinoma cells (180). Whether this relationship exists in bone during SNS activation remains to be studied. Manipulation of the transcriptional activity of Hif1-α through mutation or shRNA-mediated knockdown in osteoblasts would illuminate its possible involvement in isoproterenol-induced increases in Vegf-a.

Secondly, certain MMPs have been linked to developmental and tumor angiogenesis in the literature. Proteins that belong to the MMP family cleave ECM components for tissue remodeling and development, as well as certain ECM substrates like growth factors and cytokines that also induce structural and physiological changes. It is well understood that many MMPs are directly involved in the vascular invasion that accompanies formation of the primary and secondary ossification centers during bone development (79, 181). MMP13, a collagenase, and MMP9, a gelatinase, are two of the principal MMPs associated with this process, as genetic ablation of either of these proteinases results in defects in ossification and a disorganized hypertrophic chondrocyte zone (181). Regarding bone metastatic lesions, both MMP13 and MMP9 seem to exert key promotional roles. Nannuru and co-authors revealed that mammary tumors exhibit increased levels of MMP13 at the invasive tumor front that physically contacts the bone (182). This observation also correlated with increased active MMP9 and linked MMP13 to tumor angiogenesis and breast cancer bone lesion colonization (183, 184). Furthermore, MMP13 derived from multiple myeloma was sufficient to promote osteoclast fusion and osteolytic bone destruction (185). Expression, protein, and activity of MMP13 and MMP9 should be tested *in vivo* and

in osteoblasts to determine if these proteins could be related to elevated VEGF-A and vascular density amounts induced by SNS activation.

Link between SNS-induced Vascular Expansion and Activation of Dormant Tumor Cells

Stress and its influences on cellular communication may play a role in awakening dormant tumors, specifically through altering vascular potential and the availability of certain growth factors based on the research presented in this dissertation as well as that of others in the field. Dormancy is defined in biology as cells being in a non-diving state and suspending their physiological functions (186-188). This concept, when applied to tumor biology, has implications for the clinic and for research. Clinically, dormant tumors mean patients have residual disease but are asymptomatic. It is known that many cancer patients will relapse, and this occurs in up to 45% of patients with breast or prostate cancer (189, 190). Many of the residual tumors discovered in these patients will be in their bones, and a majority of the mechanisms behind why these tumors arise, sometimes decades after treatment of the initial tumor, and how to properly treat them, need to be understood (186).

Multiple groups have begun dissecting the mechanisms surrounding tumor dormancy and the specific pathways involved. Primary samples from prostate cancer patients showed that ones with no evidence of disease had increased levels of proteins linked to p38 signaling, suggesting p38 might be a residual disease indicator for prostate cancer (191). Clinical reports regarding breast cancer patients show that low expression of the Leukemia Inhibitory Factor Receptor (LIFR) correlates with bone metastases. Johnson and colleagues further explored this relationship, revealing that loss of LIFR in MCF7s, breast cancer cells with low metastatic potential, caused this cell line to induce greater osteolytic disease in a mouse model. Additionally, knockdown of LIFR alters a wide array of genes associated with dormancy and stem cell behavior (192). Ghajar and collaborators showed that breast

cancer cell dormancy is linked to angiogenic signals in the bone marrow. Tumor cells that did not actively divide resided in vascular niches that contained high levels of thrombospondin-1 (TSP-1), a potent anti-angiogenic protein (193). Indeed, increases in vascular density in the bone microenvironment caused by chronic SNS activation, as explained in Chapter II of this dissertation, would suggest an affect linked to the results found by Ghajar *et al.* Increasing levels of VEGF-A might activate endothelial cells to form vessels and concomitantly reduce TSP-1, a result that may awaken dormant breast cancer cells (178). Also, results from Chapter III are connected to the LIF:LIFR data from Johnson *et al.* IL-6 and LIF belong to the same family of cytokines and have distinct effects of tumor biology (198). The levels of LIF in the context of stress have not been explored, however the data in this dissertation would suggest that high levels of IL-6 would potentially awaken dormant tumors at the expense of pro-dormancy proteins such as LIF. Exposing mouse models of tumor dormancy to chronic stress and assessing dormancy gene profiles, tumor burden, and cancer progression in the bone microenvironments may reveal a mechanism of how stress drives cancer progression by activating dormant tumors.

Social Implications of This Work

The work documented in this dissertation regarding chronic SNS activation and its effect on bone vasculature and breast cancer progression reaches beyond the science, directly impacting many of the health disparities and complications cancer patients experience during a fight with the disease. It has been well chronicled that racial and socioeconomic statuses are linked to cancer progression, treatment, and survival (195). Regarding breast cancer, African-American women tend to be diagnosed at an earlier age, have more aggressive forms of breast cancer such as triple negative breast cancer (TNBC), and have poorer overall survival compared to White and Asian American women. Latina women also displayed a similar pattern (196). As previously mentioned, chronic activation of the SNS via chronic

stress or depression has been linked to breast cancer recurrence and worse overall survival. Poverty and constant discrimination, both at a social and institutional level, can lead to chronic anxiety, stress, and depression. Similar patterns are seen for prostate, lung, and colorectal cancer; screening rates for colorectal cancer are lower in African-American men, and changes in smoking patterns directly correlate with the decreasing deaths in both Black and Latino communities and the interesting increase in deaths among White women (195).

One disturbing observation is that these discriminations regarding cancer continue on even during survivorship (197). Cancer survivors living in low socioeconomic neighborhoods and/ or with low education have a shorter time to recurrence and reduced overall survival. This result could be linked to being uninsured or not being able to afford proper initial care, and scientifically linked to the potential awakening of dormant micrometastatic lesions. In order to resolve this problem, more outreach to these communities and understanding of the groups that need to be treated is required by clinicians and healthcare professionals. Former President of the United States, Barack Obama, signed into the law The Affordable Care Act (ACA), which requires all US citizens to have health insurance and attempts to make coverage and treatments more affordable, regardless of socioeconomic status (198). Greater access to and coverage for preventative care and screens, such as mammograms and colonoscopies, could help reduce cancer rates and deaths. Although more research connecting psychosocial and emotional factors to cancer progression is needed, it is clear that stress, in multiple ways, exacerbates cancer and needs to be focused on during treatment.

APPENDIX A

Extraction and Culture of Primary Mouse Bone Marrow Endothelial Cells (BMECs)

Introduction

Cell culture has become an integral part of biological research over the past century. Generally, cell culture involves the removal of tissue or cells from their natural environment and placement into an artificial one that best represents an appropriate *in vivo* setting. Cell culture overarchingly incorporates the usage of both primary cells, cells taken directly from an animal, and established cell lines that have been passaged *in vitro* for long periods of time. Most notably, the questionably unscrupulous culture of the HeLa cervical carcinoma cell line by Gey and colleagues at Johns Hopkins in 1952 and the design of defined cell culture medium by Eagle in 1955 were crucial catalysts in cell culture becoming routine in wet science labs in the biological sciences (199). The development of cell culture techniques has lead to many discoveries regarding cellular behavior, understanding of myriad of diseases, and genetic manipulation tools.

Cell lines have many beneficial attributes; they are relatively easy to culture and grow, are highly proliferative, and are widely accepted and published by many different researchers and scientific communities. Furthermore, cell lines have very long lifespans, as many of them are either immortal or continuous, and can be modified via transfections or transductions are high efficiencies. One glaring limitation of cell lines, however, is that over time, a line becomes more phenotypically and genetically different from the tissue of origin (200). When relating experimental results of non-transformed cell lines back to the tissue it represents, this delineation can be problematic.

A strong cell culture practice to circumvent cell line culturing issues is the extraction and use of primary cells. Although primary cells tend to require more maintenance and have a limited lifespan *in*

vitro, because these cells are isolated directly from tissues of interest, they are more reflective of an *in vivo* model (201). Furthermore, primary cells contain low levels of mutations and are able to behave naturally in culture.

In order for the experiments discussed in this dissertation to be relevant to bone vasculature and bone biology, it is essential that the endothelium used be derived from the bone tissue and, therefore, maintains many of its unique genetic and phenotypic properties in an artificial system. In order to do this, two existing protocols were adapted and merged, one from the Vanderbilt Center for Bone Biology that explains how to extract bone marrow stromal cells from mice, and a second from a manuscript by H. Sekiguchi *et al*. that focuses on isolation of endothelial progenitor cells from bone marrow (114). This appendix lists out the materials used in the extraction of mouse bone marrow endothelial cells and the steps of maintaining these cells in culture.

Materials

1.) Autoclaved 1.5mL and 0.5mL Eppendorf tubes (1 per pair of long bones)
2.) Appropriate Tube Racks
3.) 18-gauge Needle
4.) 4-well Chamber Slides
5.) Dissecting tools
    a. Scalpel
    b. #10 Blade
    c. Curved Scissors
    d. Forceps
6.) Kim Wipes
7.) P1000 Pipette and Pipette Tips

8.) Sterile Hood with Laminar Flow

9.) 4ug/mL Fibronectin Solution, (Life Technologies, 33016-015)

10.) 5% Endothelial Growth Medium (EGM), (ScienCell, #1001)

a. Media contains 5% Fetal Bovine Serum, 1% antibiotics, and 1% Endothelial Growth Supplement. All solutions are provided from ScienCell

Extraction Methods

1.) Prepare 4-well chamber slides by coating with 300-500uL of 4µg/mL Fibronectin solution. Warm for 30min in 37°C incubator.

2.) Pierce the 0.5mL tube bottom with the 18-gauge needle.

3.) Place 0.5ml Eppendorf tube in the 1.5ml Eppendorf tube.

4.) Add 1 ml of Endothelial growth medium (EGM) to the tubes. Note that the EGM should be allowed to pass through the hole created with the 18-gauge needle. The 0.5 ml punctured Eppendorf tube will support bone within the 1.5 ml Eppendorf tube during centrifugation step.

5.) Dissect long bones (Femur and tibia. Humeri are optional) from euthanized mouse using dissection tools.

6.) Cut off distal and proximal epiphyses of all long bones harvested. Place each pair of bones into 0.5ml punctured Eppendorf tubes containing 1mL of EGM, with the widest part of bone down (distal femur, proximal tibia, proximal humerus).

7.) Centrifuge 13.2x1000 rpm at 4°C for 2 minutes.

8.) Use P1000 pipette tip to re-suspend pellet in the endothelial cell medium by pipette.

9.) Pool cells collected from each genotype or mouse depending on the study design.

10.) Suction off the Fibronectin solution and add at least 250uLs of EGM to each well. Then, add equal number or equal volume of cells to each chamber.

Culturing BMECs Methods

1.) Culture in EGM for 6-7 days. Replace medium with fresh medium to remove non-adherent cells
2.) Replace medium every 2-3 days with fresh EGM to remove non-adherent cells and to replenish growth factors for the BMECs.
3.) Verify BMEC identity using Immunofluorescence, checking for markers such as Cd31, Cd34, and Ve-Cad. Also, Matrigel Tube Formation Assay is a functional assay to verify BMECs.

Verification Results

In order to analyze how representative of endothelial cells the BMECs were, I chose to perform two separate experiments. The first was an *in vitro* immunofluorescent assay of BMECs cultured on fibronectin-coated plastic. The imaging results show that these BMECs were CD31 positive, a protein expressed on bone vasculature (202). Additionally, certain cells were also Ng2 positive, a common marker of pericytes, which is another cell type found in the sinusoidal vascular niche of the bone. The second experiment examined the functional behaviors of these BMEC cells. After being cultured on fibronectin-coated plastic plates for 7 days, BMECs were treated with accutase, collected, and plated on matrigel coated-wells of a 24-well plate at 30,000 cells/ well. Bright field microscopy shows that after 12 hours of 50ng/mL Vegf-a treatment, BMECs formed a complex vascular network compared and tube length increased 25% when compared to PBS-treated BMECs **(Figure 30)**.

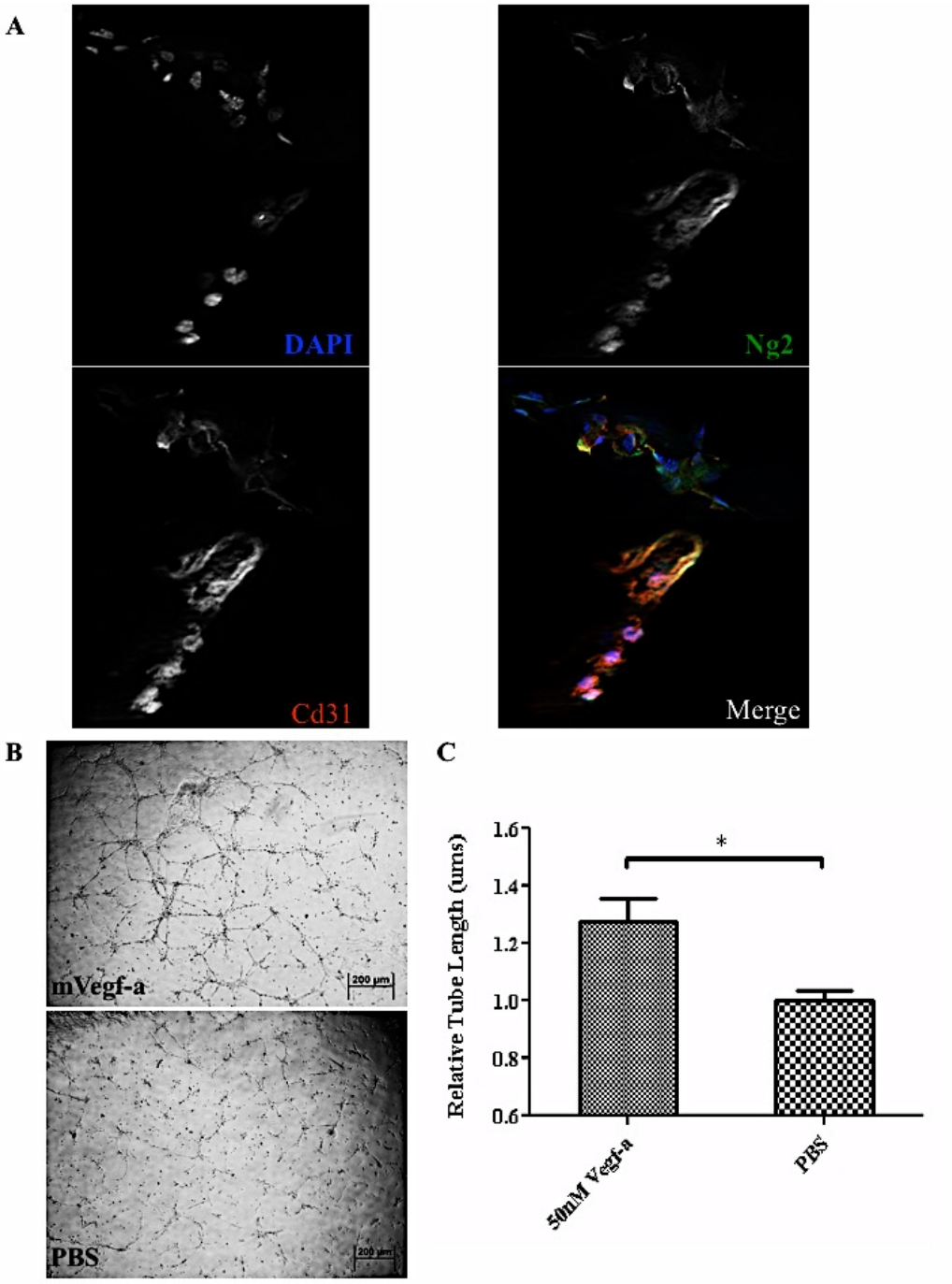

Figure 30: Endothelial Cells Harvested from Bone Marrow (BMEC) Express Endothelial Markers and Are Vegf-a Responsive. A) Fluorescent staining reveals CD31 (red) and NG2 (green) positive cells in BMEC culture. B) BMECs cultured on matrigel respond to 50ng/mL mVegf-a treatment by creating a tube network. C) Quantification of tube length of matrigel assay. (N=6, p=0.0129)

APPENDIX B

TRIzol and Alu qPCR-based Quantification of Metastatic Seeding within the Skeleton

The data presented in this appendix are published in *Nature Scientific Reports* under the same title. Some words and figures have been edited for this dissertation.

Introduction

Numerous imaging technologies exist for assessing skeletal tumor burden in preclinical cancer metastasis models, but all require a well-established tumor to generate sufficient signal. Smaller numbers of metastatic cells can be detected with flow cytometry, but this approach is costly, requires marrow flushing, and is prone to high inter-sample variability. Understanding the mechanisms that drive early skeletal establishment of metastatic cancer cells requires more sensitive and quantitative methods than those currently in common use. One such method relies on the presence of Alu tandem repeats in the human genome, which was first documented three decades ago (203). These short, interspersed fragments are ~300 bp retrotransposons, repeated more than 106 times per genome, and exclusively in higher primates. The vast number of these sequences has allowed them to be used as a very robust detection tool in anthropology and forensics for identifying human elements in ancient bone samples and remains (204, 205). The potential for using real-time qPCR amplification of human repeats to accurately quantify small numbers of cells *in vivo* in scientific investigations has been known for more than 20 years, but this technique has had limited value due to high background signals from human contamination and the challenges of consistent DNA extraction across different tissue types (206, 207).

Technical difficulties inherent in tissue extraction of DNA are compounded in bone. The

entrapment of DNA in the calcified organic material of bone and shells is beneficial for archaeologists and paleontologists, as these chemical interactions can stabilize and preserve DNA for centuries (208, 209). However, these same interactions make the process of extracting DNA from bone difficult, as it binds with hydroxyapatite and matrix proteins such as collagen (210-212). Our objectives were to improve upon existing methods of nucleic acid extraction from bone and to utilize genomic human Alu repeats in xenograft models to establish a fast, reliable, inexpensive and highly-sensitive technique for earlier quantification of bone metastatic human tumor cells within skeletal tissues. Specifically, we set out to find a method which would allow researchers to easily acquire DNA and RNA from the same sample of bone tissue and then use these samples to accurately quantify disseminated tumor cells and corresponding host gene expression in order to determine which stromal factors contribute to metastatic establishment.

Methods

TRIzol DNA and RNA Extraction

1 mL of TRIzol reagent was added to each powdered tissue sample (30-90 mg fresh tissue weight) on ice, followed by 10–30 sec of vortexing, to ensure that any clumps of tissue were dispersed. Samples were incubated at RT for 5 min to allow for lysis and disruption of cells. To each tube 200 µ L of chloroform was added, followed by 30 sec of shaking/inversion and a 5 min incubation at RT. Samples were then centrifuged at 16000 Å~ g for 10 min at 4 °C to separate RNA into aqueous phase. 350 µ L of aqueous phase were carefully transferred to another microcentrifuge tube, and the RNA was precipitated with 500 µ L of isopropanol at RT for 5 min. Samples were centrifuged at 16000 Å~ g for 10 min at 4 °C to pellet RNA. Supernatant was removed and the pellet was washed with 1 mL of 70% EtOH, followed by a brief centrifugation at 5000 Å~ g for 5 min. The supernatant was carefully

removed and samples resuspended in 40-100 µ L of DEPC-treated water, then incubated at 65 °C for 30 min to dissolve the RNA.

After RNA extraction, the remaining aqueous layer from each sample was very carefully removed. Brief centrifugation for 5 min at 16000 Å~ g was necessary to separate phases if interphase disruption had occurred. To each sample, 400 µL Back Extraction Buffer (BEB), which is an aqueous solution of 4 M guanididium thiocyanate, 50 nM sodium citrate and 1 M Tris, was added. After 10–30 sec of vortexing, the samples were centrifuged at 16000 Å~ g for 15 min at RT. The aqueous phase was transferred to a new tube and DNA precipitated with 400 µL of isopropanol for 5 min at RT.

DNA Purification

DNeasy Blood & Tissue Kit from QIAGEN was used according to the manufacturer's instructions. Briefly, bone samples were snap frozen in liquid nitrogen, then pulverized using a mortar and pestle, and up to 100 mg of sample were placed into a 2 mL microcentrifuge tube in order to begin the purification. The steps described by the kit involve lysing of samples with a proteinase K-containing buffer, binding the DNA to the DNeasy Membrane of the DNeasy mini spin columns during centrifugation, 2 wash steps to remove impurities and enzyme inhibitors in the samples, and elution of the desired DNA in TE buffer or water.

Proteinase K method: samples were snap frozen in liquid nitrogen, then pulverized with a mortar & pestle and placed into a 2 mL microcentrifuge tube. 1 mL of Proteinase K lysis buffer (10 nM Tris, 100 mM NaCl, 10 nM EDTA, 0.5% SDS, 400 µ g/mL Proteinase K) was added to each bone sample and then mixed by vortexing and pipetting. Samples were incubated for 2 hr at 60˚C, with intermittent mixing before debris were precipitated with excess NaCl (6 M). After centrifugation, supernatant was removed and DNA precipitated with isopropanol. Each pellet was washed with 70% EtOH and

resuspended in TE or water. Cell number data was approximated using a standard curve established by adding log-fold dilutions of human MDA-231 cells to whole murine bones *ex vivo*.

Quantitative PCR

Real-time PCR was performed using TaqMan gene expression assays or SYBR Green on a BioRad CFX96 Real Time System. Taqman probes/primers were from Applied Biosystems. For RNA experiments, cDNA was generated using the High Capacity Reverse Transcriptase Kit (Applied Biosystems #438814). Results were analyzed using standard curve quantification or ddCt methods. The following primers and conditions were used: Human Alu, Fw: YB8-ALU-S68 5′ -GTCAGGAGATCGAGACCATCCT-3′, Rev: YB8-ALU-AS244 were 5′ -AGTGGCGCAA TCTCGGC-3′, Probe: YB8-ALU-167 5′ -6-FAM-AGCTACTCGGGAGGCTGAGGCAGGATAMRA-3′ . Mouse β -actin (Mm00607939_s1) was used as an endogenous control to normalize each sample and gene. PCR reactions were performed in a 10 μL volume using 0.5 μ l TaqMan probe, 100 ng cDNA template, 5 μL TaqMan Gene Expression Master Mix (Applied Biosystems, Foster City, CA), and 2.5 μL DNase/RNase molecular grade water (Ambion, Austin, TX).

All TaqMan assays were performed using the following PCR conditions: denaturation at 95 °C for 15 min followed by 40 cycles of denaturing at 95 °C for 10 sec, and annealing at 60 °C for 1 min. Reactions were run in duplicate.

All SYBR Green primer pairs were validated for specificity using a Tm gradient protocol prior to the experiments performed in this manuscript. eGFP expression was assessed from RNA that was isolated from hindlimb bones of athymic nude fox3pnu/nu female mice aged 4–6 weeks, which contained a certain spiked number of GFP-transduced MDA-231VU human breast cancer cells. RNA was converted to cDNA using the High Capacity cDNA Kit from Life Technologies as per the

manufacturer's instructions, and we utilized SYBR Green technology to measure gene expression. A serial dilution of MDA-231VUs was used to create a standard curve for eGFP expression. The expression of mouse HPRT, a common housekeeping gene, was also measured to assess the quality of the samples. Each reaction was performed in triplicate, and each sample was plated in technical triplicates. Using the Ct value of the y-intercept of the standard curve as a representation of 1 cancer cell, we were able to correlate the number of cancer cells the eGFP qRT-PCR yielded to the number of cells spiked into the mouse bones.

Animal Models

All experiments using live mice were performed in accordance with the Guidelines and Regulations for the Care and Use of Laboratory Animals in AAALAC-accredited facilities, and were approved by the Institutional Animal Care and Use Committee at Vanderbilt University Medical Center. Mice were group housed in plastic cages (n = 5/cage) under standard laboratory conditions with a 12-h dark, 12-h light cycle, a constant temperature of 20 °C, and humidity of 48%. Mice were fed a standard rodent diet (Pharma Serv, Purina Rodent Laboratory Chow 5001; Framingham, MA). Nude mice were housed in sterile conditions and fed autoclaved standard chow.

Intracardiac MDA-MB-231 Model

MDA-231VU cells were selected by serial *in vivo* passaging of GFP-expressing MDA-MB-231 cells. Briefly, cells were injected via intracardiac method, and GFP-positive cells were harvested from the long bones. The highest 10% of GFP-expressing cells were sorted via FACS. MDA-231VU cells were cultured in 10% FBS DMEM with 1% penicillin/streptomycin. Cells were trypsinized at 70–90% confluence, rinsed and re-suspended in cold PBS at 106 cells/mL. Athymic nude fox3pnu/nu female

mice aged 4–6 weeks were anesthetized and injected in the left cardiac ventricle with 100 μL of cell suspension (10^5 MDA-231VU cells).

Chronic Immobilization Stress (CIS)

CIS was carried out by placing fox3pnu/nu in 50 mL laboratory conical tubes, perforated for adequate air supply, 2 hours daily, for 10 days until the time of intracardiac injection.

Intratibial Injections of MDA-231VU Cells

MDA-231VU cells were cultured as previously stated. Cells were trypsinized at 70–90% confluence, rinsed, and re-suspended in cold PBS at 107 cells/mL. Athymic nude fox3pnu/nu female mice aged 4–6 weeks were anesthetized using isoflurane, and the mice were injected in the tibias at the proximal epiphysis with 10 μ L of cell suspension (ranging from 0–105 MDA-231VU cells). Mice we sacrificed after a certain number of days, and whole hindlimb DNA was harvested in order to perform Alu and β -actin qPCR.

Imaging

Fluorescence data were obtained with the Maestro™ *in-vivo* fluorescence imaging system (Cambridge Research & Instrumentation) using 480 nm excitation and 515 emission filters to discriminate eGFP. Luminescence data were acquired with the IVIS 200® (Perkin Elmer) imaging platform.

FACS

BMSCs and MDA-231VU cells were trypsinized and counted. MDA-231VU cells were spiked

into $3e^6$ mouse BMSCs. Cells were discriminated based on cell size and granularity using forward and side-scatter analysis. Nonviable cells were gated out of further analysis. GFP gating was based on MDA- 231VU run alone without BMSCs as a positive control and BMSCs run alone without MDA-231VU as a negative control. GFP analyses were conducted on a BD LSRII flow cytometer (Franklin Lakes, New Jersey, USA).

For cell-sorting experiments, MDA-231VU cells were trypsinized and sorted into 10 μL of media using a BD FACS Aria III cell sorter. Cells were discriminated based on cell size and granularity using forward and side-scatter analysis. Nonviable cells were gated out of further analysis.

Results

Several established nucleic acid extraction techniques were systematically evaluated and we found that a modification of the TRIzolTM protocol using a back extraction buffer (TRIzol-BEB method) allowed for the most efficient extraction of DNA from bones. Yields were superior to those obtained with a commercial kit (DNeasy kit, Qiagen) and another commonly used protocol based on proteinase K digestion (**Figure 31a-b**). It is important to note here that RNA expression data and DNA can be extracted from the same sample with the TRIzol-BEB method, while the other techniques yield only genomic information to be quantified. Other methods of DNA extraction from bone, which did not consistently yield serviceable DNA, included using EDTA decalcification, NaOH and boiling, or other TRIzol modifications recommended by the manufacturer (data not shown). For TRIzol-BEB DNA extraction, frozen samples were pulverized using a carbon steel mortar and pestle, previously cooled in liquid nitrogen. By keeping the surface of the pestle between -100 and 0 °C, we were able to exploit the Leidenfrost effect, which slows the evaporation time of liquid nitrogen and allows for nucleation of the suspended sample powder on the collection tool, thereby significantly reducing contamination and

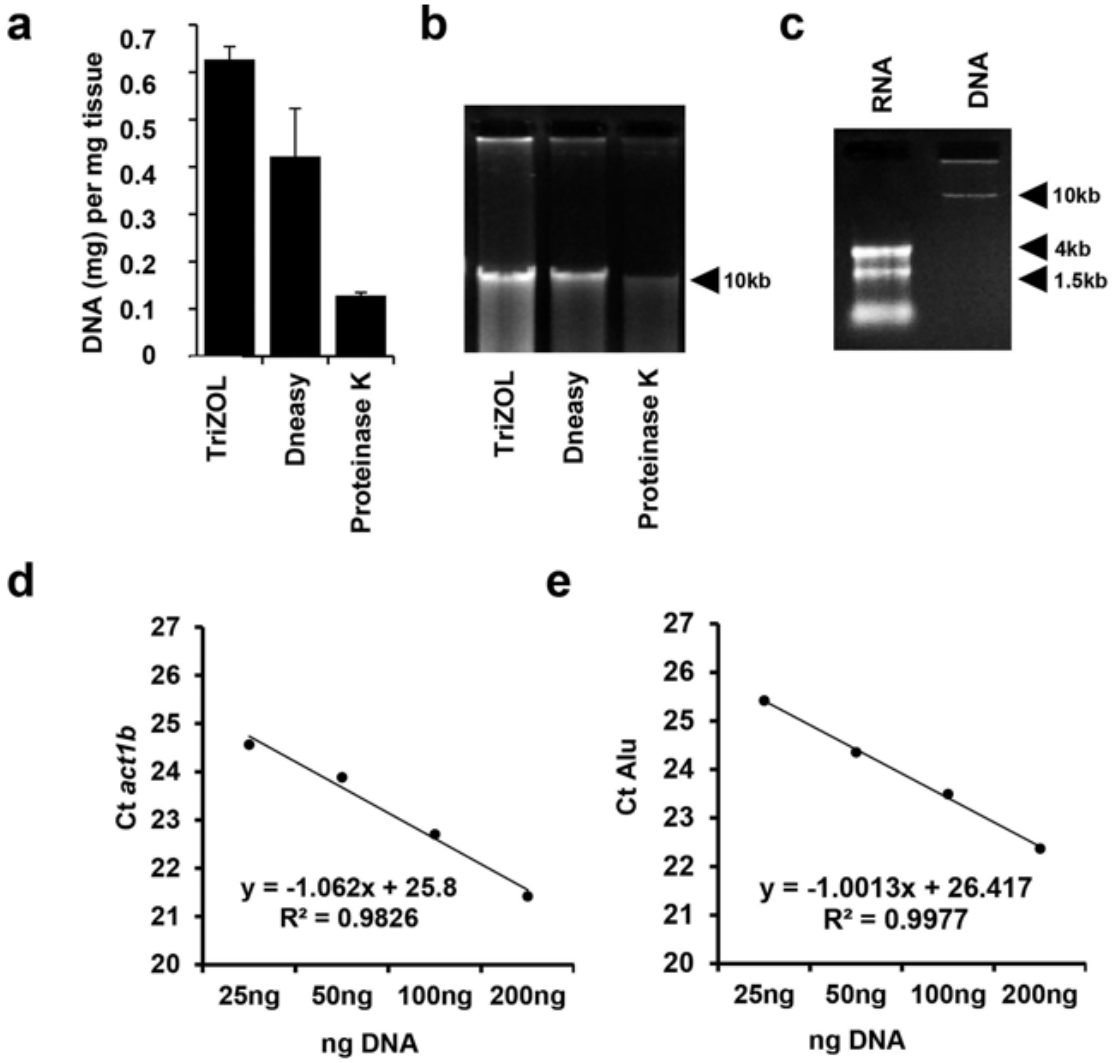

Figure 31. PCR-grade Quality DNA and RNA from TRIzol-BEB Extraction: a) The concentration of DNA samples from mouse bones using 3 different protocols was determined by measuring UV absorbance. b) Electrophoresis of DNA extracted from mouse tibiae using different protocols on a 1% (wt/vol) agarose gel in 0.5x TAE running buffer (2.0 μg of DNA loaded in each lane). c) RNA and DNA extracted with TriZOLBEB from the same bone sample were run on a denaturing gel, showing no evidence of cross contamination in the samples. d) TriZOL-BEB method allows for extraction of DNA and RNA from bone tissues. Alu qPCR of samples with 103 MDA-231 cells spiked into a mouse tibia (d) with corresponding mouse b-actin expression. e) using up to 200 ng DNA extracted from bone tissue, (n = 3).

sample loss. Powdered samples were then resuspended in TRIzol and thoroughly vortexed before proceeding with extraction and precipitation. The range of RNA yield was 0.23–1.24 μg per mg of starting tissue, ($\bar{x}$ = 0.63 μg/mg of tissue). Cross-contamination was not detectable in the RNA or DNA, which were extracted from the same sample, as shown by gel electrophoresis (**Figure 31c**).

In addition to problems from RNA-DNA cross-contamination, efficient PCR of nucleic acid extracts from bone can be inhibited by excess Ca2+ ions and protein impurities, which are not detectable on agarose gel analyses, but RNA and DNA extracted with the TriZOL-BEB method showed no evidence of PCR inhibition, as shown by: A260/A280 ratios between 1.71 and 1.97 ($\bar{x}$= 1.85 for DNA) and 1.54 and 2.10 ($\bar{x}$ = 1.89 for RNA) (**Figure 32a–d**), and linear qPCR amplification values of bone mouse β-actin in serial dilutions (**Figure 31d),** with starting DNA concentrations as high as 200 ng. Alu detection of 103 human MDA-MB-231 breast cancer cells in 20ul PBS pipetted directly, "spiked", into bone samples (~75 mg of tissue), by qPCR showed no evidence of either degradation or inhibitors in the extracted samples, as shown by slope and R2 of Ct Alu plot (**Figure 31e**), even at 10-fold DNA concentration. In both RNA and DNA extraction, inhibitor carryover at the precipitation step could be greatly reduced by using isopropanol extraction rather than ethanol and salt (213).

Though qPCR of primate Alu repeats has been used routinely in forensics and anthropology, attempts at using Alu qPCR to quantify human tumor cells in xenograft models have been hampered by extraction difficulties and background signal from human DNA contamination. Genomic DNA extracted using our modified TRIzol-BEB protocol was used for Alu qPCR and gave accurate linear quantification of 101 to 106 human cell numbers from serial dilutions of MDA-MB-231 cells spiked into 106 murine bone marrow cells (**Figure 33a**). Accurate cell number counts were also seen when Alu qPCR was used

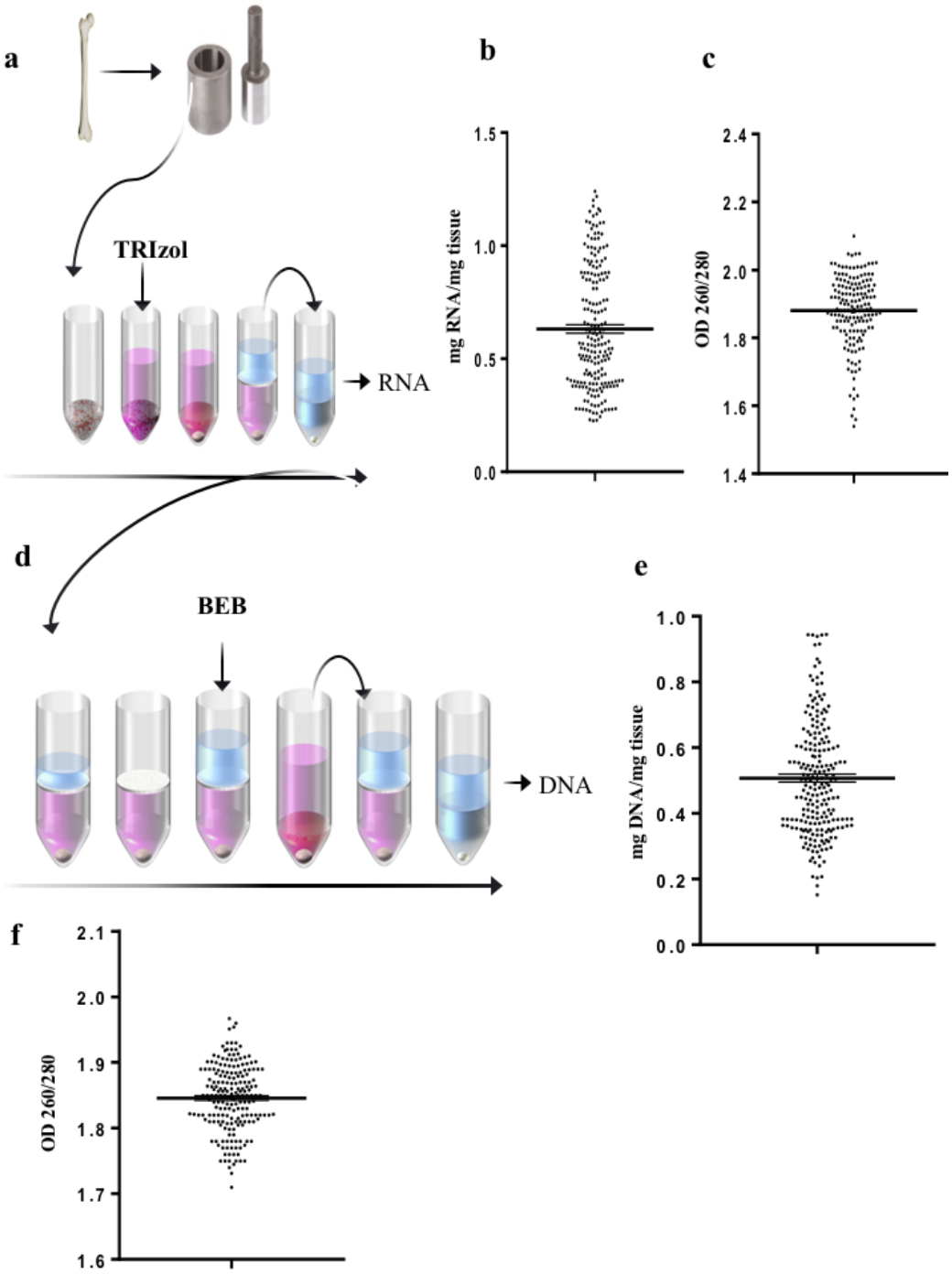

Figure 32. TriZOL-BEB Extraction Overview: a) Frozen tissue was pulverized, then TriZOL was added to each sample and immediately vortexed. After chloroform extraction, RNA was precipitated with Isoproranol, washed, and resuspended. Average RNA yield and 260/280 from mouse bones (b, c) n=200. Following RNA extraction, residual aqueous layer was removed, BEB was added followed by at least 30s of vortexing of each sample (d). Aqueous layer was removed and sample DNA precipitated with isopropanol, washed, and resuspended. e) & f) Average DNA yield and OD 260/280 after TriZOL/BEB method, n=200. Images created by JPC.

to count MDA-MB-231 cells that were spiked directly into entire pulverized mouse femora (**Figure 33b**), demonstrating that the combined methods of TRIzol-BEB extraction and Alu qPCR provide a sensitive method to quantify disseminated human metastatic cells in bone tissue.

Although we were able to detect the presence of 1 human cell within 106 mouse bone cells (**Figure 33a**) and 10 human cells per bone (**Figure 33b**), the accuracy of these data is limited by the inherent imprecision of using serial dilutions to isolate a single cell. To overcome this technical limitation and determine the maximum sensitivity of the method, we used fluorescence assisted cell sorting (FACS) to single-cell sort between 1 and 64 GFP-expressing MDA-MB-231 cells into 10 μL of media, which was added directly to an entire crushed mouse humerus, containing approximately 107 bone cells. After using TRIzol-BEB extraction to obtain gDNA from these samples and performing Alu qPCR, we were able to distinguish the difference in signal between 1 and 2 cells (**Figure 33c**), both of which were above background.

Among currently used techniques for quantifying cell numbers, flow cytometry at present has the most sensitivity, theoretically capable of detecting a single cell within any population of cells. We compared its sensitivity to the TRIzol-BEB-Alu qPCR technique for quantifying cell numbers *ex vivo*, by serial dilution of human MDA-MB-231 cells into bone marrow cells flushed from mouse femora. Quantification of MDA-MB-231 cells by flow cytometry, though very precise, estimated the cell counts at 1/3 of the actual number (**Figure 33d-e**). Furthermore, the background signal in the flushed marrow limited the sensitivity to 1 in 105 cells, which is less than what was achieved with qPCR of Alu sequences (**Figure 33c**). These results demonstrate that qPCR of Alu repeats is more accurate, precise, and sensitive than FACS for the detection of human cancer cells in mouse bones. In addition to being more expensive, flow cytometric methods are also technically hampered by the requisite of flushing the marrow from the bone in order to obtain cells. Though marrow extraction techniques have been in the

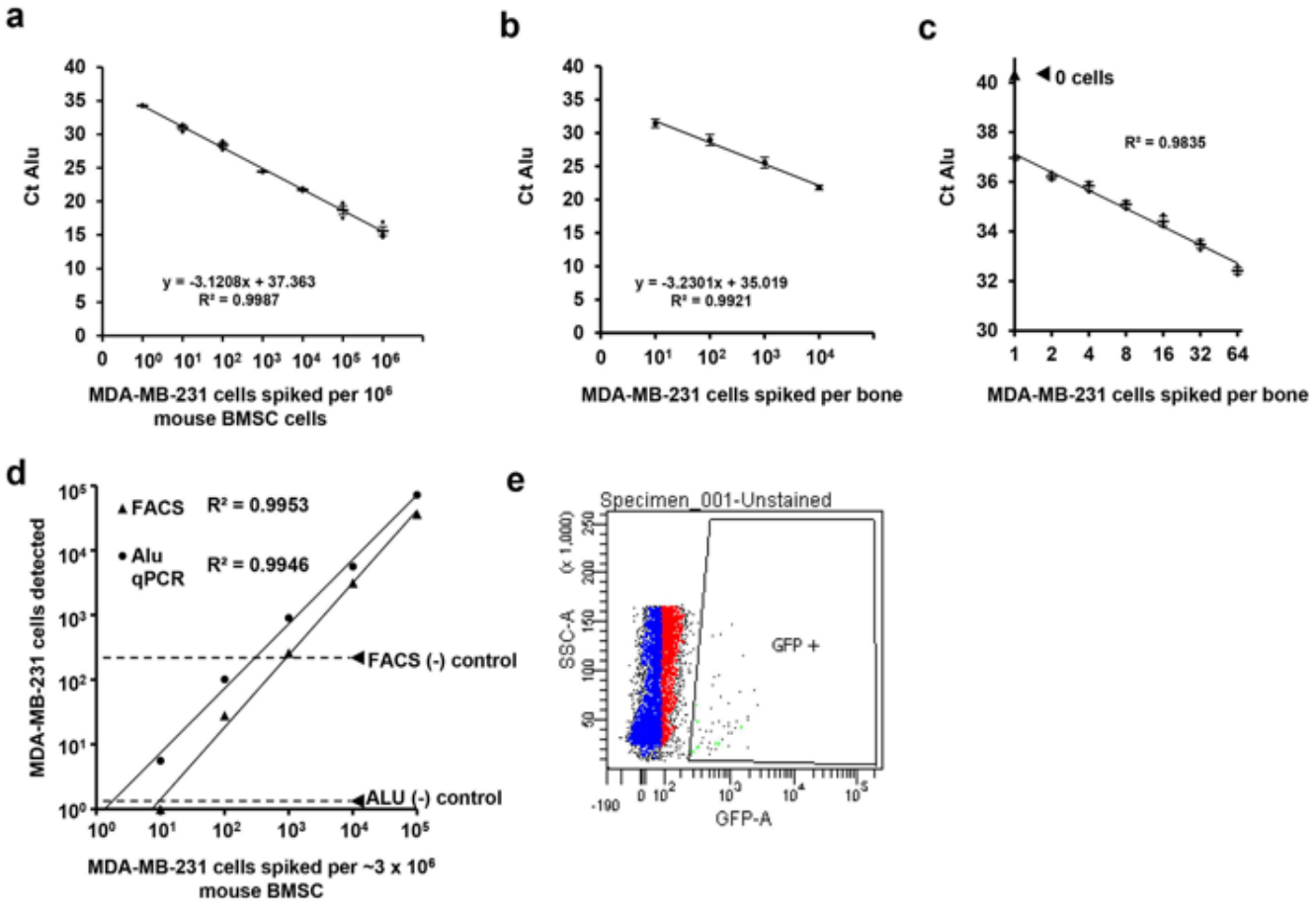

Figure 33. Alu PCR Is a Sensitive Technique for Detecting Xenograft Cells within the Bone: Correlation of ct of Alu with number of human MDA-MB-231 cells spiked into murine BMSC (a) and whole mouse femora (b). c) Cell number could be quantified by Alu qPCR from low numbers of MDA-MB-231GFP sorted into entire mouse humerii. Comparison of sensitivity of FACS with Alu qPCR (d) in detecting MDA-MB- 231-GFP cells spiked into 106 mouse BMSCs. Dashed lines are placed at the level of background signal from negative controls (no human cells) using the gating for eGFP shown in (e), n = 3.

literature since 1945, these methods do not allow an exhaustive removal of cells from the bone, which is needed to consistently locate small tumor foci by FACS or histology. Metastatic tumor cells in bone typically colonize near metaphyses rather than in the diaphyseal marrow and most of these cells remain undisturbed after marrow flushing (**Figure 34a–d**), thereby preventing subsequent FACS analysis of the tumor cells detection.

In the commonly used preclinical models of bone metastasis, it has been speculated that very few of the metastatic cells survive, and that most die over the course of the first week, resulting in a trough of bioluminescent signal during this first week. Attempts have been made with fluorescence or bioluminescence approaches to quantify the events in the early hours or days of metastatic establishment, but these techniques are limited by low reporter gene expression seen in metabolically quiescent cells, limited depth of penetration and scattering of signal, multiple layers of tissue between deep metastatic cells and the detector, and by the relative opacity of dense tissues like bone (214, 215). Given these limitations, we applied the Alu qPCR technique to reveal the fate of bone metastatic cells in the intracardiac mouse metastasis model, and compared the results with eGFP fluorescence data and eGFP RNA expression from the same samples. According to Alu qPCR, 10–100 cells arrested in any one long bone at 3 hours post intracardiac injection, and cell number increased steadily until mice were sacrificed at 14 days (**Figure 35a**). In contrast to the increasing number of cells quantified by Alu qPCR, eGFP qPCR of MDA-MB-231 cells that express eGFP driven by the CMV promoter (**Figure 36a**) showed a decrease from d1 to d7 that would suggest a reduction in cell number in the tissues. When *in vitro* eGFP and Alu qPCR signals were compared from MDA-MB-231 cells alone, the slopes were not significantly different (**Figure 36a–b**) which excludes the possibility of differences in qPCR efficiency between eGFP cDNA and Alu genomic DNA. The discrepancy between *in vivo* and *in vitro* Alu DNA vs. eGFP RNA signal may be due to metabolic changes in tumor cells, which are known to affect

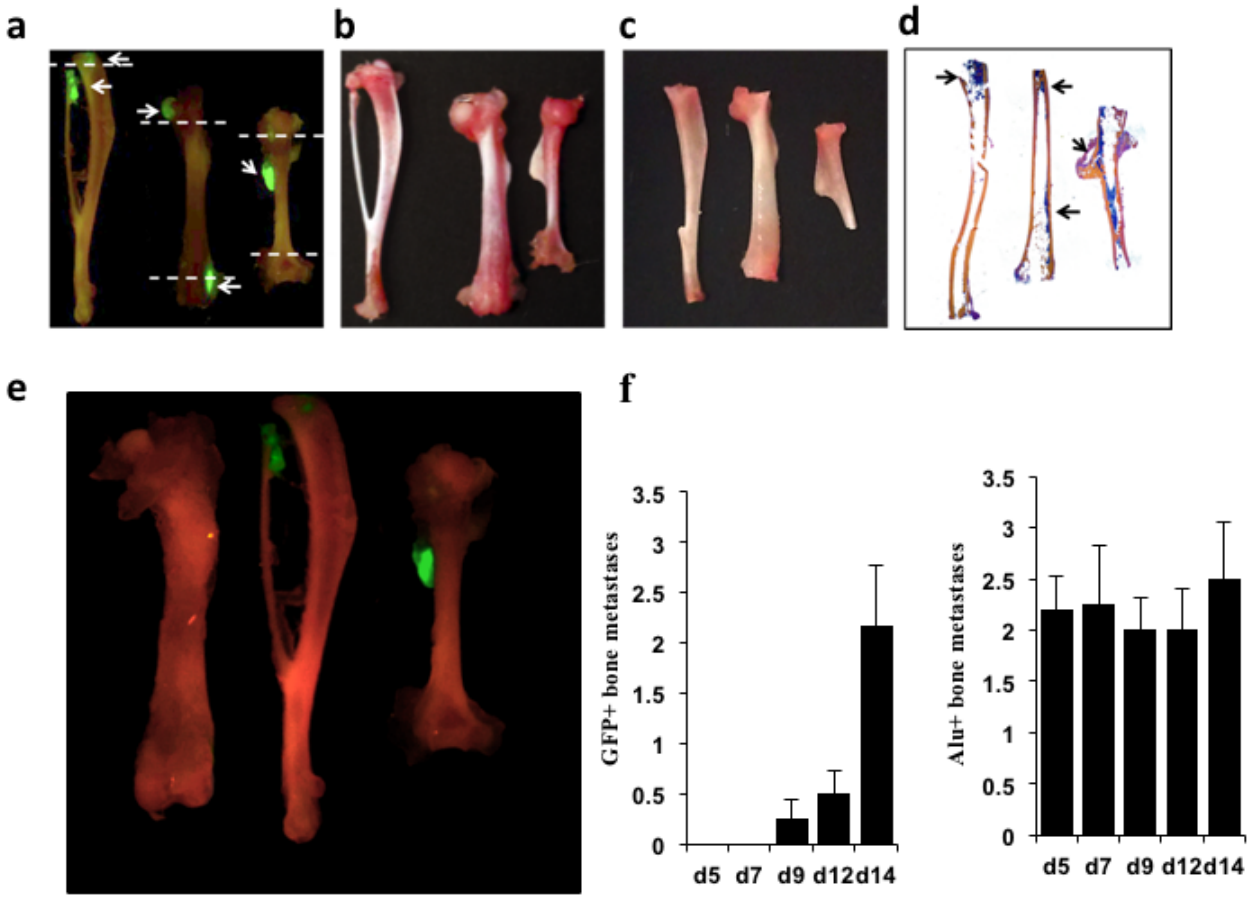

	femur	tibia	humerus
Cell # (ALU+)	3.7 x 10^4	1.8 x 10^4	5.2 x 10^3
GFP (arbitrary units)	no signal	1.6 x 10^4	4 x 10^4

Figure 34. Early Stage Metastasis Is Detectable with Alu qPCR but not Fluorescence Imaging: a) Fluorescence *ex vivo* imaging of mouse bones with GFP+ tumors (arrows). Bones have been cleaned of excess tissue, (b) and have visible red marrow. Image of bones after ends have been cut and the marrow removed by flushing and/or centrifugation techniques (c). After fixation and staining, large amounts of cells and tumor remain in the bone (d). Comparison of cell number quantification by Alu with fluorescent signal in the same bones (e) showing great variability in fluorescence intensity depending on depth of tumor and angle of bone. f) Comparison of number of bone metastases detected with GFP vs Alu qPCR (n=5).

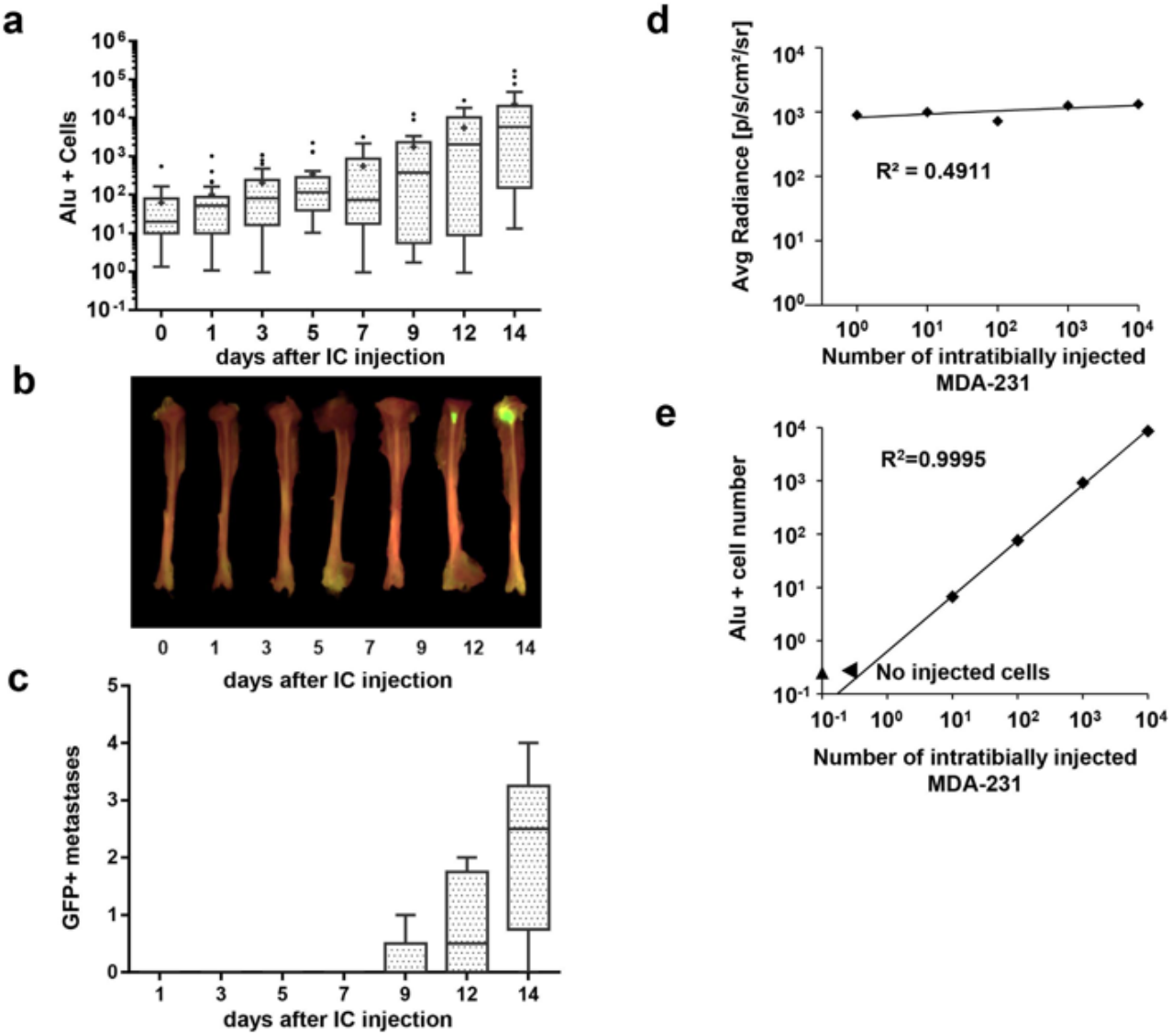

Figure 35. Alu PCR Accurately Quantifies Tumor Cell Establishment in the Bone: Representative ex vivo imaging of tibiae at different time points after intracardiac injection of MDA-231 tumor cells (b) and quantification of GFP+ bone tumors per mouse (a, c) (n = 5) with representative GFP images (b). BLI of tibiae injected with known numbers of MDA-231 cells expressing Luciferase (d) and corresponding Alu qPCR from the same bones (e), n = 2.

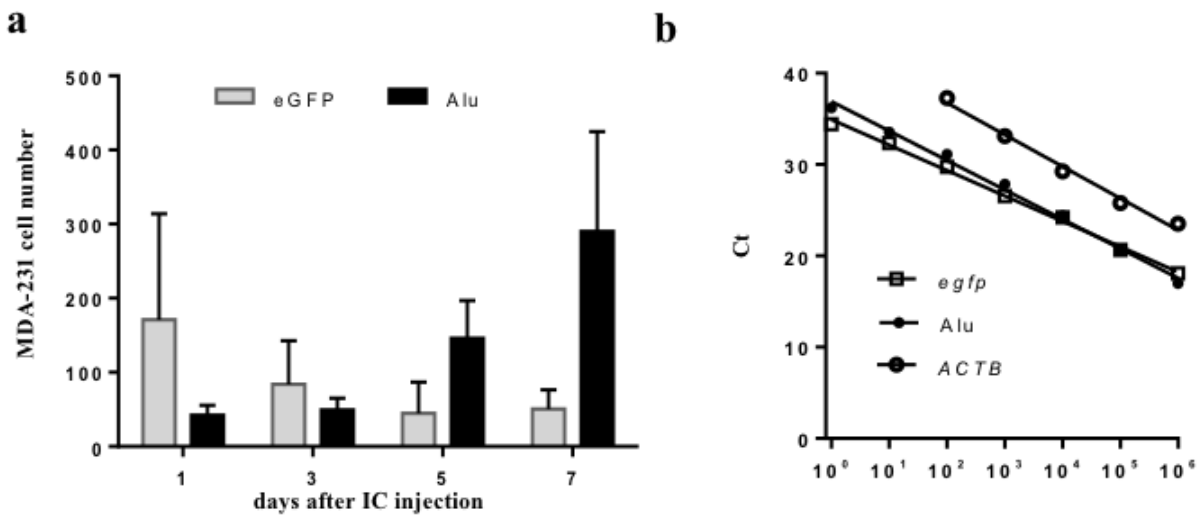

Figure 36. eGFP mRNA Expression Can Be Used to Quantify Cancer Cell Number: a) *In vivo* comparison of eGFP and Alu qPCR quantification of metastatic tumor cell number in femora of mice after intracardiac injection (n=5 mice at each time point). b) *In vitro* comparison of ct values from qPCR of egfp, Alu, and ACTB after Trizol RNA and DNA extraction of differing numbers of MDA-MB-231VU cells (n=3).

expression of reporter genes, even when under the control of a constitutive promoter (216).

Using fluorescence imaging, we did not observe an *ex vivo* signal in bone until 9 days after injection, which corresponded to >1000 cells (**Figure 35b**), consistent with previous findings regarding the sensitivity of spectral imaging *in vivo* (217). Furthermore, many large tumor foci were rendered undetectable by *ex vivo* fluorescence; by simply adjusting the positional angle of the bone during imaging and fluorescence, the resulting data- used to quantify tumor burden- were highly variable (data not shown). Interestingly, the number of bones with detectable metastases (more than 10 Alu + cells) did not increase over two weeks, though detectable metastases by *ex vivo* fluorescence appeared to increase (**Figure 34f**). This observation further supports the advantage of Alu detection to precisely quantify the number of metastatic tumor cells in the skeleton (and other tissues) at the earliest stage of metastasis, and reinforces the recent observation that circulating tumor cell clusters may have higher metastatic potential than isolated tumor cells (218).

We next considered that possible artifacts, such as clonal expansion of cells with low eGFP expression, decrease reporter expression in less metabolically active foci, or that hypoxic conditions in the bone metastatic site could attenuate the GFP signal and thus decrease the sensitivity of fluorescent detection methods. In order to control for these variables, we intratibially injected between 101 and 105 MDA-MB-231 cells which expressed both luciferase and GFP. We quantified tumor signal within 1 hour using luminescence and fluorescence, both *in vivo* and *ex vivo*, before extracting DNA and performing Alu qPCR. We used this short time course to minimize large scale changes in eGFP RNA that could affect the sensitivity of imaging modalities. Neither fluorescence nor luminescence imaging modalities could consistently detect < 1000 tumor cells *in vivo*, and though both methods were sensitive for detection *ex vivo*, they could not accurately quantify absolute or relative numbers of cancer cells within bone (**Figure 35c-d**). Alu qPCR, however, was able to both detect and accurately quantify tumor

cells from within the bone of all the samples (**Figure 35e**).

We previously reported that chronic stress-induced expression of RANKL by osteoblasts mediates an increase in MDA-231VU metastasis to the skeleton, as measured at end point (28 days post inoculation) by *ex vivo* GFP fluorescence imaging (51). In order to determine if the same neuroendocrine stimuli could cause quantifiable changes in tumor cell number at early post-inoculation time points, we subjected mice to chronic immobilization stress (CIS) for 10 days prior to intracardiac injection of tumor cells. Without any further treatment, we were able to measure a significant increase in the number of metastatic cells 5 days post-inoculation in the CIS group compared to controls (**Figure 37a–b**), confirming that Alu qPCR can be used to quantify changes in tumor cell number at the earliest stages of metastatic establishment.

Discussion

The TRIzol-BEB extraction and Alu qPCR methods discussed herein is both more accurate and precise than existing imaging modalities for measuring absolute numbers of metastatic tumor cells in skeletal tissues, while allowing gene expression studies from the same bone biopsies. In addition to high sensitivity, the quantification of metastasis by Alu qPCR allows one to quantify disseminated tumor without requiring stable transfection for imaging, which can drastically change the phenotype of the tumor cells. This advantage is critical in patient derived xenograft studies where minimal manipulation of the tumor is desired in order to maintain patient phenotype and more accurately predict patient outcomes. Additionally, Alu qPCR relies on amplification of a robust and stable genomic signal, allowing a more sensitive, consistent and accurate cell number quantification than the inherently variable mRNA expression data of reporter genes. Importantly, this method allows for simultaneous quantification of gene expression from host mRNA and precise cell number from tumor DNA. We

validated the Alu qPCR method with the two most widely used *in vivo* models of skeletal metastasis, which allowed us to precisely control both the number of cancer cells and time that samples were collected. Further studies with orthotopic xenograft models and with other cancer cell types than breast cancer will need to be performed in order to validate the combined techniques' utility in determining the time to metastasis and the number of disseminated cells in each organ. An obvious limitation of this method is that information about the specific location of disseminated metastatic cells within the tissue is lost during pulverization. However, when combined with imaging modalities, this technique should prove a powerful tool in the study of host stromal influences on the early phases of metastatic establishment in xenograft models.

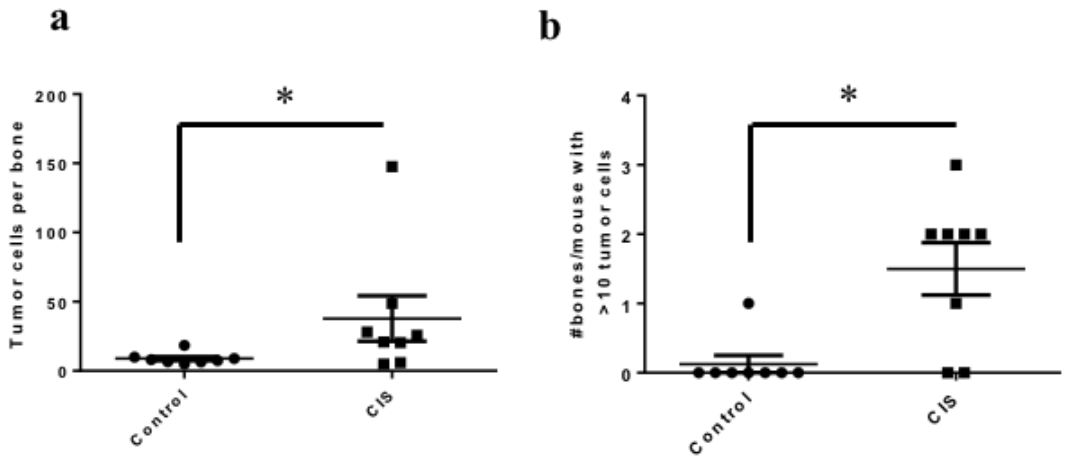

Figure 37. Alu qPCR Can Quantify Changes in Bone Metastatic Cell Number in a Murine Stress Model: mRNA expression of IL-6 according to number of tumor cells (a) in bones harvested at 3-7 days after intracardiac injection of MDA-231VU with MDA-231VU cells detected by ALU qPCR 5 days after intracardiac injection. Number of MDA-231VU cells detected in femora (b) of control mice vs. chronically immobilized stress treated mice (CIS) (n=8, $p<0.005$, t-test with Welch's correction). Number of bones with more than 10 detected cells per mouse, day 3 (n=8, $p<0.005$, Fisher's exact test).

REFERENCES:

1. Siegel, R.L., Miller, K.D., Jemal, A. (2017). Cancer Statistics, 2017. *CA Cancer JClin, 67*(1), 7-30. doi:10.3322/caac.21387
2. Ballinger, M.L., Mitchell, G., Thomas, D.M. (2015). Surveillance recommendations for patients with germline TP53 mutations. *Curr Opin Oncol, 27*(4), 332-337. doi:10.1097/CCO.0000000000000200
3. Marusyk, A., Almendro, V., Polyak, K. (2012). Intra-tumour heterogeneity: a looking glass for cancer? *Nat Rev Cancer, 12*(5), 323-334. doi:10.1038/nrc3261
4. Hanahan, D., & Weinberg, R. A. (2000). The hallmarks of cancer. *Cell, 100*(1), 57-70.
5. Hanahan, D., Weinberg, R. A. (2011). Hallmarks of cancer: the next generation. *Cell, 144*(5), 646-674. doi:10.1016/j.cell.2011.02.013
6. Aguirre-Ghiso, J. A. (2007). Models, mechanisms and clinical evidence for cancer dormancy. *Nat Rev Cancer, 7*(11), 834-846. doi:10.1038/nrc2256
7. Paget, S. (1989). The distribution of secondary growths in cancer of the breast. 1889. *Cancer Metastasis Rev, 8*(2), 98-101.
8. Weilbaecher, K. N., Guise, T. A., McCauley, L. K. (2011). Cancer to bone: a fatal attraction. *Nat Rev Cancer, 11*(6), 411-425. doi:10.1038/nrc3055
9. Hynes, N.E., Watson, C.J. (2010). Mammary gland growth factors: roles in normal development and in cancer. *Cold Spring Harb Perspect Biol, 2*(8), a003186. doi:10.1101/cshperspect.a003186
10. Harris, J. R. (2000). Notes on the Ontario trial in the context of breast-conserving therapy for early-stage breast cancer. *J Clin Oncol, 18*(21 Suppl), 43S-44S.
11. Pal, S. K., Blazer, K., Weitzel, J., Somlo, G. (2009). An association between invasive breast cancer and familial idiopathic hyperparathyroidism: a case series and review of the literature. *Breast Cancer Res Treat, 115*(1), 1-5. doi:10.1007/s10549-008-0056-8
12. Dai, X., Li, T., Bai, Z., Yang, Y., Liu, X., Zhan, J., Shi, B. (2015). Breast cancer intrinsic subtype classification, clinical use and future trends. *American Journal of Cancer Research*, *5*(10), 2929–2943.
13. Costa, L., Badia, X., Chow, E., Lipton, A., Wardley, A. (2008). Impact of skeletal complications on patients' quality of life, mobility, and functional independence. *Support Care Cancer, 16*(8), 879-889. doi:10.1007/s00520-008-0418-0
14. Mundy, G.R. Metastasis to Bone: Causes, Consequences, and Therapeutic Opportunities. Nat. Rev. Cancer. 2002 Aug 4;2(8):584-93
15. Elefteriou, F. Chronic stress, sympathetic activation and skeletal metastasis of breast cancer cells. Bonekey Rep. 2015 Jan 4;4:693.
16. Buenrostro, D., Mulcrone, P.L., Owens, P., Sterling, J.A. (2016). The Bone Microenvironment: a Fertile Soil for Tumor Growth. *Curr Osteoporos Rep, 14*(4), 151-158. doi:10.1007/s11914-016-0315-2
17. Cheng, M. L., Fong, L. (2014). Effects of RANKL-Targeted Therapy in Immunity and Cancer. *Frontiers in oncology*, *3*, 329. doi:10.3389/fonc.2013.00329
18. Mundy, G.R., Yoneda, T., Hiraga, T. (2001). Preclinical studies with zoledronic acid and other bisphosphonates: impact on the bone microenvironment. *Semin Oncol, 28*(2 Suppl 6), 35-44.
19. Bauer, D. C. (2011). Discontinuation of odanacatib and other osteoporosis treatments: here today and gone tomorrow? *J Bone Miner Res, 26*(2), 239-241. doi:10.1002/jbmr.335

20. Otto, F., Thornell, A.P., Crompton, T., Denzel, A., Gilmour, K.C., Rosewell, I.R., … Owen, M. J. (1997). Cbfa1, a candidate gene for cleidocranial dysplasia syndrome, is essential for osteoblast differentiation and bone development. *Cell*, *89*(5), 765–71.
21. Clarke, B. (2008). Normal bone anatomy and physiology. *Clin J Am Soc Nephrol, 3 Suppl 3*, S131-139. doi:10.2215/CJN.04151206
22. Yasuda, H., Shima, N., Nakagawa, N., Yamaguchi, K., Kinosaki, M., Mochizuki, S., Tomoyasu, A., Yano, K., Goto, M., … Suda, T. Osteoclast differentiation factor is a ligand for osteoprotegerin/osteoclastogenesis-inhibitory factor and is identical to TRANCE/RANKL. Proc. Natl. Acad. Sci. U.S.A. 1998 Mar 2;95(7):3597–602.
23. Roodman, G.D. (2001). Biology of osteoclast activation in cancer. *J Clin Oncol, 19*(15), 3562-3571. doi:10.1200/JCO.2001.19.15.3562
24. Bonewald, L.F. (2011). The amazing osteocyte. *J Bone Miner Res, 26*(2), 229-238. doi:10.1002/jbmr.320
25. Zhou, J.Z., Riquelme, M.A., Gao, X., Ellies, L.G., Sun, L.Z., Jiang, J.X. (2015). Differential impact of adenosine nucleotides released by osteocytes on breast cancer growth and bone metastasis *Oncogene*. 2015 Apr 2;34(14):1831-42. doi:10.1038/onc.2014.113. Epub 2014 May 19.
26. Sottnik, J. L., Dai, J., Zhang, H., Campbell, B., & Keller, E. T. (2015). Tumor-induced pressure in the bone microenvironment causes osteocytes to promote the growth of prostate cancer bone metastases. *Cancer Res, 75*(11), 2151-2158. doi:10.1158/0008-5472.CAN-14-2493
27. Delgado-Calle, J., Anderson, J., Cregor, M. D., Hiasa, M., Chirgwin, J. M., Carlesso, N., . . . Bellido, T. (2016). Bidirectional Notch Signaling and Osteocyte-Derived Factors in the Bone Marrow Microenvironment Promote Tumor Cell Proliferation and Bone Destruction in Multiple Myeloma. *Cancer Res, 76*(5), 1089-1100. doi:10.1158/0008-5472.CAN-15-1703
28. Ikeda, T., Kasai, M., Utsuyama, M., Hirokawa, K. Determination of three isoforms of the receptor activator of nuclear factor-kappaB ligand and their differential expression in bone and thymus. Endocrinology. 2001;142:1419–1426.
29. Suzuki, J., Ikeda, T., Kuroyama, H., Seki, S., Kasai, M.,… Hirokawa, K. Regulation of osteoclastogenesis by three human RANKL isoforms expressed in NIH3T3 cells. Biochem Biophys Res Commun. 2004 Feb 20;314(4):1021-7.
30. Santini, D., Perrone, G., Roato, I., Godio, L., Pantano F., … Tonini, G. Expression pattern of receptor activator of NFκB (RANK) in a series of primary solid tumors and related bone metastases. J. Cell. Physiol. [Internet]. 2011 Mar 2;226(3):780–4.
31. Boyce, B. F., Xing, L. (2008). Functions of RANKL/RANK/OPG in bone modeling and remodeling. *Archives of Biochemistry and Biophysics*, *473*(2), 139–146. http://doi.org/10.1016/j.abb.2008.03.018
32. Pitari, M. R., Rossi, M., Amodio, N., Botta, C., Morelli, E., Federico, C., … Tassone, P. (2015). Inhibition of miR-21 restores RANKL/OPG ratio in multiple myeloma-derived bone marrow stromal cells and impairs the resorbing activity of mature osteoclasts. *Oncotarget*, *6*(29), 27343–27358.
33. Tawara, K., Oxford, J. T., Jorcyk, C. L. (2011). Clinical significance of interleukin (IL)-6 in cancer metastasis to bone: potential of anti-IL-6 therapies. *Cancer Manag Res, 3*, 177-189. doi:10.2147/CMR.S18101
34. Lust, J. A., Donovan, K. A., Kline, M. P., Greipp, P. R., Kyle, R. A., Maihle, N. J. (1992). Isolation of an mRNA encoding a soluble form of the human interleukin-6 receptor. *Cytokine, 4*(2), 96-100.

35. Mullberg, J., Oberthur, W., Lottspeich, F., Mehl, E., Dittrich, E., Graeve, L., . . . Rose-John, S. (1994). The soluble human IL-6 receptor. Mutational characterization of the proteolytic cleavage site. *J Immunol, 152*(10), 4958-4968.
36. Johnson, R. W., Brennan, H. J., Vrahnas, C., Poulton, I. J., McGregor, N. E., Standal, T., . . . Sims, N. A. (2014). The primary function of gp130 signaling in osteoblasts is to maintain bone formation and strength, rather than promote osteoclast formation. *J Bone Miner Res, 29*(6), 1492-1505. doi:10.1002/jbmr.2159
37. Wallace, A., Cooney, T. E., Englund, R., Lubahn, J. D. (2011). Effects of interleukin-6 ablation on fracture healing in mice. *Journal of orthopaedic research : official publication of the Orthopaedic Research Society*, *29*(9), 1437–42. doi:10.1002/jor.21367
38. Zimmers, T. A., Fishel, M. L., Bonetto, A. (2016). STAT3 in the systemic inflammation of cancer cachexia. *Semin Cell Dev Biol, 54*, 28-41. doi:10.1016/j.semcdb.2016.02.009
39. Bonetto, A., Aydogdu, T., Jin, X., Zhang, Z., Zhan, R., Puzis, L., . . . Zimmers, T. A. (2012). JAK/STAT3 pathway inhibition blocks skeletal muscle wasting downstream of IL-6 and in experimental cancer cachexia. *Am J Physiol Endocrinol Metab, 303*(3), E410-421. doi:10.1152/ajpendo.00039.2012
40. Hartman, Z. C., Poage, G. M., den Hollander, P., Tsimelzon, A., Hill, J., Panupinthu, N., . . . Brown, P. H. (2013). Growth of triple-negative breast cancer cells relies upon coordinate autocrine expression of the proinflammatory cytokines IL-6 and IL-8. Cancer Res, 73(11), 3470-3480. doi:10.1158/0008-5472.CAN-12-4524-T
41. Zheng, Y., Chow, S. O., Boernert, K., Basel, D., Mikuscheva, A., Kim, S., . . . Seibel, M. J. (2014). Direct crosstalk between cancer and osteoblast lineage cells fuels metastatic growth in bone via auto-amplification of IL-6 and RANKL signaling pathways. *J Bone Miner Res, 29*(9), 1938-1949. doi:10.1002/jbmr.2231
42. Rodriguez-Barrueco, R., Yu, J., Saucedo-Cuevas, L. P., Olivan, M., Llobet-Navas, D., Putcha, P., . . . Silva, J. M. (2015). Inhibition of the autocrine IL-6-JAK2-STAT3-calprotectin axis as targeted therapy for HR-/HER2+ breast cancers. *Genes Dev, 29*(15), 1631-1648. doi:10.1101/gad.262642.115
43. Hill, E.L., Elde, R. Distribution of CGRP-, VIP-, D H-, SP-, and NPY-immunoreactive nerves in the periosteum of the rat. Cell and tissue research [Internet]. Springer; 1991;264(3):469–80.
44. Ma, Y., Nyman, J.S., Tao, H., Moss, H.H., Yang, X., Elefteriou F. β2-Adrenergic receptor signaling in osteoblasts contributes to the catabolic effect of glucocorticoids on bone. Endocrinology. 2011 Apr 5;152(4):1412–22.
45. Katayama, Y., Battista, M., Kao, W. M., Hidalgo, A., Peired, A. J., Thomas, S. A., Frenette, P. S. (2006). Signals from the sympathetic nervous system regulate hematopoietic stem cell egress from bone marrow. *Cell, 124*(2), 407-421. doi:10.1016/j.cell.2005.10.041
46. Elefteriou, F., Ahn, J. D., Takeda, S., Starbuck, M., Yang, X., Liu, X., . . . Karsenty, G. (2005). Leptin regulation of bone resorption by the sympathetic nervous system and CART. *Nature, 434*(7032), 514-520. doi:10.1038/nature03398
47. Vignaux, G., Ndong, J. D., Perrien, D. S., Elefteriou, F. (2015). Inner Ear Vestibular Signals Regulate Bone Remodeling via the Sympathetic Nervous System. *J Bone Miner Res, 30*(6), 1103-1111. doi:10.1002/jbmr.2426
48. Hassan, S., Karpova, Y., Baiz, D., Yancey, D., Pullikuth, A., … Kulik, G. Behavioral stress accelerates prostate cancer development in mice. J. Clin. Invest. 2013 Feb 5;123(2):874–86.
49. Pratt, L.A., Brody, D.J. Depression in the U.S. Household Population, 2009-2012. NCHS Data Brief. No. 172, 2014.

50. Palesh, O, Butler, L.D., Koopman, C., Giese-Davis, J., Carlson, R., Spiegel, D. Stress History and Breast Cancer Recurrence. *Journal of psychosomatic research*. 2007;63(3):233-239.
51. Campbell, J.P., Karolak, M.R., Ma, Y., Perrien, D.S., Masood-Campbell, S.K., Penner, N.L., Munoz, S.A., Zijlstra, A., Yang, X., Sterling, J.A., Elefteriou, F. Stimulation of host bone marrow stromal cells by sympathetic nerves promotes breast cancer bone metastasis in mice. PLoS Biol. 2012 Jul;10(7)
52. Zhang, L., Teng, Y., Zhang, Y., Liu, J., Xu, L., … Qu, X. (2012) Receptor activator for nuclear factor kappa B expression predicts poor prognosis in breast cancer patients with bone metastasis but not in patients with visceral metastasis. J Clin Pathol 65: 36–40.
53. Jones, D.H., Nakashima, T., Sanchez, O.H., Kozieradzki, I., Komarova, S.V., Sarosi, I., … Penninger, J.M. (2006). Regulation of cancer cell migration and bone metastasis by RANKL. *Nature*,*440*(7084), 692–6. doi:10.1038/nature04524
54. Latek, D., Modzelewska, A., Trzaskowski, B., Palczewski, K., Filipek, S. (2012). G protein-coupled receptors--recent advances. *Acta Biochim Pol, 59*(4), 515-529.
55. Dorsam, R. T., & Gutkind, J. S. (2007). G-protein-coupled receptors and cancer. *Nat Rev Cancer, 7*(2), 79-94. doi:10.1038/nrc2069
56. Weiner, H. **Perturbing the Organism: The Biology of Stressful Experience** (Univ. of Chicago Press, 1992)
57. Sapolsky, R.M. **Why Zebras Don't Get Ulcers: A Guide to Stress-Related Diseases, and Coping** (Freeman, 1994)
58. Sherwood, L. **Human Physiology: From Cells to Systems** (Cengage Learning, 2015)
59. Grujic, D., Susulic, V. S., Harper, M. E., Himms-Hagen, J., Cunningham, B. A., Corkey, B. E., Lowell, B. B. (1997). Beta3-adrenergic receptors on white and brown adipocytes mediate beta3-selective agonist-induced effects on energy expenditure, insulin secretion, and food intake. A study using transgenic and gene knockout mice. *J Biol Chem, 272*(28), 17686-17693
60. Lorton, D., Bellinger, D.L. (2015). Sympathetic Nervous System Regulation of Th Cells in Autoimmunity: Beyond Th1 and Th2 Cell Balance. *J Clin Cell Immunol* 6: 356. doi:10.4172/2155-9899.1000356
61. Schuler, Y., Lee-Thedieck, C., Geiger, K., Kaiser, T., Ino, Y., Aicher, W. K., Klein, G. (2012). Osteoblast-secreted factors enhance the expression of dysadherin and CCL2-dependent migration of renal carcinoma cells. *Int J Cancer, 130*(2), 288-299. doi:10.1002/ijc.25981
62. Kasbohm, E.A., Guo, R., Yowell, C. W., Bagchi, G., Kelly, P., Arora, P., … Daaka, Y. (2005). Androgen receptor activation by G(s) signaling in prostate cancer cells. *The Journal of biological chemistry*, *280*(12), 11583–9. doi:10.1074/jbc.M414423200
63. Thaker, P.H., Han, L.Y., Kamat, A.A., Arevalo, J.M., Takahashi, R., Lu. C, …, Sood A.K. Chronic stress promotes tumor growth and angiogenesis in a mouse model of ovarian carcinoma. Nat. Med. [Internet]. 2006 Aug 2;12(8):939–44.
64. Nagaraja, A.S., Dorniak, P.L., Sadaoui, N.C., Kang ,Y., Lin, T., Armaiz-Pena, G., Wu, S.Y., …, Sood, A.K. Sustained adrenergic signaling leads to increased metastasis in ovarian cancer via increased PGE2 synthesis. Oncogene. 2016 May 4;35(18):2390–7.
65. Eng, J.W., Kokolus, K.M., Reed, C.B., Hylander, B.L., Ma, W.W., Repasky, E.A. (2014). A nervous tumor microenvironment: the impact of adrenergic stress on cancer cells, immunosuppression, and immunotherapeutic response. *Cancer Immunol Immunother, 63*(11), 1115-1128. doi:10.1007/s00262-014-1617-9
66. Barron, T. I., Sharp, L., Visvanathan, K. (2012). Beta-adrenergic blocking drugs in breast cancer: a perspective review. *Ther Adv Med Oncol, 4*(3), 113-125. doi:10.1177/1758834012439738

67. Fitzgerald, P. J. (2012). Beta blockers, norepinephrine, and cancer: an epidemiological viewpoint. *Clin Epidemiol, 4*, 151-156. doi:10.2147/CLEP.S33695
68. Wang, H.M., Liao, Z.X., Komaki, R., Welsh, J.W., O'Reilly, M.S., Chang, J.Y., Zhuang, Y., Levy, L.B., Lu, C., Gomez, D.R. Improved survival outcomes with the incidental use of beta-blockers among patients with non-small-cell lung cancer treated with definitive radiation therapy. Ann Oncol [Internet]. 2013;24:1312–9.
69. Jansen, L., Below, J., Chang-Claude, J., Brenner, H., Hoffmeister, M. (2012). Beta blocker use and colorectal cancer risk: population-based case-control study. *Cancer, 118*(16), 3911-3919. doi:10.1002/cncr.26727
70. Ji, Y., Chen, S., Li, K., Xiao, X., Zheng, S., Xu, T. The role of β-adrenergic receptor signaling in the proliferation of hemangioma-derived endothelial cells. Cell Div [Internet]. 2013 Jan 2;8(1):1.
71. Creed, S.J., Le, C.P., Hassan, M., Pon, C.K., Albold, S., Chan, K.T., . . . Sloan, E. K. (2015). beta2-adrenoceptor signaling regulates invadopodia formation to enhance tumor cell invasion. *Breast Cancer Res, 17*(1), 145. doi:10.1186/s13058-015-0655-3
72. Sood, A.K., Fletcher, M. S., Coffin, J. E., Yang, M., Seftor, E. A., Gruman, L. M., … Hendrix, M. J. (2004). Functional role of matrix metalloproteinases in ovarian tumor cell plasticity.*American journal of obstetrics and gynecology*, *190*(4), 899–909. doi:10.1016/j.ajog.2004.02.011
73. Kanemi, O., Zhang, X., Sakamoto, Y., Ebina, M., Nagatomi, R. (2005), Acute stress reduces intrapareymal lung natural killer cells via beta-adrenergic stimulation. Clinical & Experimental Immunology, 139: 25–34. doi:10.1111/j.1365-2249.2005.02672.x
74. Kuebler, U., Wirtz, P. H., Sakai, M., Stemmer, A., Ehlert, U. (2013). Acute Stress Reduces Wound-Induced Activation of Microbicidal Potential of Ex Vivo Isolated Human Monocyte-Derived Macrophages. *PLoS ONE*, *8*(2), e55875.
75. Sloan, E.K., Priceman, S.J., Cox, B.F., Yu, S., Pimentel, M.A., Tangkanangnukul, V., Arevalo, J.M., Morizono, K., Karanikolas, B.D., Wu, L., Sood, A.K., Cole, S.W. The sympathetic nervous system induces a metastatic switch in primary breast cancer. Cancer Res. [Internet]. 2010 Sep 3;70(18):7042–52.
76. Pasquier, E., Street, J., Pouchy, C., Carre, M., Gifford, A. J., Murray, J., . . . Kavallaris, M. (2013). beta-blockers increase response to chemotherapy via direct antitumour and anti-angiogenic mechanisms in neuroblastoma. *Br J Cancer, 108*(12), 2485-2494. doi:10.1038/bjc.2013.205
77. Carulli, C., Innocenti, M., Brandi, M. L. (2013). Bone vascularization in normal and disease conditions. *Front Endocrinol (Lausanne), 4*, 106. doi:10.3389/fendo.2013.00106
78. Ferrara, N., Gerber, H.P., LeCouter, J. (2003). The Biology of VEGF and Its Receptors. *Nat Med.* Jun;9(6):669-76.
79. Maes, C. (2013). Role and regulation of vascularization processes in endochondral bones. *Calcif Tissue Int, 92*(4), 307-323. doi:10.1007/s00223-012-9689-z
80. Sullivan, L.A., Brekken, R.A. The VEGF family in cancer and antibody-based strategies for their inhibition. MAbs. 2010 Jan 5;2(2):165–75.
81. Olsson, A.K., Dimberg, A., Kreuger J., Claesson-Welsh L. (2006). VEGF Receptor Signaling- In Control of Vascular Function. *Nature Reviews Molecular Cell Biology* 7, 359-371 (May 2006) doi:10.1038/nrm1911
82. Ramasamy, S.K., Kusumbe, A.P., Wang, L., Adams, R.H. Endothelial Notch activity promotes angiogenesis and osteogenesis in bone. Nature. 2014 Mar 4;507(7492):376–80

83. Geudens, I., Gerhardt, H. (2011). Coordinating cell behaviour during blood vessel formation. *Development (Cambridge, England)*, *138*(21), 4569–83. doi:10.1242/dev.062323
84. Kronenberg, H. M. (2003). Developmental regulation of the growth plate. *Nature, 423*(6937), 332-336. doi:10.1038/nature01657
85. Liu, Y., Olsen, B. R. (2014). Distinct VEGF functions during bone development and homeostasis. *Arch Immunol Ther Exp (Warsz), 62*(5), 363-368.
86. Filipowska, J., Tomaszewski, K. A., Niedzwiedzki, L., Walocha, J. A., Niedzwiedzki, T. (2017). The role of vasculature in bone development, regeneration and proper systemic functioning. *Angiogenesis*. doi:10.1007/s10456-017-9541-1
87. Hu, K., Olsen, B. R. (2016). Osteoblast-derived VEGF regulates osteoblast differentiation and bone formation during bone repair. *The Journal of Clinical Investigation*, *126*(2), 509–526. http://doi.org/10.1172/JCI82585
88. Kusumbe, A. P., Ramasamy, S. K., Itkin, T., Mae, M. A., Langen, U. H., Betsholtz, C., . . . Adams, R. H. (2016). Age-dependent modulation of vascular niches for haematopoietic stem cells. *Nature, 532*(7599), 380-384. doi:10.1038/nature17638
89. Sivaraj, K. K., Adams, R. H. (2016). Blood vessel formation and function in bone. *Development, 143*(15), 2706-2715. doi:10.1242/dev.136861
90. Kusumbe, A. P., Ramasamy, S. K., Adams, R. H. (2014). Coupling of angiogenesis and osteogenesis by a specific vessel subtype in bone. *Nature, 507*(7492), 323-328. doi:10.1038/nature13145
91. Zhou, B.O., Yue, R., Murphy, M.M., Peyer, J., Morrison, S. J. (2014). Leptin Receptor-expressing mesenchymal stromal cells represent the main source of bone formed by adult bone marrow. *Cell Stem Cell*, *15*(2), 154–168.
92. Duncan, C.P., Shim S.S. J. Edouard Samson Address: the autonomic nerve supply of bone. An experimental study of the intraosseous adrenergic nervi vasorum in the rabbit. J Bone Jt Surg Br. 1977;59:323–330
93. Borgström, P., Bourdon, M.A., Hillan, K.J., Sriramarao, P., Ferrara, N. (1998). Neutralizing anti-vascular endothelial growth factor antibody completely inhibits angiogenesis and growth of human prostate carcinoma micro tumors in vivo. *Prostate,* Apr. 1;35(1):1-10.
94. FDA begins process to remove breast cancer indication from avastin label [Internet] U.S. Food and Drug Administration; 2010. [updated 12/16/2010. Available from: http://www.fda.gov/newsevents/newsroom/pressannouncements/ucm237172.htm.
95. Montero, A. J., Escobar, M., Lopes, G., Gluck, S., Vogel, C. (2012). Bevacizumab in the treatment of metastatic breast cancer: friend or foe? *Curr Oncol Rep, 14*(1), 1-11. doi:10.1007/s11912-011-0202-z
96. Bauerle, T., Hilbig, H., Bartling, S., Kiessling, F., Kersten, A., Schmitt-Graff, A., . . . Berger, M. R. (2008). Bevacizumab inhibits breast cancer-induced osteolysis, surrounding soft tissue metastasis, and angiogenesis in rats as visualized by VCT and MRI. *Neoplasia, 10*(5), 511-520.
97. Fishman, M.N., Tomshine, J., Fulp, W.J., Foreman, P.K. A systematic review of the efficacy and safety experience reported for sorafenib in advanced renal cell carcinoma (RCC) in the post-approval setting. PLoS ONE. 2015;10:e0120877 doi: 10.1371/journal.pone.0120877
98. Roland, C.L., Dineen, S.P., Lynn, K.D., Sullivan, L.A., Dellinger, M.T., Sadegh L., Sullivan J.P., Shames D.S., Brekken R.A. Inhibition of vascular endothelial growth factor reduces angiogenesis and modulates immune cell infiltration of orthotopic breast cancer xenografts. Mol. Cancer Ther. 2009 Jul 3;8(7):1761–71.
99. Tang, C., Hess, K., Jardim, D. L., Gagliato Dde, M., Tsimberidou, A. M., Falchook, G., . . .

Hong, D. S. (2014). Synergy between VEGF/VEGFR inhibitors and chemotherapy agents in the phase I clinic. *Clin Cancer Res, 20*(23), 5956-5963. doi:10.1158/1078-0432.CCR-14-1582
100. American Cancer Society. Cancer Facts & Figures 2016. Atlanta: American Cancer Society; 2016.
101. Campbell, J.P., Merkel, A.R., Masood-Campbell, S.K., Elefteriou, F., Sterling, J.A. Models of Bone Metastasis. *J. Vis. Exp.* (67), e4260, doi:10.3791/4260 2012.
102. Preston Campbell, J., Mulcrone, P., Masood, S.K., Karolak, M., Merkel, A., Hebron, K., Zijlstra, A., Sterling, J., Elefteriou, F. TRIzol and Alu qPCR-based quantification of metastatic seeding within the skeleton. Sci Rep. 2015 Jan 4;5:12635.
103. Chida, Y., Hamer, M., Wardle, J., Steptoe, A. Do stress-related psychosocial factors contribute to cancer incidence and survival? Nat Clin Pract Oncol. 2008 Aug 5;5(8):466–75.
104. Melhem-Bertrandt ,A., Chavez-Macgregor, M., Lei, X., Brown, E., Lee, R., Meric-Bernstam, F., Sood, A., Conzen, S., Hortobagyi, G., Gonzalez-Angulo, A-M. Beta-blocker use is associated with improved relapse-free survival in patients with triple-negative breast cancer. Journal of Clinical Oncology: official journal of the American Society of Clinical Oncology. 2011;29(19):2645–52.
105. Takeda S., Elefteriou F., Levasseur R., Liu X., Zhao L., Parker K.L., Armstrong D., Ducy P., Karsenty G. Leptin regulates bone formation via the sympathetic nervous system. Cell. 2002 Nov 5;111(3):305–17.
106. Asada N., Katayama Y., Sato M., Minagawa K., Wakahashi K., Kawano H., Kawano Y., Sada A., Ikeda K., Matsui T., Tanimoto M. Matrix-embedded osteocytes regulate mobilization of hematopoietic stem/progenitor cells. Cell Stem Cell. 2013 Jun 4;12(6):737–47.
107. Itoh Y., Yamada M., Suematsu N., Matsushita M., Otomo E. An immunohistochemical study of centenarian brains: a comparison. J. Neurol. Sci. 1998 Apr 3;157(1):73–81.
108. Sullivan L.A., Carbon J.G., Roland C.L., Toombs J.E., Nyquist-Andersen M., Kavlie A., Schlunegger K., Richardson J.A., Brekken R.A. R84, a novel therapeutic antibody against mouse and human VEGF with potent anti-tumor activity and limited toxicity induction. PloS ONE. 2010 Jan 5;5(8):e12031.
109. Dacquin R., Starbuck M., Schinke T. Mouse α1 (I)-collagen promoter is the best known promoter to drive efficient Cre recombinase expression in osteoblast. Developmental … [Internet]. 2002;
110. Kajimura D., Hinoi E., Ferron M., Kode A., Riley K.J., Zhou B., Guo X.E., Karsenty G. Genetic determination of the cellular basis of the sympathetic regulation of bone mass accrual. J. Exp. Med. 2011 Apr 1;208(4):841–51.
111. Yoneda T., Williams P.J., Hiraga T., Niewolna M., Nishimura R. A Bone-Seeking Clone Exhibits Different Biological Properties from the MDA-MB-231 Parental Human Breast Cancer Cells and a Brain-Seeking Clone In Vivo and In Vitro. JBMR 2001:16
112. Pasic L., Eisinger-Mathason T., Velayudhan B., Moskaluk C., Brenin D., Macara I., Lannigan D. Sustained activation of the HER1-ERK1/2-RSK signaling pathway controls myoepithelial cell fate in human mammary tissue. Gene Dev. 2011;25(15):1641–53.
113. Deckers M.M., Smits P., Karperien M., Ni J., Tylzanowski P., Feng P., Parmelee D., Zhang J., Bouffard E., Gentz R., Löwik C.W., Merregaert J. Recombinant human extracellular matrix protein 1 inhibits alkaline phosphatase activity and mineralization of mouse embryonic metatarsals in vitro. Bone. 2001 Jan 1;28(1):14–20.

114. Sekiguchi H., Ii M., Jujo K., Yokoyama A., Hagiwara N., Asahara T. Improved culture-based isolation of differentiating endothelial progenitor cells from mouse bone marrow mononuclear cells. PloS ONE. 2011 Jan 6;6(12):e28639.
115. Golbidi S., Frisbee J.C., Laher I. Chronic stress impacts the cardiovascular system: animal models and clinical outcomes. Am. J. Physiol. Heart Circ. Physiol. 2015 Jun 1;308(12):H1476–98
116. Madden K.S., Szpunar M.J., Brown E.B. B-Adrenergic receptors (β-AR) regulate VEGF and IL-6 production by divergent pathways in high β-AR-expressing breast cancer cell lines. Breast Cancer Res. Treat. [Internet]. 2011 Dec 4;130(3):747–58.
117. Stiles J.M., Amaya C., Rains S., Diaz D., Pham R., Battiste J., Modiano J.F., Kokta V., Boucheron L.E., Mitchell D.C., Bryan B.A. Targeting of beta adrenergic receptors results in therapeutic efficacy against models of hemangioendothelioma and angiosarcoma. PloS ONE [Internet]. 2013;8:e60021.
118. Roland C.L., Lynn K.D., Toombs J.E., Dineen S.P., Udugamasooriya D.G., Brekken R.A. Cytokine levels correlate with immune cell infiltration after anti-VEGF therapy in preclinical mouse models of breast cancer. *PloS ONE*. 2009;4(11)
119. Yang L., Kwon J., Popov Y., Gajdos G.B., Ordog T., Brekken R.A., Mukhopadhyay D., Schuppan D., Bi Y., Simonetto D., Shah V.H. Vascular endothelial growth factor promotes fibrosis resolution and repair in mice. Gastroenterology. 2014 May 4;146(5):1339–50.e1.
120. Gu X., Yu X., Dai H. Intravitreal injection of ranibizumab for treatment of age-related macular degeneration: effects on serum VEGF concentration. Curr. Eye Res. 2014 May 4;39(5):518–21.
121. Yu L., Wu X., Cheng Z., Lee C.V., LeCouter J., Campa C., Fuh G., Lowman H., Ferrara N. Interaction between bevacizumab and murine VEGF-A: a reassessment. Invest. Ophthalmol. Vis. Sci. 2008 Feb 5;49(2):522–7.
122. Gao D., Nolan D.J., Mellick A.S., Bambino K., McDonnell K., Mittal V. Endothelial progenitor cells control the angiogenic switch in mouse lung metastasis. Science [Internet]. 2008 Jan 5;319(5860):195–8.
123. Song F-N., Duan M., Liu L-Z., Wang Z-C., Shi J-Y., Yang L-X., … Wang X.Y. (2014) RANKL Promotes Migration and Invasion of Hepatocellular Carcinoma Cells via NF-κB-Mediated Epithelial-Mesenchymal Transition. PLoS ONE 9(9)
124. Armstrong A.P., Miller R.E., Jones J.C., Zhang J., Keller E.T., Dougall W.C. RANKL acts directly on RANK-expressing prostate tumor cells and mediates migration and expression of tumor metastasis genes. Prostate. 2008 Jan 2;68(1):92–104.
125. Le C.P., Nowell C.J., Kim-Fuchs C., Botteri E., Hiller J.G., Ismail H., Pimentel M.A., Chai M.G., Karnezis T., Rotmensz N., Renne G., Gandini S., Pouton C.W., Ferrari D., Möller A., Stacker S.A., Sloan E.K. Chronic stress in mice remodels lymph vasculature to promote tumour cell dissemination. Nat Commun. 2016 Jan 5;7:10634
126. Nagaraja A.S., Dorniak P.L., Sadaoui N.C., Kang Y., Lin T., Armaiz-Pena G., Wu S.Y., Rupaimoole R., Allen J.K., Gharpure K.M., Pradeep S., Zand B., Previs R.A., Hansen J.M., Ivan C., Rodriguez-Aguayo C., Yang P., Lopez-Berestein G., Lutgendorf S.K., Cole S.W., Sood A.K. Sustained adrenergic signaling leads to increased metastasis in ovarian cancer via increased PGE2 synthesis. Oncogene. 2016 May 4;35(18):2390–7.
127. Hulsurkar M., Li Z., Zhang Y., Li X., Zheng D., Li W. Beta-adrenergic signaling promotes tumor angiogenesis and prostate cancer progression through HDAC2-mediated suppression of thrombospondin-1. Oncogene. 2016 Sep 1;

128. Sastry K.S., Karpova Y., Prokopovich S., Smith A.J., Essau B., Gersappe A., Carson J.P., Weber M.J., Register T.C., Chen Y.Q., Penn R.B., Kulik G. Epinephrine protects cancer cells from apoptosis via activation of cAMP-dependent protein kinase and BAD phosphorylation. J. Biol. Chem. 2007 May 5;282(19):14094–100.
129. Saito T., Fukai A., Mabuchi A., Ikeda T., Yano F., Ohba S., Nishida N., Akune T., Yoshimura N., Nakagawa T., Nakamura K., Tokunaga K., Chung U-I.I., Kawaguchi H. Transcriptional regulation of endochondral ossification by HIF-2alpha during skeletal growth and osteoarthritis development. Nat. Med. 2010 Jun 2;16(6):678–86.
130. Zelzer E., Levy Y., Kahana C., Shilo B.Z., Rubinstein M., Cohen B. Insulin induces transcription of target genes through the hypoxia-inducible factor HIF-1alpha/ARNT. EMBO J. 1998 Sep 2;17(17):5085–94.
131. Dy G.K., Adjei A.A. Understanding, recognizing, and managing toxicities of targeted anticancer therapies. CA Cancer J Clin. 2013 Jan 2;63(4):249–79.
132. Elefteriou F, Campbell P, Ma Y. Control of Bone Remodeling by the Peripheral Sympathetic Nervous System. *Calcified tissue international*. 2014;94(1):140-151. doi:10.1007/s00223-013-9752-4.
133. Pasquier E., Ciccolini J., Carre M., Giacometti S., Fanciullino R., ... Andre N.. Propranolol potentiates the anti-angiogenic effects and anti-tumor efficacy of chemotherapy agents: implication in breast cancer treatment. Oncotarget. 2011:2:797-809
134. Cole, S. W., Nagaraja, A. S., Lutgendorf, S. K., Green, P. A., Sood, A. K. (2015). Sympathetic nervous system regulation of the tumour microenvironment. *Nat Rev Cancer, 15*(9), 563-572. doi:10.1038/nrc3978
135. Cole, S. W., Sood, A. K. (2012). Molecular pathways: beta-adrenergic signaling in cancer. *Clin Cancer Res, 18*(5), 1201-1206. doi:10.1158/1078-0432.CCR-11-0641
136. Elefteriou, F. (2016). Role of sympathetic nerves in the establishment of metastatic breast cancer cells in bone. *J Bone Oncol, 5*(3), 132-134. doi:10.1016/j.jbo.2016.03.003
137. Chi, D. S., Fitzgerald, S. M., Pitts, S., Cantor, K., King, E., Lee, S. A., . . . Krishnaswamy, G. (2004). MAPK-dependent regulation of IL-1- and beta-adrenoreceptor-induced inflammatory cytokine production from mast cells: implications for the stress response. BMC Immunol, 5, 22. doi:10.1186/1471-2172-5-22
138. Pietras, K., Ostman, A. (2010). Hallmarks of cancer: interactions with the tumor stroma. *Exp Cell Res, 316*(8), 1324-1331. doi:10.1016/j.yexcr.2010.02.045
139. Geng, Y., Chandrasekaran, S., Hsu, J. W., Gidwani, M., Hughes, A. D., King, M. R. (2013). Phenotypic switch in blood: effects of pro-inflammatory cytokines on breast cancer cell aggregation and adhesion. PLoS One, 8(1), e54959. doi:10.1371/journal.pone.0054959
140. Chen, Q., Massague, J. (2012). Molecular pathways: VCAM-1 as a potential therapeutic target in metastasis. Clin Cancer Res, 18(20), 5520-5525. doi:10.1158/1078-0432.CCR-11-2904
141. Barthel, S. R., Hays, D. L., Yazawa, E. M., Opperman, M., Walley, K. C., Nimrichter, L., . . . Dimitroff, C. J. (2013). Definition of molecular determinants of prostate cancer cell bone extravasation. Cancer Res, 73(2), 942-952. doi:10.1158/0008-5472.CAN-12-3264
142. De Luca, A., Lamura, L., Gallo, M., Maffia, V., Normanno, N. (2012). Mesenchymal stem cell-derived interleukin-6 and vascular endothelial growth factor promote breast cancer cell migration. J Cell Biochem, 113(11), 3363-3370. doi:10.1002/jcb.24212
143. Taherian, A., Li, X., Liu, Y., Haas, T. A. (2011). Differences in integrin expression and signaling within human breast cancer cells. *BMC Cancer, 11*, 293. doi:10.1186/1471-2407-11-293

144. Richard, C., Thibaudeau K., Charreau, B., Loirat, M.J., Naulet, J., Blanchard, D., Soulillou, J.P., & Bouhours, J.F. (1998). Characterization of a murine monoclonal antibody specific for swine beta1 integrin. *Xenotranslplantation,* 1998 Feb;5(1):75-83
145. Huang, C. R., Lee, C. T., Chang, K. Y., Chang, W. C., Liu, Y. W., Lee, J. C., Chen, B. K. (2015). Down-regulation of ARNT promotes cancer metastasis by activating the fibronectin/integrin beta1/FAK axis. *Oncotarget, 6*(13), 11530-11546. doi:10.18632/oncotarget.3448
146. Zhao, Y., Bachelier, R., Treilleux, I., Pujuguet, P., Peyruchaud, O., Baron, R., . . . Clezardin, P. (2007). Tumor alphavbeta3 integrin is a therapeutic target for breast cancer bone metastases. *Cancer Res, 67*(12), 5821-5830. doi:10.1158/0008-5472.CAN-06-4499
147. Page, J. M., Merkel, A. R., Ruppender, N. S., Guo, R., Dadwal, U. C., Cannonier, S. A., . . . Sterling, J. A. (2015). Matrix rigidity regulates the transition of tumor cells to a bone-destructive phenotype through integrin beta3 and TGF-beta receptor type II. *Biomaterials, 64*, 33-44. doi:10.1016/j.biomaterials.2015.06.026
148. Bakewell, S. J., Nestor, P., Prasad, S., Tomasson, M. H., Dowland, N., Mehrotra, M., . . . Weilbaecher, K. N. (2003). Platelet and osteoclast beta3 integrins are critical for bone metastasis. *Proc Natl Acad Sci U S A, 100*(24), 14205-14210. doi:10.1073/pnas.2234372100
149. Carter, R.A., Wicks, I.P. (2001). Vascular Cell Adhesion Molecule (CD106): a Multifaceted Regulator of Joint Inflammation. *Arthritis Rheum.* 2001 May;44(5):985-94
150. Chen, Q., Zhang, X. H., Massague, J. (2011). Macrophage binding to receptor VCAM-1 transmits survival signals in breast cancer cells that invade the lungs. *Cancer Cell, 20*(4), 538-549. doi:10.1016/j.ccr.2011.08.025
151. Ding, Y. B., Chen, G. Y., Xia, J. G., Zang, X. W., Yang, H. Y., Yang, L. (2003). Association of VCAM-1 overexpression with oncogenesis, tumor angiogenesis and metastasis of gastric carcinoma. *World J Gastroenterol, 9*(7), 1409-1414. doi:10.1016/j.abb.2008.03.016
152. Lu, X., Mu, E., Wei, Y., Riethdorf, S., Yang, Q., Yuan, M., . . . Kang, Y. (2011). VCAM-1 promotes osteolytic expansion of indolent bone micrometastasis of breast cancer by engaging alpha4beta1-positive osteoclast progenitors. *Cancer Cell, 20*(6), 701-714. doi:10.1016/j.ccr.2011.11.002
153. Ley, K. (2003). The role of selectins in inflammation and disease. *Trends Mol Med, 9*(6), 263-268
154. Galustian, C., Childs, R. A., Stoll, M., Ishida, H., Kiso, M., Feizi, T. (2002). Synergistic interactions of the two classes of ligand, sialyl-Lewis(a/x) fuco-oligosaccharides and short sulpho-motifs, with the P- and L-selectins: implications for therapeutic inhibitor designs. *Immunology, 105*(3), 350-359.
155. Schweitzer, K. M., Drager, A. M., van der Valk, P., Thijsen, S. F., Zevenbergen, A., Theijsmeijer, A. P., . . . Langenhuijsen, M. M. (1996). Constitutive expression of E-selectin and vascular cell adhesion molecule-1 on endothelial cells of hematopoietic tissues. *Am J Pathol, 148*(1), 165-175.
156. Yang, T., Grafe, I., Bae, Y., Chen, S., Chen, Y., Bertin, T. K., . . . Lee, B. (2013). E-selectin ligand 1 regulates bone remodeling by limiting bioactive TGF-beta in the bone microenvironment. *Proc Natl Acad Sci U S A, 110*(18), 7336-7341. doi:10.1073/pnas.1219748110
157. Wein, M., Sterbinsky, S. A., Bickel, C. A., Schleimer, R. P., Bochner, B. S. (1995). Comparison of human eosinophil and neutrophil ligands for P-selectin: ligands for P-selectin differ from those for E-selectin. *Am J Respir Cell Mol Biol, 12*(3), 315-319.

doi:10.1165/ajrcmb.12.3.7532979
158. Dallas, M. R., Chen, S. H., Streppel, M. M., Sharma, S., Maitra, A., Konstantopoulos, K. (2012). Sialofucosylated podocalyxin is a functional E- and L-selectin ligand expressed by metastatic pancreatic cancer cells. *Am J Physiol Cell Physiol, 303*(6), C616-624. doi:10.1152/ajpcell.00149.2012
159. Tremblay, P.-L., Auger, F.A., Hout, J. Regulation of transendothelial migration of colon cancer cells by E-selectin-mediated activation of p38 and ERK MAP kinases. *Oncogene* (2006) **25,** 6563–6573. doi:10.1038/sj.onc.1209664; published online 22 May 2006
160. Coupland, L. A., Chong, B. H., Parish, C. R. (2012). Platelets and P-selectin control tumor cell metastasis in an organ-specific manner and independently of NK cells. *Cancer Res, 72*(18), 4662-4671. doi:10.1158/0008-5472.CAN-11-4010
161. Nasti, T. H., Bullard, D. C., Yusuf, N. (2015). P-selectin enhances growth and metastasis of mouse mammary tumors by promoting regulatory T cell infiltration into the tumors. *Life Sci, 131*, 11-18. doi:10.1016/j.lfs.2015.02.025
162. Szasz, A. M., Lanczky, A., Nagy, A., Forster, S., Hark, K., Green, J. E., . . . Gyorffy, B. (2016). Cross-validation of survival associated biomarkers in gastric cancer using transcriptomic data of 1,065 patients. *Oncotarget, 7*(31), 49322-49333. doi:10.18632/oncotarget.10337
163. Rincon, M. (2012). Interleukin-6: from an inflammatory marker to a target for inflammatory diseases. Trends Immunol, 33(11), 571-577. doi:10.1016/j.it.2012.07.003
164. Hunter C.A., Jones S.A. (2015). IL-6 as a Keystone Cytokine in Health and Disease. *Nat Immunol,* May;16(5):448-57. doi: 10.1038/ni.3153. Review
165. Korkaya, H., Kim, G. I., Davis, A., Malik, F., Henry, N. L., Ithimakin, S., . . . Wicha, M. S. (2012). Activation of an IL6 inflammatory loop mediates trastuzumab resistance in HER2+ breast cancer by expanding the cancer stem cell population. Mol Cell, 47(4), 570-584. doi:10.1016/j.molcel.2012.06.014
166. Ara, T., Declerck, Y. A. (2010). Interleukin-6 in bone metastasis and cancer progression. Eur J Cancer, 46(7), 1223-1231. doi:10.1016/j.ejca.2010.02.026
167. Yasmin-Karim, S., King, M. R., Messing, E. M., Lee, Y. F. (2014). E-selectin ligand-1 controls circulating prostate cancer cell rolling/adhesion and metastasis. *Oncotarget, 5*(23), 12097-12110. doi:10.18632/oncotarget.2503
168. Liu, Z. J., Tian, R., Li, Y., Zhang, L., Shao, H., Yang, C., Velazquez, O. C. (2016). SDF-1alpha-induced dual pairs of E-selectin/ligand mediate endothelial progenitor cell homing to critical ischemia. *Sci Rep, 6*, 34416. doi:10.1038/srep34416
169. Ferro A., Queen L.R., Priest R.M., Xu B., Ritter J.M., Poston L., Ward J.P. Activation of nitric oxide synthase by beta 2-adrenoceptors in human umbilical vein endothelium in vitro. Br J Pharmacol. 1999;126:1872–1880.
170. Ciccarelli M., Sorriento D., Cipolletta E., Santulli G., Fusco A., Zhou R.-H., … Iaccarino, G. (2011). Impaired neoangiogenesis in β_2–adrenoceptor gene-deficient mice: restoration by intravascular human β_2–adrenoceptor gene transfer and role of NFκB and CREB transcription factors. *British Journal of Pharmacology*, *162*(3), 712–721. http://doi.org/10.1111/j.1476-5381.2010.01078.x
171. Fizazi, K., Bosserman, L., Gao, G., Skacel, T., Markus, R. (2013). Denosumab treatment of prostate cancer with bone metastases and increased urine N-telopeptide levels after therapy with intravenous bisphosphonates: results of a randomized phase II trial. *J Urol, 189*(1 Suppl), S51-57; discussion S57-58. doi:10.1016/j.juro.2012.11.022
172. Nelson, C. J., Cho, C., Berk, A. R., Holland, J., Roth, A. J. (2010). Are gold standard depression

measures appropriate for use in geriatric cancer patients? A systematic evaluation of self-report depression instruments used with geriatric, cancer, and geriatric cancer samples. *J Clin Oncol, 28*(2), 348-356. doi:10.1200/JCO.2009.23.0201
173. Kristensen, T. B., Knutsson, M. L. T., Wehland, M., Laursen, B. E., Grimm, D., Warnke, E., Magnusson, N. E. (2014). Anti-Vascular Endothelial Growth Factor Therapy in Breast Cancer. *International Journal of Molecular Sciences*, *15*(12), 23024–23041. http://doi.org/10.3390/ijms151223024
174. Bachelier, R., Confavreux, C. B., Peyruchaud, O., Croset, M., Goehrig, D., van der Pluijm, G., Clezardin, P. (2014). Combination of anti-angiogenic therapies reduces osteolysis and tumor burden in experimental breast cancer bone metastasis. *Int J Cancer, 135*(6), 1319-1329. doi:10.1002/ijc.28787
175. Haider, M. T., Hunter, K. D., Robinson, S. P., Graham, T. J., Corey, E., Dear, T. N., . . . Holen, I. (2015). Rapid modification of the bone microenvironment following short-term treatment with Cabozantinib in vivo. *Bone, 81*, 581-592. doi:10.1016/j.bone.2015.08.003
176. Varkaris, A., Corn, P.G., Parikh, N.U., Efstathiou, E., Song, J.H., Lee, Y.C., . . . Gallick, G.E. (2016). Integrating Murine and Clinical Trials with Cabozantinib to Understand Roles of MET and VEGFR2 as Targets for Growth Inhibition of Prostate Cancer. *Clin Cancer Res, 22*(1), 107-121. doi:10.1158/1078-0432.CCR-15-0235
177. Schadler, K.L., Thomas, N.J., Galie, P.A., Bhang, D.H., Roby, K.C., Addai, P., . . . Ryeom, S. (2016). Tumor vessel normalization after aerobic exercise enhances chemotherapeutic efficacy. *Oncotarget, 7*(40), 65429-65440. doi:10.18632/oncotarget.11748
178. Ghajar, C.M., Peinado, H., Mori, H., Matei, I.R., Evason, K.J., Brazier, H., . . . Bissell, M.J. (2013). The perivascular niche regulates breast tumour dormancy. *Nat Cell Biol, 15*(7), 807-817. doi:10.1038/ncb2767
179. Rivera, L.B., Bergers, G. (2014). Angiogenesis. Targeting vascular sprouts. *Science, 344*(6191), 1449-1450. doi:10.1126/science.1257071
180. Park, S. Y., Kang, J. H., Jeong, K. J., Lee, J., Han, J. W., Choi, W. S., . . . Lee, H. Y. (2011). Norepinephrine induces VEGF expression and angiogenesis by a hypoxia-inducible factor-1alpha protein-dependent mechanism. *Int J Cancer, 128*(10), 2306-2316. doi:10.1002/ijc.25589
181. Aiken, A., Khokha, R. (2010). Unraveling metalloproteinase function in skeletal biology and disease using genetically altered mice. *Biochim Biophys Acta, 1803*(1), 121-132. doi:10.1016/j.bbamcr.2009.07.002
182. Nannuru, K. C., Futakuchi, M., Varney, M. L., Vincent, T. M., Marcusson, E. G., Singh, R. K. (2010). Matrix metalloproteinase (MMP)-13 regulates mammary tumor-induced osteolysis by activating MMP9 and transforming growth factor-beta signaling at the tumor-bone interface. *Cancer Res, 70*(9), 3494-3504. doi:10.1158/0008-5472.CAN-09-3251
183. Kudo, Y., Iizuka, S., Yoshida, M., Tsunematsu, T., Kondo, T., Subarnbhesaj, A., . . . Takata, T. (2012). Matrix metalloproteinase-13 (MMP-13) directly and indirectly promotes tumor angiogenesis. *J Biol Chem, 287*(46), 38716-38728. doi:10.1074/jbc.M112.373159
184. Shah, M., Huang, D., Blick, T., Connor, A., Reiter, L. A., Hardink, J. R., . . . Thompson, E. W. (2012). An MMP13-selective inhibitor delays primary tumor growth and the onset of tumor-associated osteolytic lesions in experimental models of breast cancer. *PLoS One, 7*(1), e29615. doi:10.1371/journal.pone.0029615
185. Fu, J., Li, S., Feng, R., Ma, H., Sabeh, F., Roodman, G. D., . . . Lentzsch, S. (2016). Multiple myeloma-derived MMP-13 mediates osteoclast fusogenesis and osteolytic disease. *J Clin Invest, 126*(5), 1759-1772. doi:10.1172/JCI80276

186. Price, T. T., Burness, M. L., Sivan, A., Warner, M. J., Cheng, R., Lee, C. H., . . . Sipkins, D. A. (2016). Dormant breast cancer micrometastases reside in specific bone marrow niches that regulate their transit to and from bone. *Sci Transl Med, 8*(340), 340ra373. doi:10.1126/scitranslmed.aad4059
187. Ranganathan, A. C., Adam, A. P., Aguirre-Ghiso, J. A. (2006). Opposing roles of mitogenic and stress signaling pathways in the induction of cancer dormancy. *Cell Cycle, 5*(16), 1799-1807. doi:10.4161/cc.5.16.3109
188. Naumov, G. N., Akslen, L. A., Folkman, J. (2006). Role of angiogenesis in human tumor dormancy: animal models of the angiogenic switch. *Cell Cycle, 5*(16), 1779-1787. doi:10.4161/cc.5.16.3018
189. Pfitzenmaier, J., Ellis, W. J., Arfman, E. W., Hawley, S., McLaughlin, P. O., Lange, P. H., Vessella, R. L. (2006). Telomerase activity in disseminated prostate cancer cells. *BJU Int, 97*(6), 1309-1313. doi:10.1111/j.1464-410X.2006.06194.x
190. Weckermann, D., Muller, P., Wawroschek, F., Harzmann, R., Riethmuller, G., Schlimok, G. (2001). Disseminated cytokeratin positive tumor cells in the bone marrow of patients with prostate cancer: detection and prognostic value. *J Urol, 166*(2), 699-703.
191. Chery, L., Lam, H. M., Coleman, I., Lakely, B., Coleman, R., Larson, S., . . . Morrissey, C. (2014). Characterization of single disseminated prostate cancer cells reveals tumor cell heterogeneity and identifies dormancy associated pathways. *Oncotarget, 5*(20), 9939-9951. doi:10.18632/oncotarget.2480
192. Johnson, R. W., Finger, E. C., Olcina, M. M., Vilalta, M., Aguilera, T., Miao, Y., . . . Giaccia, A. J. (2016). Induction of LIFR confers a dormancy phenotype in breast cancer cells disseminated to the bone marrow. *Nat Cell Biol, 18*(10), 1078-1089. doi:10.1038/ncb3408
193. Ghajar, C. M. (2015). Metastasis prevention by targeting the dormant niche. *Nat Rev Cancer, 15*(4), 238-247. doi:10.1038/nrc3910
194. Johnson, R. W., Schipani, E., Giaccia, A. J. (2015). HIF targets in bone remodeling and metastatic disease. *Pharmacol Ther, 150*, 169-177. doi:10.1016/j.pharmthera.2015.02.002
195. O'Keefe, E. B., Meltzer, J. P., Bethea, T. N. (2015). Health disparities and cancer: racial disparities in cancer mortality in the United States, 2000-2010. *Front Public Health, 3*, 51. doi:10.3389/fpubh.2015.00051
196. Shariff-Marco, S., Yang, J., John, E. M., Kurian, A. W., Cheng, I., Leung, R., . . . Gomez, S. L. (2015). Intersection of Race/Ethnicity and Socioeconomic Status in Mortality After Breast Cancer. *J Community Health, 40*(6), 1287-1299. doi:10.1007/s10900-015-0052-y
197. Surbone, A., Halpern, M. T. (2016). Unequal cancer survivorship care: addressing cultural and sociodemographic disparities in the clinic. *Support Care Cancer, 24*(12), 4831-4833. doi:10.1007/s00520-016-3435-4
198. Obama, B. (2016). United States Health Care Reform: Progress to Date and Next Steps. *JAMA, 316*(5), 525-532. doi:10.1001/jama.2016.9797
199. Skloot, Rebecca. **The Immortal Life of Henrietta Lacks**. New York: Crown Publishers, 2010. Print.
200. Hughes, P. The costs of using unauthenticated, over-passaged cell lines: how much more data do we need? BioTechniques 43:575-586 (November 2007)
201. Pan, C., Kumar, C., Bohl, S., Klingmueller, U., Mann, M. Comparative Proteomic Phenotyping of Cell Lines and Primary Cells to Assess Preservation of Cell Type-specific Functions. *Molecular & Cellular Proteomics : MCP*. 2009;8(3):443-450. doi:10.1074/mcp.M800258-MCP200.

202. Kim, H., Cho, H-J., Kim, S-W., Liu, B., Choi, Y.J., Lee, J., Sohn, Y-D., … Yoon, Y-S. $CD31^+$ Cells Represent Highly Angiogenic and Vasculogenic Cells in Bone Marrow *Circulation Research*. 2010;107:602-614, originally published September 2, 2010
203. Schmid, C. W., Deininger, P. L. Sequence organization of the human genome. *Cell* 6, 345–358 (1975).
204. Paabo, S. Molecular cloning of Ancient Egyptian mummy DNA. *Nature* 314, 644–645 (1985).
205. Tyler, M. G., Kirby, L. T., Wood, S., Vernon, S., Ferris, J. A. Human blood stain identification and sex determination in dried blood stains using recombinant DNA techniques. *Forensic Science International* 31, 267–272 (1986).
206. McKenzie, B.A., Barrieux, A., Varki, N.M. A novel detection system for submicroscopic human metastases in athymic mice. *Cancer Communications* 3, 15–19 (1991).
207. Burkhart, C.A., Norris, M.D., Haber, M. A simple method for the isolation of genomic DNA from mouse tail free of real-time PCR inhibitors. *Journal of Biochemical and Biophysical Methods* 52, 145–149 (2002).
208. Collins M. J., Nielsen-Marsh, C.M., Hiller J., Smith C.I., Roberts J.P., … Turner-Walker G. The survival of organic matter in bone: a review. *Archaeometry* 44, 383–394 (2002).
209. Oskam, C. L., Haile J., McLay E., Rigby P., Allentoft M.E., … Bunce M. Fossil avian eggshell preserves ancient DNA. *Proceedings of the Royal Society B: Biological Sciences* Jul 7; 277(1690):1991–2000 (2010).
210. Collins, M.J., Riley, M.S., Child, A.M., Turner-Walker, G. A Basic Mathematical Simulation of the Chemical Degradation of Ancient Collagen. *Journal of Archaeological Science* 22, 175–183 (1995).
211. Brundin, M., Figdor, D., Sundqvist, G., Sjögren, U. DNA Binding to Hydroxyapatite: A Potential Mechanism for Preservation of Microbial DNA. *Journal of Endodontics* 39, 211–216 (2013).
212. Rosenberg, A.M., Prokopchuk, P.A. The binding of dsDNA and ssDNA to human types I, II and IV collagens. *The Journal of Rheumatology* 13, 512–516 (1986).
213. Hanni, C., Brousseau, T., Laudet, V., Stehelin, D. Isopropanol precipitation removes PCR inhibitors from ancient bone extracts. *Nucleic Acids Research* 23, 881–882 (1995).
214. Herbst, K.J., Allen, M.D., Zhang, J. The cAMP-dependent protein kinase inhibitor H-89 attenuates the bioluminescence signal produced by Renilla Luciferase. *PloS One* 4, e5642 (2009).
215. Kim, J.B., Urban, K., Cochran, E., Lee, S., Ang, A., … Lassota P. Non-invasive detection of a small number of bioluminescent cancer cells. *PloS One* 5, e9364 (2010).
216. Coralli, C., Cemazar, M., Kanthou, C., Tozer ,G.M., Dachs, G.U. Limitations of the reporter green fluorescent protein under simulated tumor conditions. *Cancer Research* 61, 4784–4790 (2001).
217. Tam, J.M., Upadhyay, R., Pittet, M.J., Weissleder, R., Mahmood, U. Improved in vivo whole-animal detection limits of green fluorescent protein-expressing tumor lines by spectral fluorescence imaging. *Molecular Imaging* 6, 269–276 (2007).
218. Aceto, N., Bardia, A., Miyamoto, D.T., Donaldson, M.C., … Maheswaran, S. Circulating tumor cell clusters are oligoclonal precursors of breast cancer metastasis. *Cell* 158, 1110–1122 (2014).